Acoustic wave propagation in a duct with varying temperatures

Craig Massey-Hicks

A research report submitted to the Faculty of Engineering and the Built Environment, University of the Witwatersrand, Johannesburg, in partial fulfilment of the requirements for the degree of Master of Science in Engineering.

Johannesburg, September 2017

Declaration

I declare that this research report is my own, unaided work, except where otherwise acknowledged. It is being submitted for the degree of Master of Science in Engineering in the University of the Witwatersrand, Johannesburg. It has not been submitted before for any degree or examination at any other university.

Signed this _____ day of _____20___ .

_____.

Craig Massey-Hicks

Acknowledgements

I would like to thank my supervisor, Prof. Craig Law, for the advice and guidance he has provided over the course of this project. The feedback I received while writing this report was particularly valuable and has made a significant contribution to my academic development.

I would also like to thank the many friends, family and colleagues who supported and advised me over the course of my studies. Particular thanks must go to my Grandfather, Mr George Lezard, whose keen interest and encouragement were a crucial factor in keeping me going when things got difficult, thanks Papa.

Abstract

This project examines the propagation of an acoustic wave through a composite duct. The geometry of the duct is selected to approximate that of a gas turbine combustor and a temperature field is applied to this geometry. The temperature field was obtained from a CFD model of a working gas turbine combustor and the acoustic modelling was performed in the ANSYS Mechanical Acoustic ACT extension, using Finite Element methods. The CFD models were validated by comparing their results with data from the manual for the engine used as the basis for these models. The acoustic models were verified and validated by comparing them with the results of a 1 dimensional, theoretical model implemented in various Matlab scripts. The final model presents the Sound Pressure level in the composite duct with an applied temperature field at a frequency of 600Hz and with an excitation of $1\mathrm{m}.\mathrm{s}^{-1}$ representing the noise generated by the flame.

The use of the Finite Element approach and the assumptions central to the theoretical model were found to be reasonable for the conditions encountered in the combustor. The Finite Element models showed good agreement with the theoretical models and the next steps in the development of these models were presented.

Table of Contents

Acknowledgements ... iii

Abstract ... iv

Table of Contents ... v

Figures ... vii

Tables ... viii

1. Introduction ... 1

1.1. Motivation ... 1

1.2. Research question and objectives ... 2

1.3. Report Overview ... 3

2. Literature survey ... 5

2.1. Combustor Design ... 5

2.2. Combustor Noise ... 6

2.3. Thermoacoustics ... 7

2.4. Aeroacoustics ... 10

2.5. Fluid Structure Interaction ... 11

2.6. Problem conceptualisation ... 14

3. Method ... 20

3.1. Geometry ... 22

3.2. Model 1 ... 24

3.3. Models 2 & 5 ... 28

3.4. Models 3 & 4 ... 31

3.5. Models 6 & 7 ... 36

3.6. Equipment used ... 39

3.7. Assumptions and Limitations ... 39

4. Results ... 43

4.1. Model 1 ... 43

4.2. Model 2 and Model 5 ... 46

4.3. Model 3 ... 48

4.4. Model 4 ... 50

4.5. Model 6 ... 54

4.6. Model 7 ... 58

5. Conclusions ... 61

6. Recommendations ... 64

6.1. Lessons Learned ... 64

6.2. Future work 65
6.2.1. Suggested further projects 65
6.2.2. Software Tutorials 67
References 70
A - Gas Turbine Combustor Design ..... Ai
B - Proteus Combustor ..... Bi
C - ANSYS CFX Models Ci
D - ANSYS FEA Acoustic Models ..... Di
E - Transfer Matrices ..... Ei
F - Theoretical Models in MATLAB ..... Fi

Figures

Figure 1: Combustion zones and components of typical combustor (Hossaini, 2013) 5
Figure 2: Acoustic multi-port of duct with heat source (Polifke, et al., 2001) 8
Figure 3: Simple model of gas turbine combustor geometry (Dowling & Stow, 2003) 9
Figure 4: "Burner" region in a pre-mix combustor (Dowling & Stow, 2003) 10
Figure 5: Coupling action of FSI (Lefrancois & Boufflet, 2010) 12
Figure 6: Interactions between phenomena of interest (Huls, 2006) 15
Figure 7: Approaches to analysing effects of combustion dynamics in gas turbine combustors (Huls, 2006) 16
Figure 8: Conceptualisation of the interactions between the physical phenomena that result in the effect of acoustics on the combustor liner 16
Figure 9: Proteus Gas Turbine Engine with combustor visible 23
Figure 10: 3D model of full combustor assembly 24
Figure 11: Mesh and geometry of Model 1 (24epw) 25
Figure 12: Comparison of FLUID220 and FLUID30 elements used in ANSYS Acoustic ACT (Howard & Cazzolato, 2014) 27
Figure 13: Model 2 geometry and mesh 28
Figure 14: Sections and endpoints of Model 5 29
Figure 15: Nodes along axis of ANSYS Model 30
Figure 16: Cross section of mesh used in Model 4 (note the use of hex mesh in interior) 32
Figure 17: Boundary conditions in CFX Pre for Model 3 33
Figure 18: Mesh and Boundaries of CFX simulation for Model 4 34
Figure 19: Planes for sampling temperatures through fired combustor 35
Figure 20: Mesh of Model 6b, with multiple planes for the various temperatures 37
Figure 21: Geometry and Mesh of Model 7 38
Figure 22: Temperature inputs for variable temperature field of Model 7 38
Figure 24: SPL for Model 1, theory vs ANSYS with multiple meshes used 44
Figure 23: First four modes of simple duct (Clockwise from top left) 45
Figure 25: SPL for Model 2, ANSYS vs Theory 47
Figure 26: Mode 4 of Model 2 showing non-planar behaviour around swirler 47
Figure 27: Velocity vector and field at inlet of cold combustor 49
Figure 28: Velocity field in XY plane of Combustor (no flame) 49
Figure 29: Mach number through fired combustor liner 51
Figure 30: Temperature field, with velocity vector in ZY plane of fired combustor 52

Figure 31: Temperatures at various sample points 52
Figure 32: Linear and variable temperature profiles along combustor liner 53
Figure 33: Linearly varying temperature across Model 6 55
Figure 34: SPL for Model 6a, ANSYS vs Theory 56
Figure 35: Varying temperature field of Model 6 57
Figure 36: SPL for Model 6b, ANSYS vs Theory 57
Figure 37: SPL for Model 7a, ANSYS vs Theory 59
Figure 38: SPL for Model 7b, ANSYS vs Theory 59
Figure 39: SPL of Model 7b, open duct 60
Figure 40: Steps of suggested tutorial on CFD modelling of combustor 68

Tables

Table 1: Models used through the course of the project 21
Table 2: Verification of results from Model 3 49
Table 3: Boundary conditions input to CFX-Pre for Model 4 50
Table 4: Verification of Model 4 53
Table 5: Validation of Model 4 54

1. Introduction

The acoustic component of the loads experienced by the liner of a gas turbine combustor have, traditionally, been regarded as negligible. However, modern emission requirements have forced designers to reduce the temperature of combustion in order to reduce NO_x products in the combustion gases. One way in which this is achieved is to make use of a Lean Premix Prevaporise combustor design (LPP).

An LPP combustor operates very close to the lower explosion limit of the air fuel equivalence ratio. While this achieves the goal of reducing the temperature of combustion, it has the side effect of greatly increasing the instability of the flame and, therefore, the noise of combustion.

While the nature and magnitude of the acoustic load produced by flame noise has been well studied, the resultant load experienced by the combustion liner, and its role in causing liner failure have not been regarded as significant in the past (Huls, 2006). Instead, failures of combustion liners have been attributed to thermal creep and fatigue due to thermal cycling as the load on the combustor varies (Tinga, 2006).

The noise produced in a gas turbine combustor has the potential to reach amplitudes and frequencies that may cause significant structural damage to the combustor assembly in general and liner in particular. If this noise were to occur at or near the resonant frequencies of the liner, there is the potential for a severe level of vibration to be produced. Given the already harsh operating environment and long operating life requirements, this vibration may have a significant effect on the failure modes of the liner (Pożarlik, 2010).

1.1. Motivation

The ability to quantify the effect of noise on the liner would allow for an improvement of both the design of the component and the prediction of its lifespan.

In addition to the increased levels of noise within the combustor, the consumption of air in the premixing phase of an LPP combustor leaves less air available to travel in the annulus for cooling and dilution compared to a traditional combustor design.

This annular air flow would previously have had a damping effect on the pressure fluctuations.

The interactions of fluid and structure in the context of combustion chambers have been well studied in the form of vibrations induced in rocket engines. The most notable subject of these studies being the notorious “pogo effect” in the rockets used in the 60s and 70s (Culick & Yang, 1995). The fluctuations in pressure in the combustion chambers of the rockets fluctuated with an amplitude of 10% about the mean (Polifke, et al., 2001). These vibrations are higher than those experienced in a gas turbine combustor. However, as the mission life of the rocket is much lower than that of a gas turbine, the material fatigue induced by these vibrations was of little to no concern (so long as they remained below a critical level). What this does show is that combustion induced vibration can be a legitimate cause of concern for the long term operation of these combustors.

In order to apply and integrate the various disciplines, each discipline needs to be mastered to a sufficient level. Once this mastery is achieved, the results of each step may be used as quality building blocks for the, more complex, overall model. If any of the physical processes is not fully understood, the quality of the overall solution will be significantly diminished. Therefore, if an organisation is able to solve this problem, it serves as a means of both developing and proving the capacity in the various fields outlined in the next section.

1.2. Research question and objectives

The question motivating this research is: “How does the noise produced by the operation of a gas turbine combustor interact with its structure?”

In order to complete the first step towards answering this question, the objective of this project was to develop a numerical model of the acoustic field within the combustor. The outcomes of this objective are:

- A CFD model that illustrates the velocity and temperature fields within a typical gas turbine combustor
- A finite element acoustic model, of the geometry of the combustor used above, that takes the temperature field into account.
- A comparison of the results of the finite element model with those of a 1-Dimensional, theoretical model.

The Computational Fluid Dynamics model will increase the understanding of the design of the combustor and behaviour of the flow therein. This provides a context for the problem and informs decisions on the assumptions and simplifications used. This context also allows for more intelligent selection of boundary conditions for the models produced. The flow of gas and, in particular, the temperature distribution of this gas play a significant role in the propagation of the acoustic waves through the combustor. As such, they are a necessary starting point for any acoustic analysis of this equipment.

A Finite Element model will allow for the initial analysis of the propagation of acoustic waves through the geometry of the combustor to be conducted at a lower computational cost than that of a CFD based investigation. The Finite Element method will be used for the analysis of stresses and strains in the structure (when such a point is reached) and the fluid structure interaction will be easier to develop if both aspects of the problem are approached with the same method.

With experimental modelling outside of the scope of this project, the analytical 1-Dimensional models will be used to validate the acoustic analysis performed in the Finite Element models. With this being a first attempt at this research, it is useful to have the analytical model as a bridge between the theory and numerical and later experimental models.

1.3. Report Overview

This report begins by examining the literature on the various aspects of the physical phenomena that underpin the research question. The design of a gas turbine combustor is briefly described, as is the nature of combustor noise experienced in practice. This is followed by a review of the disciplines of thermoacoustics aeroacoustics, and fluid structure interaction (FSI). With these disciplines covered, an overview is given of previous approaches that have been taken towards answering the research question. Finally, a conceptualisation of the problem is presented, with each of the various physical processes (and their interactions) examined.

After going through the literature that informs the method of this project, the method itself is presented in the form of a description of each of the models produced and their function. The models are presented in the order in which they build on one another. The processes and decisions made in producing each of the three types of model, those in ANSYS Acoustic, CFX and MATLAB, are described as these

models are presented. The limitations and assumptions used are noted along the way, with the effects of these limitations discussed at the end of the section.

After detailing each of the models in the description of the method, the results of these models are presented. Some of the results illustrate the validity of the assumptions and simplifications used in the project, while new limitations in the method are exposed by other results. The final result is presented as the Sound Pressure Level distribution of a composite duct with a varying temperature profile. This model is presented as a reasonable prediction of the behaviour of an acoustic wave in a gas turbine combustor at a given frequency and for a given excitation.

Conclusions are then drawn, based on these results and, finally, recommendations are made based on these conclusions. The recommendations are divided into two sections, one on the lessons learned while undertaking this project and another on the recommended future work that could build on that done in this project.

Appendices containing more detailed description of gas turbine combustor design, the actual combustor used as the basis for the geometry of the models in this project and the derivations of the transfer matrices that are used in the theoretical model are included at the end of the report for interest.

2. Literature survey

This section presents an overview of the current techniques for quantifying the effects of the flame produced acoustic load on the life of a gas turbine combustor liner. The layout of a typical combustor is described before different components of the problem are categorised and the physical processes of the interactions between these categories described.

2.1. Combustor Design

For a traditional combustor design, the airflow may be divided into 3 zones of distinct behaviour. The first of these is the primary zone, where the air entering the combustor is deliberately swirled to create a vortex that allows for fuel and air to mix as well as anchoring the flame in place. The second is the intermediate zone, where additional air is provided to the flow to ensure 100% combustion takes place. The third and final zone before exiting the combustor is the dilution zone that adds the remaining air to the flow, lowering the temperature and altering the temperature distribution of the combustor outlet. The length of the dilution zone is typically 55 – 65 % of the combustor (Lefebvre & Ballal, 2010). Figure 1 shows a typical combustor, with the discussed zones and components annotated.

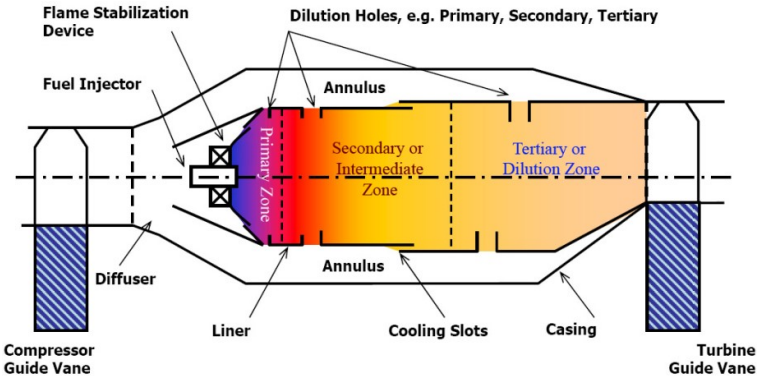


Figure 1: Combustion zones and components of typical combustor (Hossaini, 2013)

The primary zone represents the location of the flame and, therefore, the source of the majority of noise within the combustor. The geometry of the combustor and its components determines the nature of the flow of combustion gases and the temperature profile of these gases, which has a significant effect on the propagation of the noise through the combustion chamber.

2.2. Combustor Noise

There are two sources of combustion noise. The first is that arising from the highly turbulent flow throughout the combustor. This flow is a source of noise in all three of the flow zones of the combustor ((Bragg, 1963), as referred to in (Lefebvre, 2010). This source is due to the aeroacoustic effect discussed in section 2.4 of this report.

The second source of noise within the combustor is direct noise resulting from the burning of the flame. This produces acoustic monopoles in the region of the flame that are statistically distributed across the frequency spectrum from 100Hz to 2000Hz, with the highest concentration occurring in the 300 to 500Hz range (Lefebvre, 2010).

The production of this noise and it's interaction with the behaviour of the flame may be described in terms of the thermoacoustic effect discussed in section 2.3 of this report. The amount of noise radiated by the flame compared with the total energy produced by the flame determines the flame's thermoacoustic efficiency. Naturally, the source of this noise is predominantly located in the primary and (to a lesser extent) intermediate zones where the actual combustion is occurring.

Combustions noise occurring in the 200-500Hz range is described in industry as "Howl" and that found in the 80 to 150Hz range as "Growl", with Growl typically found only during start-up conditions ((Shivashankara & Crouch, 1977), as referred to in (Lefebvre, 2010)). Frequencies above 600Hz are typically regarded as not being as prevalent in gas turbine combustors (Kok, et al., 2010). The relatively low frequency of this noise allows for simplifications to be made in the modelling of the acoustic waves. These simplifications allow for the use of 1-dimensional analytical models to be used for the validation of the more complex numerical models presented later.

Instabilities in combustion lead to an increase in the amount of noise produced by the flame (Boyce, 2012) (Ballal & Lefebvre, 1974) Combustion instabilities may be the result of variations in the fuel flow and fuel drop size, temperature or loading of the turbine that affect the combustion directly. Alternatively, these instabilities may be the result of disturbances or fluctuations in the air supply from the compressor. The fluctuations in air supply affects the mixing of the fuel and air and lead to zones of flame extinction and re-ignition, producing greater degrees of turbulence and noise from the flame (Ballal & Lefebvre, 1974). In both cases, variations in the operation of the engine influence the noise produced and need to be taken into

account when modelling the noise within a combustor. For the modelling of the velocity and temperature fields within the combustor, a steady state simulation is typically employed (ANSYS, 2013) which is the approach used in this project.

Changes in fuel type may have a large effect on drop size, spray pattern and the speed and heat of the flame, all of which may have an effect on the stability of the flame. Fluctuations in fuel supply pressure will affect the flow of the fuel through the atomiser and have a similar effect.

Low operating temperatures and high pressures have the effect of increasing the thermoacoustic source of combustion noise. General ambient conditions contribute greatly to these effects through the temperature, pressure and moisture content of the air entering the compressor (Boyce, 2012).

Further causes of unusual combustor noise (not necessarily noise of combustion) include the fouling of the combustor liner, failure of crossover tubes and the detachment or cracking of the combustor housing, which may change the resonant properties of the chamber.

With the advent of lean burning combustors as a means of reducing emissions, combustors are now running at much lower equivalence ratios than previously, which has increased the difficulty in ensuring a stable flame and, therefore, led to an increase in the amount of noise typically produced during the combustion process (Richards, 1996). The impact of the combustion noise on the life of the combustor liner is, therefore, of greater interest now than it has been in the past (Huls, 2006)

2.3. Thermoacoustics

The primary source of noise in a gas turbine combustor is that produced by the phenomena of thermoacoustics. The term “Thermoacoustics” refers to “the dynamic coupling of heat transfer and acoustics” (Epperlein, et al., 2015). The modelling of this phenomena in gas turbines is known to be extraordinarily difficult due to the influence of combustion dynamics on the computational effort required (Polifke, et al., 2001), (Epperlein, et al., 2015).

With the direct numerical modelling of the thermoacoustic effect an extremely costly exercise from computing perspective, thermo-acoustic systems are frequently modelled as networks of acoustic multi-ports (Polifke, et al., 2001). While this is typically only performed for 1 spatial dimension and with two variables, extension to higher orders has been shown to be possible (Polifke, et al., 2001).

An example of a network of acoustic multi ports for a duct containing a heat source is shown in Figure 2.

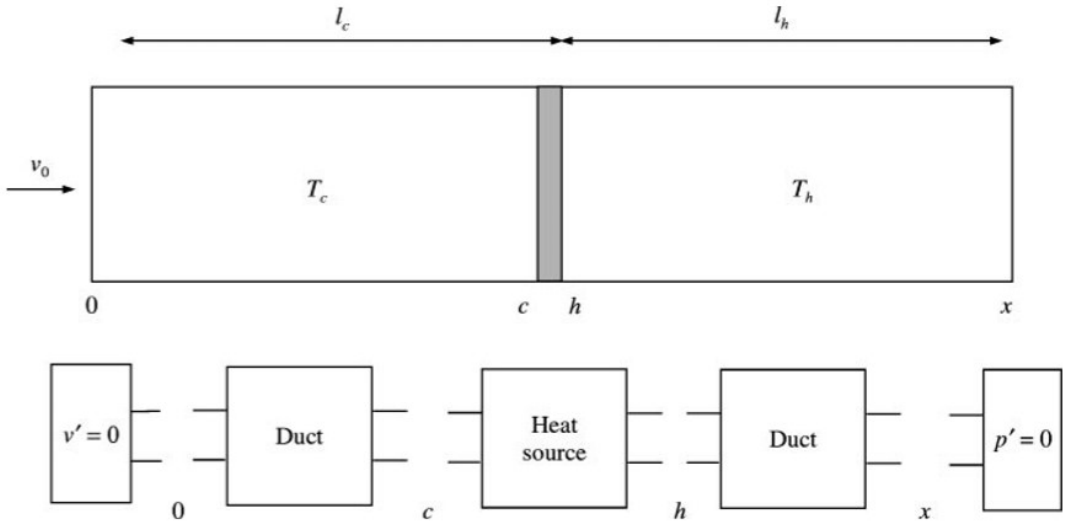


Figure 2: Acoustic multi-port of duct with heat source (Polifke, et al., 2001)

A transfer matrix for this heat source is developed analytically in (Polifke, et al., 2001) and given as:

$$\begin{pmatrix} \frac{P'_h}{Z_h} \\ v'_h \end{pmatrix} = \begin{pmatrix} \zeta & \zeta M_c\left(2n + ne^{-i\omega\tau} + \zeta\right) \\ 2n\gamma M_c & 1 - ne^{-i\omega\tau} \end{pmatrix} \begin{pmatrix} \frac{P'_c}{Z_c} \\ v'_c \end{pmatrix} \quad 1$$

Where: M_c is the Mach number at the cold side of the duct, γ the ratio of specific heats, Z the specific impedance, P'_x the acoustic pressure, v'_x the acoustic velocity and:

$$n = \frac{1}{2}\left(\frac{T_h}{T_C} - 1\right) \quad 2$$

T_x represents the temperature, with the subscripts h and c denoting the hot and cold sides of the duct respectively.

ζ and τ represent the independent variables of the pressure differential coefficient and the time lag of the system. These two factors control the dynamic characteristics of the heat source and, therefore, the stability of the thermoacoustic system.

While some of the transfer matrices for a thermoacoustic system may be determined analytically, there are cases where the complexity of the geometries involved make this approach unfeasible. Instead, the “black box” approach commonly used in communications engineering is applied (Polifke, et al., 2001). In this approach, the transfer function of the component in question is determined by its response to a perturbation, either experimentally or numerically.

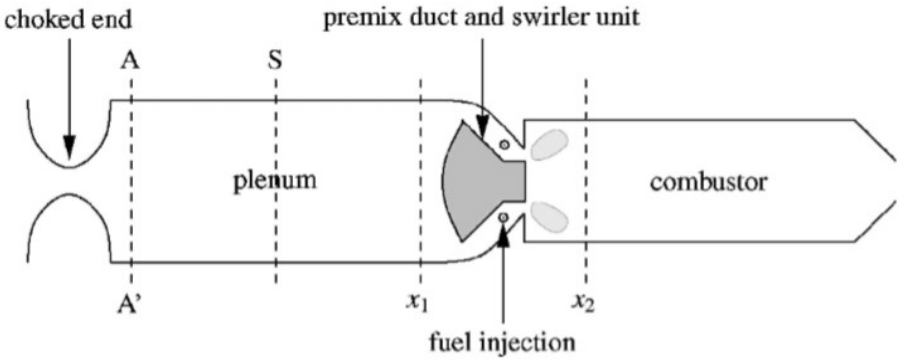


Figure 3: Simple model of gas turbine combustor geometry (Dowling & Stow, 2003)

In the case of a can type gas turbine combustor (Figure 3), the nature of the geometry lends itself to the analytical development of transfer matrices. The only area that becomes too complicated for this to be a viable strategy is that of the “burner”, which includes the swirler, injector and flame. For this area (shown as region 3 in Figure 4), the black box approach is used to determine the “burner impedance”, which is defined in (Huls, 2006) as:

$$Z_B = \left(\frac{P'}{v'}\right)_B \qquad 3$$

And is found either numerically or experimentally (Polifke, et al., 2001)

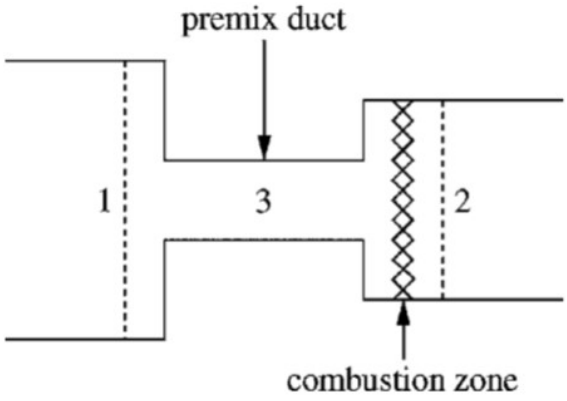


Figure 4: “Burner” region in a pre-mix combustor (Dowling & Stow, 2003)

The use of acoustic multiports as a tool for modelling the propagation of an acoustic wave generated by a thermoacoustic source is a well-established practice and has been successfully used to model the acoustics of a gas turbine combustor (A. P. Dowling, 2003) (Huls, 2006). When the geometry of the model is relatively simple, a source term may be analytically determined. However, as the geometry approaches the complexity of the burners encountered in a combustor, the source term is typically determined empirically.

2.4. Aeroacoustics

The generation and propagation of sound through a fluid or, rather, “the interaction between a background flow and an acoustic field” (COMSOL, 2017), is the subject of the study of aeroacoustics (Bodony, 2017). Aeroacoustics involves aspects of both fluid dynamics and acoustics and, as such, requires a working understanding of the Navier-Stokes, Euler, Energy and Wave Equations and their solutions as a pre-requisite to any work in this area (Bodony, 2017).

Acoustic waves are only one subset of the many different types of waves that may exist in a flow (other examples being vorticity and thermal instability). The energy of these acoustic waves constitutes a very small fraction of the total energy of a flow field. This makes the direct numerical simulation of an acoustic field in (and/or caused by) a background flow very difficult due to the accuracy of the numerical scheme required to overcome the effects of dispersion and dissipation.

The usual approach to overcome this difficulty in modelling aeroacoustics effects was first proposed by Lighthill (1952) in what is commonly known as “Lighthill’s acoustic analogy”. In the first part of this analogy, use is made of the fact that the sound field is a small perturbation of the background flow to find an approximate solution (Hirschberg & Rienstra, 2004). The flow and the acoustic field are treated as separate entities, with the solutions to the acoustic field being placed on top of those of the background flow.

In the second part, the large difference in the heat and energy scales between the source of the sound and its propagation through the fluid is taken advantage of to separate the generation and propagation of the sound into different components. The difference between the actual flow and the reference flow is taken to be a source of the sound, which may be modelled as a monopole, dipole or quadrupole source (Lighthill, 1952).

These sources, and their propagation through the flow were described by Lighthill (1952) through the re-arranging of the Navier-Stokes equations. The quadrupole was found to be the best description of the noise produced by a free, turbulent, isentropic flow (Hirschberg & Rienstra, 2004). The solutions proposed by Lighthill are regarded as being very useful for general work in getting an order of magnitude estimate, but not for detailed analysis as they tend to assign too much physical space to the source terms (Hirschberg & Rienstra, 2004). For this reason, these equations are extended into the Ffowes Williams-Hawkings and Curle's equations in most numerical applications (ANSYS, 2013).

As in thermoacoustics, the study of aeroacoustics may be simplified and understood by separating the source and propagation of the acoustic waves. For simple duct geometries, similar to that encountered in a can type gas turbine combustor, acoustic multi-ports may be used to produce 1-dimensional anlaytical models of this phenomena. Before any such models may be produced, however, it is necessary to attain sufficient mastery of the physics underlying the phenomena..

The most common engineering applications of the field of aeroacoustics are in the design of automotive exhaust systems and in the ducting of HVAC systems, as well as in the design and analysis of turbomachinery (Bodony, 2017) (COMSOL, 2017). As such, most software packages designed to handle this phenomena are done so with these applications in mind, with integration with the other physical processes encountered in a combustor (i.e. combustion) not given much consideration.

There is potential for the use of these packages in the modelling of combustion noise, where the noise from the flame may be modelled by placing a quadrupole source in the flame zone and modelling it's propagation through a pre-solved flow field. The major limitation with this approach is that it is not able to take the feedback of the acoustic field to the flame into account (ANSYS, 2013). This limitation prevents complete description of the acoustic behaviour within the combustor by this method.

2.5. Fluid Structure Interaction

The non-stationary coupling of a fluid flowing through a flexible mechanical structure is the subject of the branch of mechanics known as "Fluid Structure Interaction" (Topiwala, et al., 2016). The coupling is referred to as non-stationary due to the fact that no stable equilibrium solution is guaranteed. The fluid exerts a

pressure on the structure, which may deform under this load and affect the flow of the fluid. This interaction between the two elements may be seen in Figure 5.

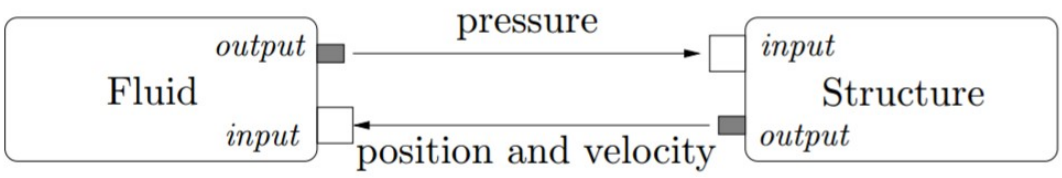


Figure 5: Coupling action of FSI (Lefrancois & Boufflet, 2010)

The coupling of the fluid and structure may be described as “strong” or “weak”. In a strongly coupled system, the interaction is in both of the directions shown in Figure 5. In a weakly coupled system, the interaction is only in one direction, with the pressure from the fluid exerting a force on the structure, but with the deformations of the structure slight enough to have a negligible effect on the fluid (Topiwala, et al., 2016). In the case of a rigid structure like the walls of a gas turbine combustor, the system is considered to be weakly coupled (Pożarlik, 2010)

While the mechanisms that govern the behaviour of both the fluid and structure are the same, their responses to these mechanisms are different. This leads to different difficulties when finding numerical solutions to these problems. As such, the two fields have developed separate commercial solver packages, such as ANSYS CFX that is optimised for the fluids portion of the problem and ANSYS Mechanical that deals with the structural portion.

The overall problem of FSI may be solved using either a monolithic or interactive approach. The differences in these approaches is best explained through the use of the Fundamental Principle of Dynamics (a general expression of Newton’s 2nd law) (Lefrancois & Boufflet, 2010).

$$m\vec{\Gamma} = \sum \vec{F} \qquad 4$$

The left hand term represents the problem to be solved for the structure, with m the mass of the structure and $\vec{\Gamma}$ the acceleration vector. The term on the right represents the sum of the forces ($\vec{F}$, in the form of pressure fluctuations) exerted by the fluid. The modelling of these forces will depend on the categorisation of the fluid.

In the study of FSI, the behaviour of the fluid are typically categorised as; compressible Navier-Stokes, incompressible Navier-Stokes or as an acoustic fluid. If the former two fluid types are to be used, an option for the modelling and coupling of the solutions to Equation 2 may be performed through the use of ANSYS FLUENT and MECHANICAL solvers to complete the fluid and solid aspects of the problem respectively (Topiwala, et al., 2016). In the simple case of the acoustic fluid, there is assumed to be no flow and the loads are modelled in the form of acoustic pressure waves and may be solved through the use of the ANSYS Acoustic ACT extension in ANSYS MECHANICAL, which transforms the solid elements of an FEA mesh into acoustic elements (Howard & Cazzolato, 2014).

In the interaction approach, the left and right hand sides of Equation A3 are solved separately, with the equals sign representing a coupling procedure that allows the two programs to share the required common data in an iterative process. This approach simplifies the mathematics required and allows for the use of standard solvers and integration packages such as ANSYS Workbench. It is also, unfortunately, very slow and requires a high level of skill in the software used in order to couple the separate programs effectively in the sequential manner required (Topiwala, et al., 2016).

When the system is modelled as having an acoustic fluid in ANSYS MECHANICAL, the coupling system, in the form of a thin layer that acts between the meshes of the fluid and structure, must satisfy:

$$[M_S]\{\ddot{u}\} + [K_S]\{u\} = \{F_s\} + [R]\{P\} \text{ (Howard \& Cazzolato, 2014)} \quad 5$$

$$[M_F]\{\ddot{P}\} + [K_F]\{P\} = \{F_F\} - \rho_0[R]^T\{\ddot{u}\} \text{ (Howard \& Cazzolato, 2014)} \quad 6$$

Where $[M_x]$, $[K_x]$ and $[R]$ represent the mass, stiffness and coupling (based of effective area) matrices respectively, with the subscripts S referring to the structure and F referring to the fluid (Howard & Cazzolato, 2014). $\{P\}$, $\{u\}$ and $\{\ddot{u}\}$ represent the Pressure, displacement and acceleration vectors respectively. Rearranging these equations and adding the effects of damping ($[C_x]$) gives (Howard & Cazzolato, 2014):

$$\begin{bmatrix} M_S & 0 \\ \rho_0 R^T & M_F \end{bmatrix}\begin{Bmatrix} \ddot{u} \\ \ddot{P} \end{Bmatrix} + \begin{bmatrix} C_S & 0 \\ 0 & C_F \end{bmatrix}\begin{Bmatrix} \dot{u} \\ \dot{P} \end{Bmatrix} + \begin{bmatrix} K_S & -R \\ 0 & K_F \end{bmatrix}\begin{Bmatrix} u \\ P \end{Bmatrix} = \begin{Bmatrix} F_S \\ F_F \end{Bmatrix} \quad 7$$

In the monolithic approach, the entire Equation is solved in a single solver. This approach allows for unified time and space discretisation and, therefore, effective paralleling of the computation and faster run times. The mathematics involved is,

however, very difficult, with large linear and non-linear equations having to be dealt with numerically (Sandberg, et al., 2009) (Lefrancois & Boufflet, 2010).

The difficulty in both approaches stems from the multi-physics, multi-faceted nature of the problem (Topiwala, et al., 2016) which requires a truly interdisciplinary approach in order to be dealt with effectively. In either case, as is emphasised repeatedly in the literature, an extensive skill set is required from those conducting the research (Topiwala, et al., 2016) (Lefrancois & Boufflet, 2010).

FSI is presented in the literature as a stand-alone area of research that is of significant interest in many applications. The weak coupling of the FSI in a gas turbine combustor means that the loads produced by the fluid on the structure may be examined independently of the structure's response to these loads. The response of the structure to a given load may then be examined as a separate investigation, with the solution to the problem that forms the basis of this project being the quantification of the FSI.

2.6. Problem conceptualisation

The literature on the topics of thermoacoustics, aeroacoustics and FSI all emphasize the multi-disciplinary nature of each area of study. With each of three areas contributing to the acoustic loading of gas turbine combustor liners, an investigation into this phenomenon is going to involve a multi-disciplinary approach. The aim of any study of this nature will be to integrate the various physical processes involved.

In every attempt to enter this field of study, mention is made of the multi-disciplinary nature of the problem, examples include (Huls, 2006) (Polifke, et al., 2001) (A. P. Dowling, 2003) and (Pożarlik, 2010). Multiple physical processes are at play simultaneously and need to be coupled effectively in order for any simulation to be valid. The actual categorisation of these processes is worth spending time on in order to view the problem in its entirety.

With this aim in mind, there is much work that has been done over the past decade at the University of Twente, in the Netherlands, as part of a European-wide project (the LIMOSINE Project) into the combustion dynamics and Flame-fluid-structure interactions of gas turbine combustors. The work has been predominantly based around the test rig built at the University of Twente and consists of both numerical modelling and experimental measurements. The DESIRE test rig, used in the LIMOSINE project, was designed specifically to facilitate the study of the

combustion dynamics of a modern gas turbine combustor (Pożarlik, 2010). These studies have illustrated some of the requirements for the integration of the physical processes involved.

A schematic of the interaction between the relevant phenomena of interest in this field may be found in (Huls, 2006). A modified version of this schematic is shown in Figure 6. The lessons learnt by the projects undertaken through the LIMOSINE project in their efforts to model these phenomenae provides useful guidence on how to break the problem down into separate components. These components may be analysed separately and the results used to provide the interfaces between them that will allow the individual solutions to be integrated into a solution for the system as a whole.

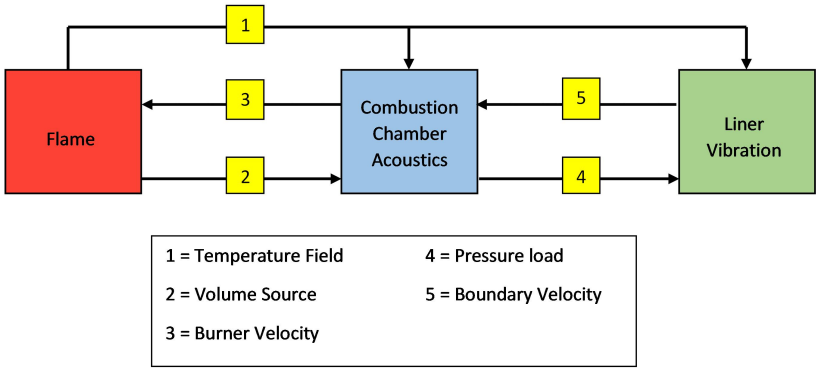


Figure 6: Interactions between phenomena of interest (Huls, 2006)

The approaches that may be taken towards modelling these interactions have been described by various contributors to the LIMOSINE/DESIRE projects, with the diagram in Figure 7 (Huls, 2006) a concise illustration of the 4 approaches that may be taken. In short, the three phenomena (the behaviour of the flame, the nature of the acoustic field it produces and the vibration induced in the structure by the fluid) may be modelled individually and the results of these models fed back and forth between them (Method 4). An alternative is to produce one monolithic model to describe the entire process (Method 1). In between these extremes, the interactions between the flame and fluid may be viewed as part of one thermo-acoustic process; and then treat the vibration of the structure (Method 2). Similarly to Method 2, the flame may be treated as an autonomous source and the pressure fluctuations of the fluid and vibrations of the structure treated as one model.

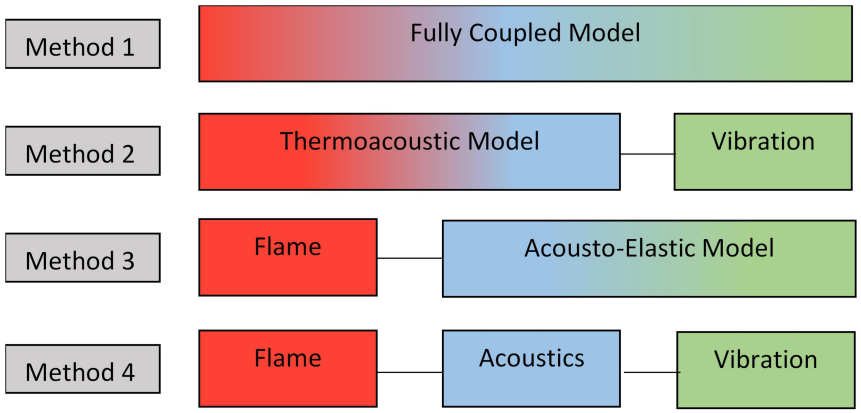


Figure 7: Approaches to analysing effects of combustion dynamics in gas turbine combustors (Huls, 2006)

An alternative to the conceptualisation of the problem developed in (Huls, 2006)) is given in Figure 8. As in Figure 6, the components of the system are depicted in the text boxes, while the interfaces between them are represented by the numbered boxes. The difference between the two conceptualisations is the separation of the Flow and Flame into individual components. This is to emphasise the distinction between the thermo-acoustic and aero-acoustic sources of noise as well as the effect of the flow on the propagation of this noise. While there are many ways in which to view the overall problem, this conceptualisation allows the use of existing disciplines, such as those described in Sections 2.3 to 2.5, to serve as the basis for each component.

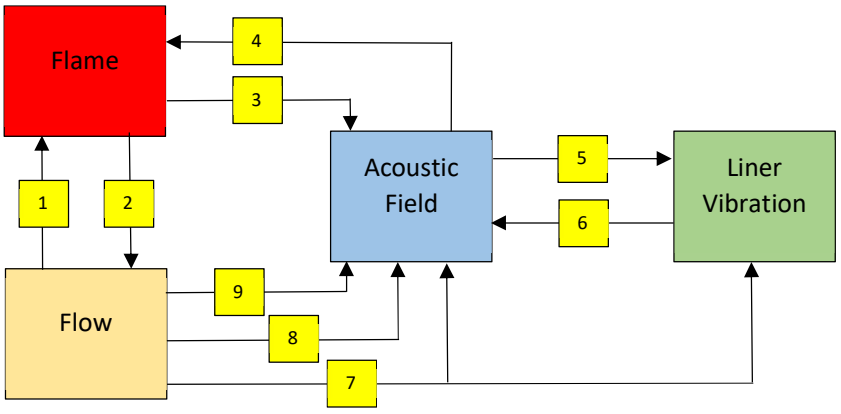


Figure 8: Conceptualisation of the interactions between the physical phenomena that result in the effect of acoustics on the combustor liner

The information passed between the phenomena in Figure 8 is identified as follows:

1. Velocity Vector
2. Energy from Flame to Flow
3. Flame Noise
4. Thermoacoustic Feedback
5. Acoustic Pressure Load
6. Noise of vibration
7. Temperature Field
8. Mean Flow
9. Flow Noise

Considering that the function of the equipment is to impart useful energy to the flow of gas through the machine, the first component of this system to be defined is the Flow. The Flow describes the movement of combustion gases and heat through the combustor. For the purpose of this conceptualisation, the flow of heat is included in this component, rather than that of the flame. While the Flame does provide the energy that gives rise to the temperature field, it is the Flow that determines the distribution of this field (Process 7).

The flow of gas interacts with the flame by a velocity profile (Process 1) with a high degree of turbulence and vorticity. The rotational nature of the velocity profile serves to anchor the flame to a specific location within the combustor and hold it to a certain shape. The turbulence and vorticity imparted by the Flow aids in the mixing of the air and fuel and is a crucial component of the combustion process. Energy is imparted to the flow from the Flame in the form of the heat of combustion (Process 2).

The Flow also acts as a source of aero-acoustic noise (Process 9), with areas of high turbulence causing pressure fluctuations about the mean pressure value that propagate through the regions of lower turbulence within the combustor. This process is the subject of the study of aero-acoustics, as discussed in section 2.4.

The Flame may be thought of as a source of noise and heat that reacts with the flow and acoustic fields. The chemical and physical processes of combustion constitute an entire field of study in and of themselves, an introduction to which may be found in (Lefebvre & Ballal, 2010). Commercial CFD packages such as FINE

Numeca and ANSYS CFX include the facility to set up a reacting mixture to model these processes of combustion (ANSYS, 2013).

As a side effect to adding heat to the flow of gas, the flame acts as a source of noise within the combustor. The production of noise due to the addition of heat is the subject of the field of study known as thermo-acoustics, which is the mechanism responsible for Processes 3 and 4 here and is discussed in section 2.3

The combination of processes 3 and 4 is governed by the Rayleigh integral, developed by Rayleigh (1896) (Rayleigh, 1896). The coupling of these processes is pivotal to any study of combustion stability and has been extensively studied. The interest here is not solely on the development of acoustic loads of the liner, but also the effect of this phenomenon on the stability of the flame itself.

In this conceptualisation, the Acoustic Field is thought of as a separate entity to the Flow, with processes 3 and 9 acting as sources that radiate through a free field within the combustor. The Acoustic Field has an additional interaction with the Flame in the form of a feedback loop that may best be visualised by imagining the interaction of a speaker and a flame where the flame is also the source of noise for the speaker. If the two processes are in phase, this could give rise to a resonant condition where the pressure fluctuations within the combustor are greatly amplified.

The Acoustic Field consists of the fluctuations of pressure and velocity about the mean values of the flow (Process 8). These acoustic values are very difficult to extract directly from the flow field and it is considered here to be preferable to separate the two, using the Flame and Flow to provide both the context in which the Acoustic Field occurs and as the sources of this field.

The final component presented in Figure 8, the Fluid Structure Interaction (FSI), concerns the imparting of vibrations into the structure of the combustor liner by the loads produced in the Acoustic Field (Process 5) and is discussed in section 2.5. The actual effect of this load on the liner will be influenced by the temperature of the liner from that of the Flow (Process 7) and, to a lesser degree, the chemical composition of the gasses of combustion and their effect on the material of the liner (process 12). While the vibration of the walls will produce some noise (Process 6), this effect was found to be negligible by Prozarlik (2010)

The effect of the FSI in generating vibrations (and, therefore, wear) will give an indication of the impact by the acoustic load on the lifecycle of the combustor liner.

The level of precision necessary for these acoustic calculations will be determined by the sensitivity of the liner to FSI induced vibration.

For all components and processes of this conceptualisation, it should be noted that the design and geometry of the combustor assembly in general, and liner in particular, plays a significant role in determining the results. The size and shape of the cavity, along with any perforations, will affect the propagation of the Acoustic Field. The positioning of any liner holes and the design of the swirler will directly affect the Flow of the combustion gases and, therefore, the behaviour of the flame. The shape, thickness and material of the liner walls will have a significant effect on the FSI and any vibrations generated, as well as their final effect on the lifecycle of the liner.

The purpose of this conceptualisation is to break the problem into components that may be analysed separately, using the tools best suited for the component in question. It may be seen from Figure 8 that the Acoustic Field lies at the heart of this breakdown, with seven of the nine interfaces of the system connecting to this component. Using the Acoustic Field as the basis for the initial models to describe the system allows for an early identification of the requirements for these interfaces and the information that is needed from the models that will describe the other components.

A limitation of using the Acoustic Field as the basis for the initial modelling is that the accuracy of the results are strongly dependent on the context provided by the Flow and on the values of the acoustic sources from the Flow and the Flame. The results of these early models will, therefore, not be representative of the exact behaviour within a gas turbine combustor. However, these may be improved through an iterative approach once the surrounding models have been produced, using the base provided by the Acoustic Field models.

3. Method

This section serves to describe the overall process taken by this project to model the acoustic field in a gas turbine combustor. The individual methods and stages are described in detail in their respective appendices, with the emphasis in this section on the integration of the various methods.

To keep track of the various geometries and models used, the progressive steps of the project were named Model 1 to Model 7, with a summary of these presented in Table 1.

The geometry of the models are described in the second column of Table 1. This geometry was increased from that of a simple duct, to that of a composite duct (a combination of several ducts of different diameters in series). Finally, the temperature of the acoustic fluid of the model (air) was made to vary, first linearly and then in accordance with what may be expected in a gas turbine combustor.

The third column of Table 1 lists the programs used in creating each model, while the final column describes the purpose of creating each model.

Table 1: Models used through the course of the project

Model	Geometry	Programs Used	Purpose
Model 1	Simple duct	ANSYS Acoustic, Matlab	Develop basic ANSYS model and Matlab script. Confirm plane wave assumption. Set mesh element size and type for subsequent models.
Model 2	Composite duct	ANSYS Acoustic, Matlab	Extend geometry of Model 1 to that of a composite duct that more closely approximates that of a gas turbine combustor
Model 3	Full combustor	ANSYS CFX	Qualitative assessment of cold air flow through combustor, obtain inputs for Model 4
Model 4	Combustor liner	ANSYS CFX	Fired model of combustor, qualitative temperature field, confirm low Mach numbers.
Model 5	Composite duct with outlet	ANSYS Acoustic, Matlab	Include combustor outlet in acoustic models
Model 6a	Simple duct	ANSYS Acoustic, ANSYS Thermal, Matlab	Confirm procedure and matrices used of modelling of simple duct with linear temperature profile
Model 6b	Simple duct	ANSYS Acoustic, ANSYS Thermal, Matlab	Test matrix for suitability of use on varying temperature profile
Model 7a	Composite duct	ANSYS Acoustic, ANSYS Thermal, Matlab	Combine Model 5 and Model 6a
Model 7b	Composite duct	ANSYS Acoustic, ANSYS Thermal, Matlab	Combine Model 5 and Model 6b

The validation of all ANSYS acoustic models was completed by comparing the results of these models with those of the Matlab scripts described in Appendix F. These scripts make use of a 1-Dimensional, theoretical model of the combustor that relies on the 4-pole transfer matrix method described in (Howard & Cazzolato, 2014) and (Singh, et al., 2008). These matrices and their derivations are discussed in detail in Appendix E.

Models 1, 2, and 5 were of a similar method, with an acoustic model from the ANSYS program being compared with that of a Matlab script, the models differing only in geometry.

Models 3 and 4 were conducted in ANSYS CFX and model the flow and combustion in the combustor. The purpose of these models was to provide the temperature profiles used in Models 6 and 7. Additional outputs of these models were the velocity profiles and Mach numbers of the flow through the combustor. These were used to justify the use of the finite element method in modelling the acoustics within a combustor, as explained in Sections 4.3 and 4.4 of this report.

Models 6 and 7 follow a similar method to 1, 2 and 5, but with the addition of a varying temperature in the liner portion of the combustor assembly. This temperature profile is, at first, a linear gradient from the maximum flame temperature to the exit temperature. For the second part of Models 6 and 7, the temperature was made to vary in accordance with the results of the simulations in Model 4.

To attempt to produce an acoustic model of a geometry that was representative of the geometry and operating conditions of a gas turbine combustor in one step would have had too many areas of uncertainty. Specific areas of uncertainty were in how to apply the variable temperature gradient to both the ANSYS Models and Matlab scripts, the suitability of using a 1-Dimensional acoustic model of the complex duct representation of the combustor and of the neglect of the effects of mean flow on the model.

The stepwise approach that was followed allowed for the verification and validation of the simpler models before extending their complexity to address each area of uncertainty. This increase in complexity built up to the final model (Model 7) that achieves the goals of producing acoustic and 1-dimensional models of the combustor with a typical temperature field. This temperature field is obtained from the results of Models 3 and 4, which produce the CFD model that illustrates the temperature and velocity profiles within a gas turbine combustor.

3.1. Geometry

The model of the combustor was based on that of the Bristol Proteus gas turbine in the North West Engineering Building at the University of the Witwatersrand (Figure 9). The reasons for basing the models on this particular design were its simplicity and the fact that there was access to an actual combustor. The data on the performance of the engine from its manual were used for the validation of Models 3 and 4. The age of the engine, built in 1954, meant that it was possible to make use of the design for this work without having to seek permission of the manufacturer.

The design of the engine and combustor are described in detail in Appendix B. The combustor was removed from the engine to provide the dimensions used in the remainder of the project.



Figure 9: Proteus Gas Turbine Engine with combustor visible

The interior of the combustor was examined and the soot patterns observed as a means of confirming the flow patterns found in the CFD models, these patterns are examined in detail in Appendix B by looking at photographs of the areas around the holes of the liner and the areas adjacent to the swirler blades. From these photographs, a strong radial component of the flow from the swirler is visible. The holes of the liner may be seen to have a lip that causes the flow of air to be angled slightly into the flow of the combustion gases. The measurements of the dimensions of this combustor were used to create a 3-D model in Solid Works CAD software. This model was then exported to the design modeller in ANSYS workbench. The model of the complete combustor assembly is shown in Figure 10. While still too complex to be used as the geometry on which to base a mesh for any of the numerical models, it does serve as a useful aid to the visualisation of the equipment being investigated and provides the bulk dimensions and properties used to define all geometries.

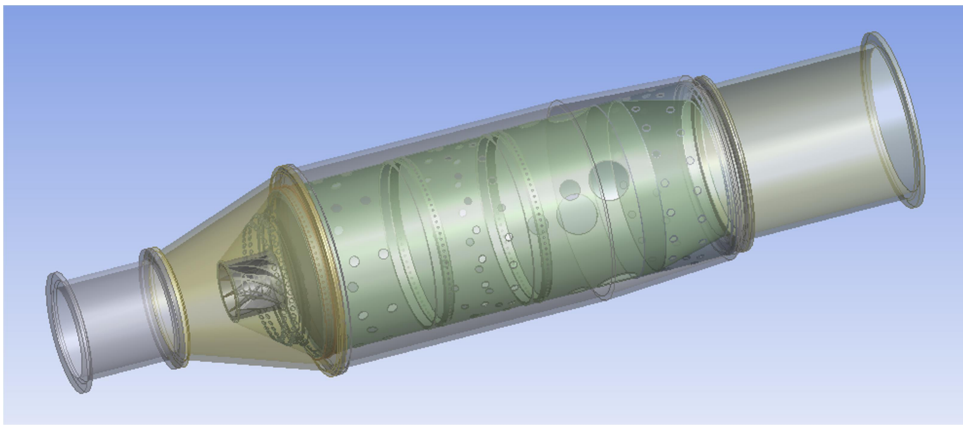


Figure 10: 3D model of full combustor assembly

3.2. Model 1

The purpose of Model 1 is, primarily, to confirm the validity of the method used in (Howard & Cazzolato, 2014). A model was produced in the ANSYS Acoustic ACT extension, with its dimensions based on those of the Proteus combustor. A harmonic analysis was conducted to produce the acoustic pressures, velocities and Sound Pressure Levels (SPLs) along the duct.

The results of the ANSYS Acoustic model were exported to, and stored in, an excel spreadsheet. A Matlab script then calculated the theoretical 1-dimensional results of these acoustic properties. These results were plotted in the Matlab script against those stored in the spreadsheet from the ANSYS Acoustic model.

The acoustic models were produced in ANSYS Mechanical, using the acoustic workbench ACT extension, as a Finite Element model and validated against the results of a 1 dimensional analytical calculation in Matlab. The geometry of Model 1 consists of a simple duct, as found in (Howard & Cazzolato, 2014) and is shown in Figure 11.

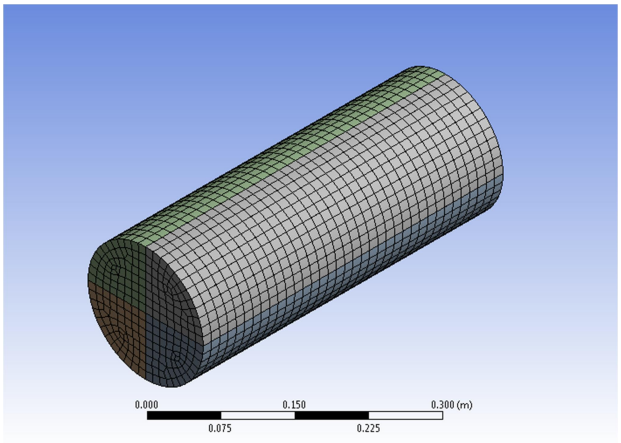


Figure 11: Mesh and geometry of Model 1 (24epw)

The Matlab script, based on that developed in Howard & Cazzolato (2014) was used to validate the acoustic model. A 4 pole transfer matrix was used to calculate the acoustic pressure and velocity along the axis of a duct by dividing it into multiple "slices" and treating these as the ends of successive ducts. The script was verified by comparing the results of the calculations from the final "slice" with the expected results at the end of the duct, using the transfer matrix across the length of the duct.

When using the transfer matrices to calculate the acoustic properties along the axis of the model, it is important to note that the direction of travel along the axis and the nomenclature of the boundary conditions is extremely important. If the direction of travel gets muddled or the inlet and outlet of the duct swapped around, the results of the calculated pressure values will be inverted about the axis (i.e. multiplied by-1). For details on the matrices that bring about this effect, see Appendix E.

The Sound Pressure Level (SPL) was calculated using Equation 7 (Howard & Cazzolato, 2014). The $\sqrt{2}$ in the denominator results in the peak SPL being calculated instead of the RMS value. This was necessary in order to agree with the results produced in the ANSYS program (Howard & Cazzolato, 2014):

$$\mathbf{SPL} = \mathbf{20}\,\mathbf{log_{10}}\frac{\mathbf{P_x'}}{(\sqrt{\mathbf{2}})(\mathbf{20}\times\mathbf{10^{-6}})} \qquad 8$$

In order for the one dimensional equations used to construct the theoretical models in Matlab to be valid, it was necessary to make the assumptions that the acoustic pressures and velocity in the duct will propagate in the form of planar waves along

the axis of the duct. The maximum theoretical frequency at which this will occur ($\boldsymbol{f_c}$) is obtained from Equation 8 (Singh, et al., 2008):

$$\boldsymbol{f_c = \frac{1.8412 C_0}{2\pi a}} \quad 9$$

Where $\boldsymbol{C_0}$ is the speed of sound of the fluid in the duct and $\boldsymbol{a}$ is its characteristic dimension (diameter)

For the geometry of the combustor, at room temperature, the cut on frequency, up to which the plane wave assumption is valid, is 1218Hz. From this, a maximum frequency of interest for this project was selected to be 1200Hz. The cut-on frequency is defined as the frequency below which only plane waves propagate inside the duct (Howard & Cazzolato, 2014).Note that any increase in temperature of the air within the combustor will lead to a higher value of $\boldsymbol{C_0}$ in Equation 8 and, therefore, a higher cut-on frequency. The use of 1200Hz as the maximum frequency of interest is reasonable in the context of the noise generated by gas turbine combustors, which typically occurs in the 500-800Hz range.

Model 1 was used to confirm this plane wave assumption by examining the mode shapes of the ANSYS Acoustic model and comparing them to the behaviour predicted by the theory. A modal analysis of the model was conducted, using this function in the ANSYS Acoustic ACT extension.

The mesh size for the liner was determined by comparing the results of the SPL along the axis of ANSYS Acoustic models of different mesh configurations with that of the analytical model. These mesh configurations consist of different element types and sizes.

The minimum effective element size to be used in the acoustic meshes of ANSYS Acoustic is 6 elements per wavelength for FLUID220 elements and 12 elements per wavelength for FLUID30 elements (Howard & Cazzolato, 2014). The reason for the different requirements is the higher number of nodes of the FLUID220 elements, which have nodes at the midpoints of each of their vertices, as shown in Figure 12.

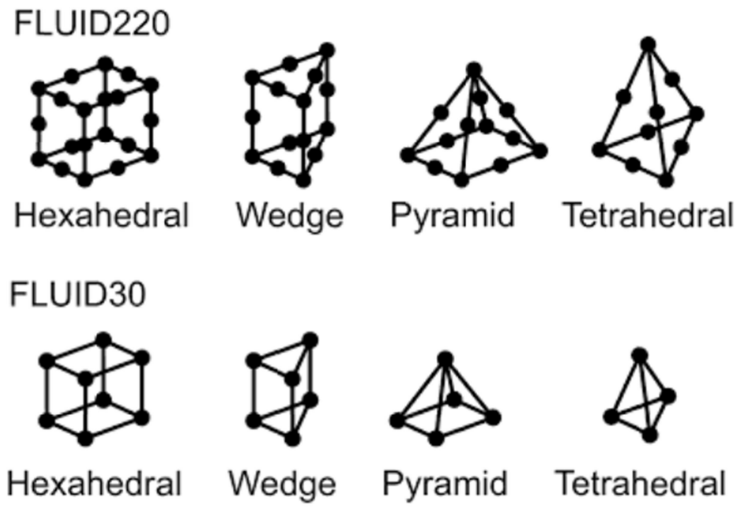


Figure 12: Comparison of FLUID220 and FLUID30 elements used in ANSYS Acoustic ACT (Howard & Cazzolato, 2014)

The wavelength (λ) under investigation was determined by the ratio of the speed of sound in the medium and the frequency (f) of the wave:

$$\lambda = \frac{c_0}{f} \tag{10}$$

The size of the elements used in the mesh were described in terms of the number of elements per wavelength (epw), in order to get a sense of the suitability of the element size for the investigation:

$$epw = \frac{\lambda}{l_{element}} \tag{11}$$

Model 1 was used to confirm the methods used in (Howard & Cazzolato, 2014), upon which later models were based. The plane wave assumption was confirmed up to a maximum frequency of 1200Hz and a mesh configuration for the ANSYS Acoustic models was determined based on this frequency. With the mesh and frequencies of interest determined, and the methods confirmed and practiced with a simple duct, the geometry could now be expanded to that of Models 2 and 5, which are a closer representation of that of the Proteus combustor.

3.3. Models 2 & 5

In Model 2, the geometry of Model 1 is expanded to that of the composite duct shown in Figure 13. This composite duct was based on the dimensions of the diffuser, swirler and liner of the Proteus combustor. The purpose of Models 2 and 5 was to confirm that the methods used in Model 1 were applicable to a composite duct, as used in (Huls, 2006).

The geometries of models 2 and 5 were very similar, both consisting of several ducts of different dimensions. The difference being that Model 5 includes an additional duct downstream of the liner (Figure 14). The form of both of these geometries is similar to that of the theoretical model described in (A. P. Dowling, 2003) and (Boudier, 2007). These geometries may be used for further development of models that include a source term for the sound produced by the flame, as in (Polifke, et al., 2001). This source term is not included in this project, with a simple acoustic velocity excitation used in its place.

The acoustic velocity for the excitation of the acoustic and theoretical models was kept at the value of $1m.s^{-1}$ used in (Howard & Cazzolato, 2014). With no flame source term being used in this project, the excitation term needed to be an arbitrary value and there was no compelling reason to deviate from that of the original. Coincidentally, the maximum SPL of Model 7 is 153dB, which is very close to the maximum SPL of 154dB measured in the experimental gas turbine described in (Bake, et al., 2005).

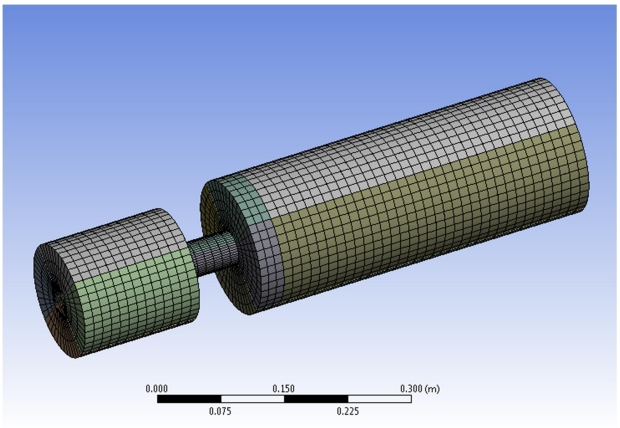


Figure 13: Model 2 geometry and mesh

As with Model 1, a harmonic analysis was conducted of the ANSYS Acoustic model to obtain the acoustic pressures, velocities and SPLs along its axis. These values

were exported to a spreadsheet and compared with the results of a 1 dimensional calculation produced by a Matlab script.

The values at the intersection between these composite ducts were calculated and used to verify the values that were later calculated along the axis of the entire model. The values at point -2(defined in Figure 14) were used to determine the pressure at point 1, which was taken as the source of the sound propagating through the duct. For the interfaces between these ducts, use was made of the continuity of acoustic mass flow and pressure across the interface.

Point 1 is located in line with the first primary air injection holes of the combustor, which corresponds to the region where the majority of combustion occurs. The origin of the coordinate system is at point 1, as with the ANSYS acoustic models.

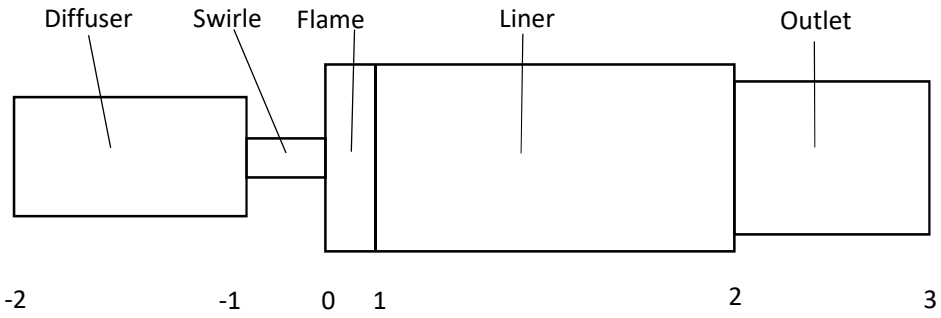


Figure 14: Sections and endpoints of Model 5

To calculate the values of the acoustic pressures ($\mathbf{P}'_{\mathbf{x}}$) and mass flow rates ($\boldsymbol{m}'_{\mathbf{x}}$) at the points shown in Figure 14, a four pole transfer matrix is defined for each section; the Liner ($[\boldsymbol{T_L}]$), Flame Zone ($[\boldsymbol{T_{FZ}}]$), Swirler ($[\boldsymbol{T_S}]$) and Diffuser ($[\boldsymbol{T_D}]$):

$$\begin{pmatrix} \mathbf{P}'_2 \\ \boldsymbol{m}'_2 \end{pmatrix} = [\boldsymbol{T_L}] \begin{pmatrix} \mathbf{P}'_1 \\ \boldsymbol{m}'_1 \end{pmatrix} \quad 12$$

$$\begin{pmatrix} \mathbf{P}'_1 \\ \boldsymbol{m}'_1 \end{pmatrix} = [\boldsymbol{T_{FZ}}] \begin{pmatrix} \mathbf{P}'_0 \\ \boldsymbol{m}'_0 \end{pmatrix} \quad 13$$

$$\begin{pmatrix} \mathbf{P}'_0 \\ \boldsymbol{m}'_0 \end{pmatrix} = [\boldsymbol{T_S}] \begin{pmatrix} \mathbf{P}'_{-1} \\ \boldsymbol{m}'_{-1} \end{pmatrix} \quad 14$$

$$\begin{pmatrix} \mathbf{P}'_{-1} \\ \boldsymbol{m}'_{-1} \end{pmatrix} = [\boldsymbol{T_D}] \begin{pmatrix} \mathbf{P}'_{-2} \\ \boldsymbol{m}'_{-2} \end{pmatrix} \quad 15$$

These transfer matrices are derived and explained in detail in Appendix E of this report. Combining Equations 12, 13 and 14 gives:

$$\begin{pmatrix} \mathbf{P}_1' \\ \boldsymbol{m}_1' \end{pmatrix} = [\boldsymbol{T_{FZ}}][\boldsymbol{T_S}][\boldsymbol{T_D}] \begin{pmatrix} \mathbf{P}_{-2}' \\ \boldsymbol{m}_{-2}' \end{pmatrix} \quad 16$$

With m_1' used as the excitation and m_{-2}' assumed to be 0 due to the choked inlet conditions of the diffuser, P_1' may be found. P_1', and m_1' may now be used as a starting point for the calculations done along the duct in either direction, using the method employed in Model 1. For all scripts, the excitation was set in terms of the acoustic velocity, to match the format used in the ANSYS models, and converted to acoustic mass flow rate in the script.

The values of the imaginary and real components of the Acoustic pressure and velocity, along with the SPL, along the axis ANSYS acoustic models described here were exported to Excel spreadsheets, using the export results function of ANSYS Mechanical. While this did not cause any difficulty for the simple geometries of Models 1 and 6, the models with multiple sections did have some complications.

When the results of the FEA models were exported to the spreadsheet, they were listed in order of node number. It may be seen from Figure 15 that, for the case of the composite section models, these nodes were not numbered in sequence along the axis of the model, meaning that the results exported to the spreadsheet require some manipulation to get them into the desired order for them to be compared to those of the theoretical models.

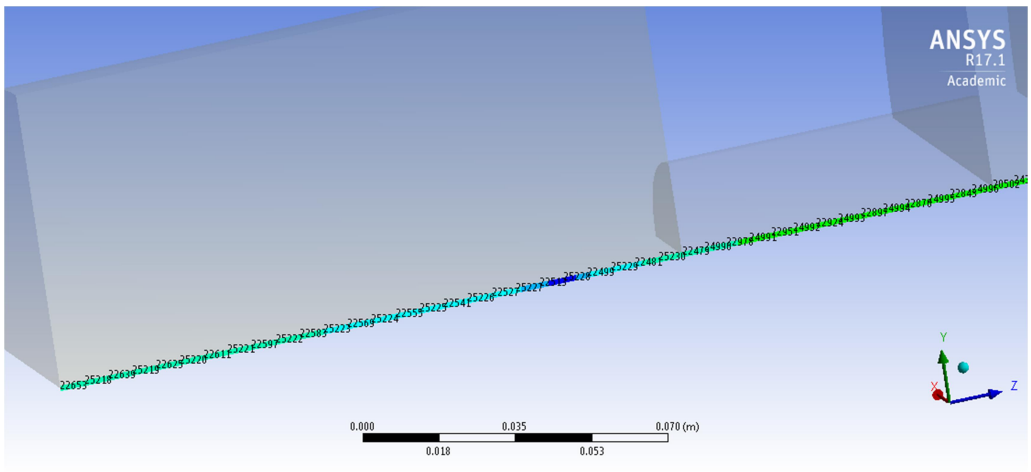


Figure 15: Nodes along axis of ANSYS Model

The position of each node along the axis was manually entered into a spreadsheet that contained the nodes in the order in which they were exported from ANSYS. This column was then copied to the spreadsheets that contained the calculated values in their exported order. The column with the node order was then sorted from smallest to largest (using the standard excel function for this task and expanding the selection to include all adjacent columns), placing the calculated values in the correct order.

Once the values of the acoustic pressures, velocities and SPLs were placed in the correct order, the results for each model were collected into one spreadsheet and saved in the working directory of the relevant MATLAB script. The Z-coordinate values were included in this spreadsheet by using the constant size of the elements as the step size along the axis.

With the validity of the composite ducts in ANSYS Acoustic and Matlab confirmed, these models were extended to include variations in temperature in the liner in later models. Before this could be done, it was necessary to obtain a temperature profile to represent that of the Proteus combustor. The CFD simulations of Models 3 and 4 were produced to obtain this profile.

3.4. Models 3 & 4

The purpose of Models 3 and 4 was to obtain a temperature field of a typical combustor that may be used in the ANSYS Acoustic models of this project. Model 3 provides the input velocities for the simplified geometry of Model 4, which includes the combustion process and provides the final temperature field.

The geometry of Figure 10 was used in creating the mesh for Model 3 in ANSYS ICEM as part of an ANSYS workbench project. This geometry includes the combustor liner, swirler, diffuser and casing. The small gap between the combustor casing and liner, along with the thin walls of the liner itself made the correct sizing of the mesh in these regions especially crucial.

In order to reduce the complexity of the geometry and associated mesh, the cooling film holes and secondary air holes were not included in this model. The complexity of certain areas of the geometry (specifically, the blades of the swirler, edges of the air holes and cooling ridges) necessitates the use of a tetrahedral mesh. After generating these elements, the quality of the mesh was measured and several iterations of refinement completed in ICEM. The sizes of the elements around the liner holes and swirler blades were also reduced in order to eliminate any

discontinuities in the mesh. The mesh quality was further improved by filling the interior of the liner with hexagonal mesh elements (shown in Figure 16), creating a more uniform pattern and improving the aspect ratio quality.

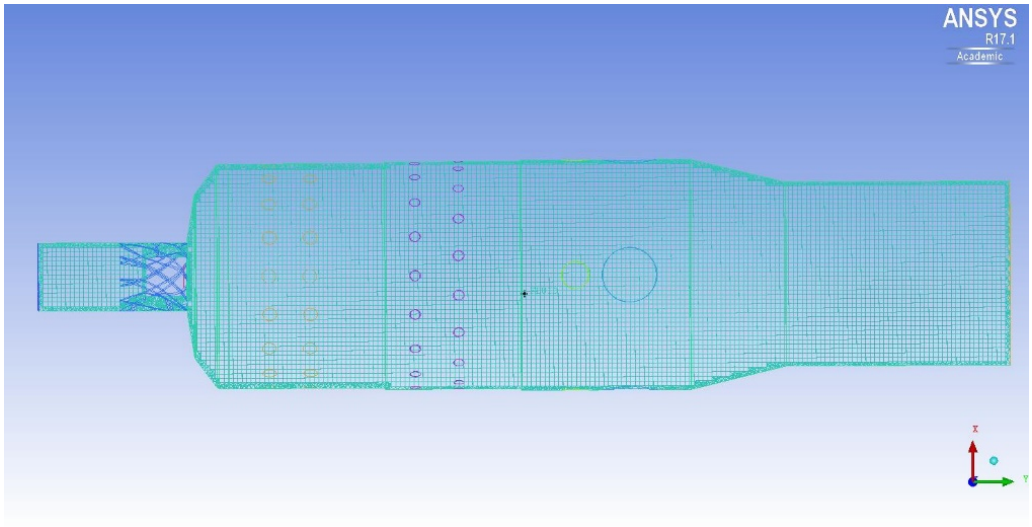


Figure 16: Cross section of mesh used in Model 4 (note the use of hex mesh in interior)

Once the mesh was developed and smoothed, it was exported to ANSYS CFX-Pre (Figure 17) to set up the boundary conditions for the calculations. The surface at the inlet to the diffuser set as an inlet with a normal velocity of $85\mathrm{m.s^{-1}}$, as per the information in the Proteus engine's manual. The outlet from the combustor, was set to a standard atmospheric pressure of 101kPa. The inlet and outlet of the model are visible from the arrows in Figure 17.

For both Model 3 and Model 4, all walls were set to the "no slip" condition, with the wall velocities set to $0m.s^{-1}$.The outlet of the model was set as an outlet with a reference pressure of $0\mathrm{kPa}$. The standard $k-\varepsilon$ turbulence model was used, which is sufficient for the general nature of the results to be obtained from this simulation. This turbulence model uses the scaleable wall model, which enables solutions of arbitrarily fine near wall grids (ANSYS, 2013). The turbulence intensity of the inlet is kept at the default value of 0.037, which is considered to be a reasonable value for a circular duct in the absence of experimental data (ANSYS, 2013).

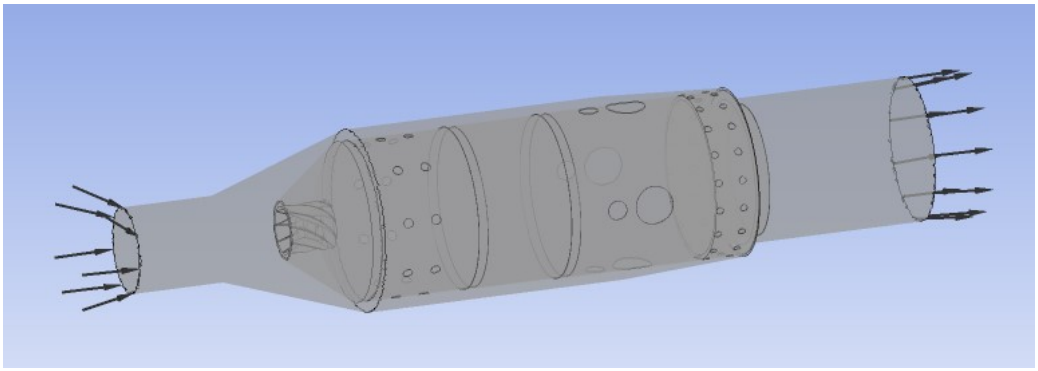


Figure 17: Boundary conditions in CFX Pre for Model 3

For Model 3, simulations of the flow through the combustor were run in ANSYS CFX without any combustion taking place. The mass flow rates of the inlet and outlet were compared as a means of verifying the model. The penetration of the jets from the liner holes and the shape of the flow in the combustion zone were compared with that predicted by the design principles described in (Lefebvre & Ballal, 2010) as a means of verifying the model.

The results of this simulation were used as the inputs for a further simulation with a simplified geometry (Model 4), where the diffuser and casing were removed. The turbulence intensities at these inlets were maintained at the standard value of 0.037, as in Model 3.

In this simulation, the chemical reaction of the fuel with the air was introduced to replicate the combustion process. This combustion process was set up in accordance with the best practices for the modelling of the combustion within a gas turbine combustor as described in Chapter 8 of the ANSYS CFX Reference guide (ANSYS, 2013). The combustion model used for these simulations was the laminar flamlet model, which is more suitable for a non-premixed flame. If a premixed design had been used as the basis of the simulation, an Eddy Dissipation Model (EDM) would have been more appropriate.

The geometry of the final simulation as displayed in CFX Pre, with inlets and outlets included, is shown in Figure 18. A typical set of values at these inlets is shown in Table 3 in section 4.4. As with Model 3, the results of this simulation were verified by comparing the mass flow rates at the inlets and outlet. Verification of the model was done by comparing the values to the temperatures and velocities with those of the theory in (Lefebvre & Ballal, 2010) and those of the Proteus manual of (Siddeley, 1961).

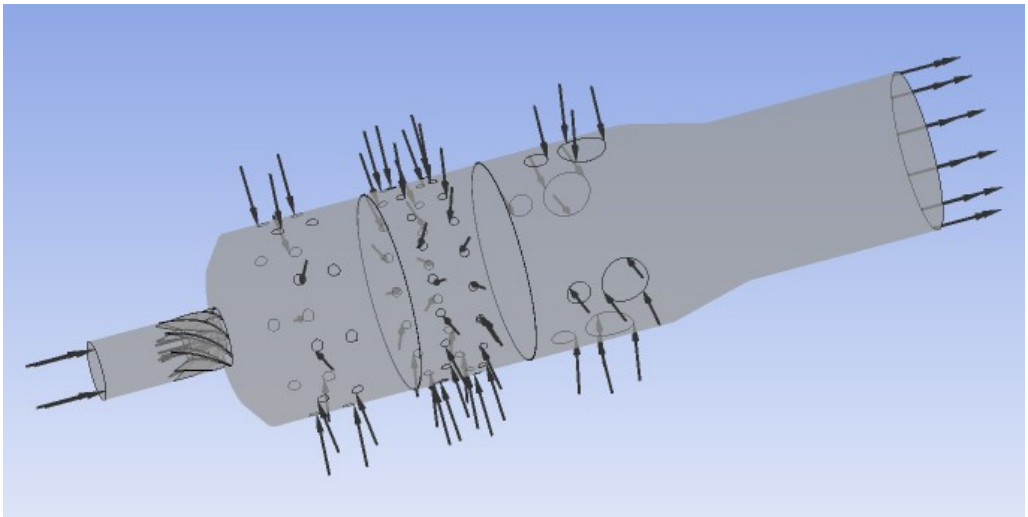


Figure 18: Mesh and Boundaries of CFX simulation for Model 4

The chemical reaction between the fuel and air was based on the input conditions of the Combustor tutorial in (ANSYS, 2013). A PDF flamelet model was used in accordance with the suggested practice of combustion modelling in (ANSYS, 2013). The fuel used for the simulation was methane, which necessitated a particularly high velocity through the nozzle modelled on that of the Proteus in order to get a realistic simulation of the flame for the mass flow rates of air in question. According to the manual, the fuel used in the Proteus combustor would have been JP4 or JP1. While the flame described in the manual, and used to validate Model 4, would have been based on these fuels. The modelling of the combustion of methane is far simpler than that of the liquid aviation fuels mentioned above as it does not have to account for the injection and subsequent vaporisation of the liquid. The reduction in the model's complexity and computational effort required were felt to outweigh the loss in accuracy of the detailed behaviour of the flame as this behaviour was not the focus of the project.

With future work likely to focus on the flames produced in Lean Premixed Pre-vaporised (LPP) combustors, the modelling of a liquid fuel would have been of limited value. Additionally, Methane is a common source of fuel in combustor test rigs such as that used in (Dowling & Stow, 2003) and (Pożarlik, 2010). Any future work done, that makes use of an experimental model for validation, is therefore likely to make use of Methane as the fuel.

A second run of the model was completed, using lower flow rates for both the inlet air and the fuel. These flow rates were similar to those of the experimental rigs cited above. While the first run of the model increased the flow of methane fuel to match

the airflow of the combustor, the second run decreased the flow of air to match the rate and type of fuel likely to be used in a test rig. A comparison of the two runs may be seen in Appendix C, with the temperature fields produced being very similar. The results of the second, slow run were used as the basis of the temperature profile for Models 6 and 7.

One of the limitations of using the Finite Element Method in modelling the acoustics of the combustor in ANSYS Acoustic ACT is that it is not able to account for the effects of mean flow. To determine the effect of this limitation, the Mach number of the flow through the combustor was examined. Flows with Mach numbers below 0.3 may be treated as incompressible, which allows the effects of mean flow to be neglected in an acoustic analysis (Hirschberg & Rienstra, 2004).

In order to make use of this temperature field in the Acoustic models, it must be mapped from ANSYS CFX to an equivalent model in ANSYS mechanical.

Instead of exporting the entire temperature field, several planes (shown in Figure 19) were created at various points of interest; such as at the axis of each set of liner holes, where the temperature could be expected to make any significant changes.

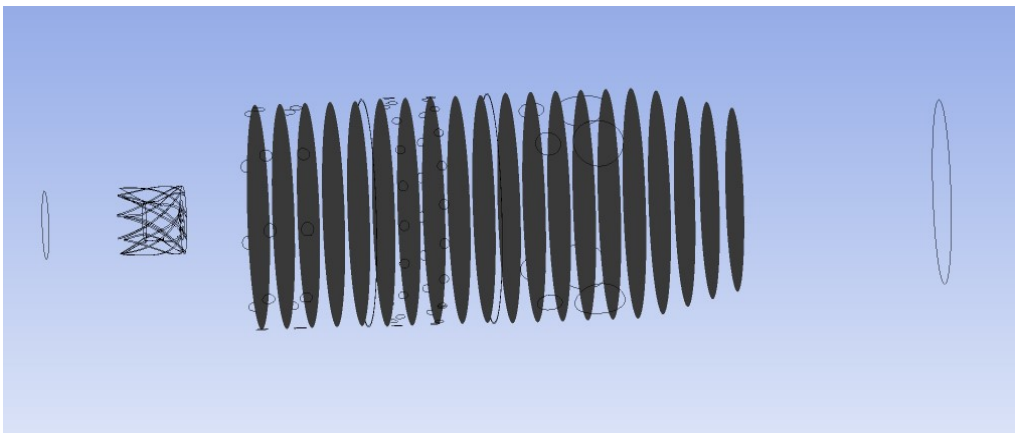


Figure 19: Planes for sampling temperatures through fired combustor

The average temperature at each of the planes in Figure 19 was calculated in CFX post and the results used to provide the temperature profiles for Model 6 and Model 7. This resultant temperature profile was now 1-dimensional, along the axis, allowing for its use in the theoretical models that provide a source of validation for the ANSYS Acoustic models. The trade-off for the use of this simplified profile is the loss of precision of the resulting acoustic models that do not include the circumferential and radial variations of temperature.

The aim of the simulations in CFX was to get an indication of the type of temperature profile that could be expected through the combustor, which may then be used in the later ANSYS Acoustic models. The results of this simulation were verified by comparing the mass flows in and out of the model. With no experimental rig available for validation, the results were validated by comparing the flow patterns with that predicted by the theory in (Boyce, 2012) and (Lefebvre & Ballal, 2010), by comparing the values of the physical characteristics of the flow (such as velocity, temperature and Mach number) with those of the Proteus Engine manual (Siddeley, 1961) and through inspection of the soot patterns of the actual combustor depicted in Appendix B.

3.5. Models 6 & 7

The geometry and mesh from Model 1 were used to create Model 6. In this model, the temperature is made to vary, first linearly in the manner described in (Howard & Cazzolato, 2014), and then to fluctuate in accordance with the temperatures obtained from Model 4 (See Appendix C – ANSYS CFX models). The temperature field was generated in the FEA model by running a thermal analysis in ANSYS mechanical, with the resulting temperatures mapped to the elements of the acoustic model. These temperatures alter the density and speed of sound accordingly throughout the model. The thermal profile of the linear case was produced by applying a temperature to the planes at either end of the cylinder.

With the material properties of the model suitably altered, a harmonic analysis was conducted with an excitation of $1\mathrm{m.s^{-1}}$ for the frequency of $600\mathrm{Hz}$. The results of this analysis were checked against those of the equivalent theoretical model developed in Matlab and described in Appendix F.

In Model 6, as with Model 1, the Matlab script was based on that described in (Howard & Cazzolato, 2014), which makes use of the special transfer matrix derived by Howard (2013) for a duct with a linear temperature variation. The terms of this matrix are detailed in Appendix E.

With the calculations of the linear temperature gradient completed and the implementation of Howard and Cazzolato (2014) verified, the more complex temperature field was introduced to the model. The temperatures obtained in Model 4 were used as the individual values of temperature along the axis of the theoretical model in MATLAB and the results calculated using the same transfer matrix as the

first version of Model 6, with the calculations being performed on a series of ducts of the same diameter.

In order to produce the varying temperature field in the ANSYS Acoustic model, the previous mesh was modified to insert the planes of different temperatures in Figure 20. These planes are at the same points as those in Figure 19 and make use of the average temperatures of the planes in Model 4. The temperature is assumed to vary linearly between each plane.

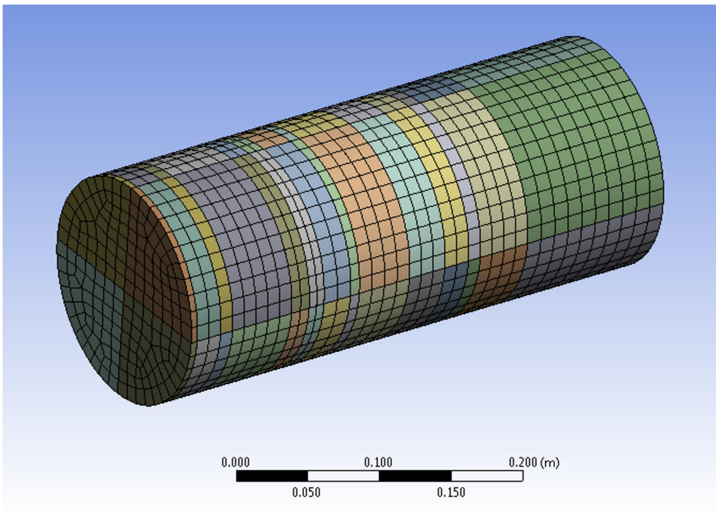


Figure 20: Mesh of Model 6b, with multiple planes for the various temperatures

The steady state thermal analysis was performed as before to change the acoustic properties of the model. These modified material properties of the model were used to perform a harmonic analysis of Model 6 at $600\mathrm{Hz}$, with an excitation of $1\mathrm{m.s}^{-1}$.

The purpose of Model 6 was to validate the method of importing the temperatures from Model 4 to conduct a thermal analysis on the solid model and then converting back to acoustic elements. The alternative transfer matrix was implemented and the results of the harmonic analyses by the two methods compared. With these tasks completed, the complexity of the geometry was increased to that of Model 7.

Model 7 was produced by combining the geometry of Model 5 with the procedure of Model 6. The diameter of the outlet was increased to that of the liner, to reduce the effect of any discontinuities on the model, with the geometry and mesh used illustrated in Figure 21.

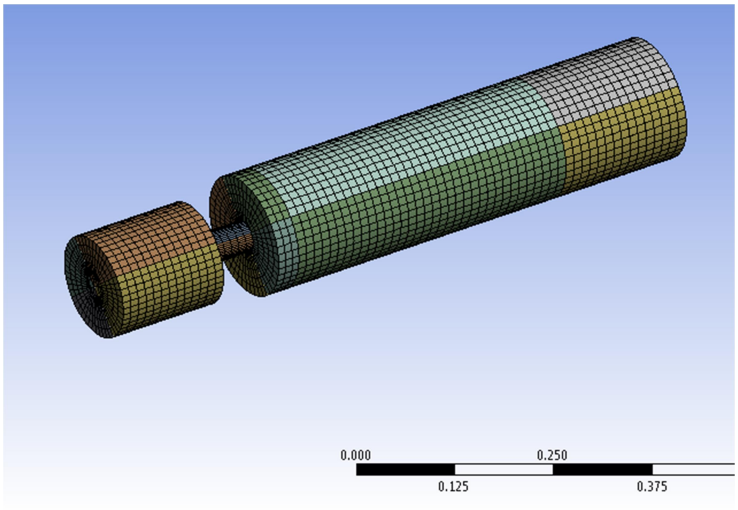


Figure 21: Geometry and Mesh of Model 7

As in Model 6, the temperature in the liner was first made to vary linearly through a thermal analysis in ANSYS Mechanical. The new material properties were then used in the model to complete a harmonic analysis and the results validated by comparing them with those of an equivalent Matlab model.

With the mesh and geometry of Model 7 validated, the temperature was made to vary in accordance with the results of Model 4, using the same procedure as Model 6. The values of the varying temperature field from Model 4 and used in Model 6b were applied to the planes shown in Figure 22. With these temperatures applied, a thermal analysis of the model was completed in ANSYS Mechanical, using the procedure from (Howard & Cazzolato, 2014) to import the temperature profile back into the acoustic model.

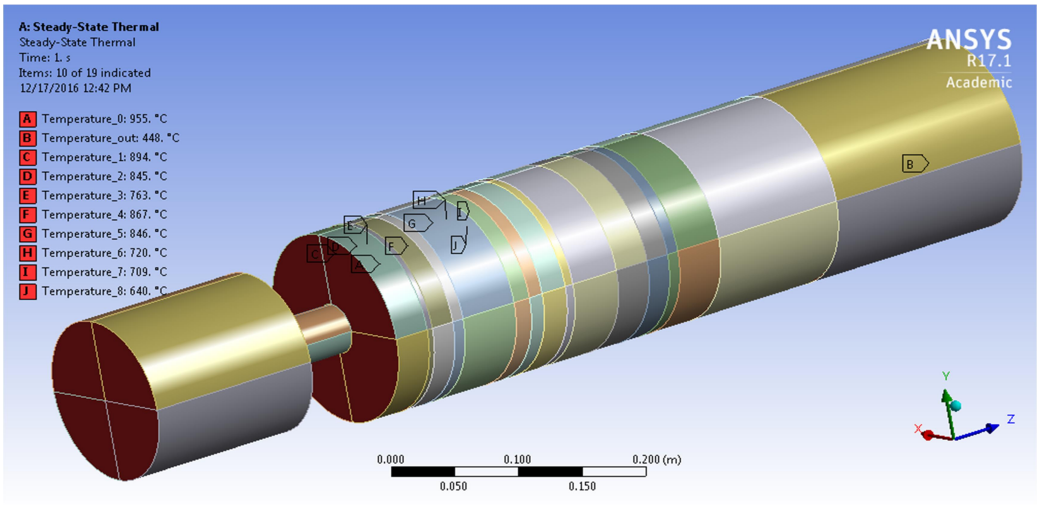


Figure 22: Temperature inputs for variable temperature field of Model 7

In the final version of Model 7, the propagation of an acoustic wave through a duct of varying temperature was simulated. The wave was generated by a source within the duct, at the location where the flame within a gas turbine combustor occurs.

3.6. Equipment used

All programs and simulations were run on a workstation. The workstation had 2 x Intel(R) Xeon(R) CPU ES520 4 core processors, running at 2.27GHz, with 16GB of Ram and a 500GB hard drive. A windows 7 x64 server was set up on this hardware and used to install the ANSYS 17.1, Matlab, Solid Edge and Microsoft office packages that were used to run the simulations. This combination of hardware and software was found to be more than adequate for the purposes of this project and remains in place for future work.

In order to gain proficiency with the ANSYS and Solid Edge programs, the series of introductory tutorials for each were run through and the lessons learnt there used in the creation of the models used in the project. In the case of the use of ANSYS and Matlab to conduct an acoustic analysis of the simplified combustor, the exercises in (Howard & Cazzolato, 2014) were used as a base. For the analysis of the combustor in CFX, the combustor tutorial in (ANSYS, 2013) was used as the basis of setting up the chemical reaction for the combustion.

All results and progress were regularly backed up to two portable 1TB drives, kept at separate physical locations. Regular backups of all written work were also made to the School of Mechanical, Industrial and Aeronautical Engineering's server.

3.7. Assumptions and Limitations

In order for the theoretical models used in Matlab to be valid, it was necessary to assume that the acoustic waves propagating through the liner do so in a planar manner along the axis of the duct. As described in section 3.2, the cut off frequency, above which this assumption is no longer valid, is 1218Hz. For this reason, the maximum frequency of interest was taken as being 1200Hz, with the size of the acoustic mesh based on this limit. Restricting the analysed frequency to a maximum of 1200Hz was considered to be acceptable for this field of study when one considers that combustor "growl" typically occurs in the range between $200 - 500\text{Hz}$ (Lefebvre, 2010).

While a full spectral analysis would have been interesting to complete in the acoustic models, with the option readily available in the ANSYS Acoustic package

used, it was felt that a more effective use of the time available for this project was to conduct a harmonic analysis at a specific frequency under increasingly complex conditions. The frequency selected to be used was based on the assumption that the majority of combustor noise occurs at or below this frequency (Kok, et al., 2010).

A requirement for the use of the finite element method in conducting an acoustic analysis was for the mean flow through the combustor to be neglected. This assumption is only valid for low Mach numbers (A. P. Dowling, 2003). The Mach numbers through the simulations of both Model 3 and Model 4 were examined and found to be well below 0.3 in all cases due to the high temperatures within the combustor and the associated high speeds of sound of the gas. These Mach numbers were considered to be low enough to justify the assumption of incompressible flow, which in turn allow for the assumption that the effects of the mean flow on the propagation of the acoustic waves in the combustor may be ignored. As such, this assumption should not have a noticeable effect on the accuracy of the results of the acoustic models produced in this project.

The geometry used for the harmonic analysis in both ANSYS and Matlab has several simplifications that would cause the results of this analysis to differ from what would be expected to occur in the actual Proteus combustor. Chief amongst these were the lack of any perforations in the acoustic models. The primary, secondary and dilution holes of the liner would be expected to have a significant effect on its acoustic properties. The jets emanating from these holes would also have to be considered as additional sources of aero-acoustic noise. While this would be a significant limitation of these models if the intention were to predict the acoustic behaviour of a traditional combustor, an analysis of an LPP combustor could still be conducted with this limitation as this design makes use of far fewer perforations.

The geometry of the swirler in the acoustic models does not include the blades, with the area of the duct taken as that of the area between the blades of the actual swirler. The impedance of this section of the combustor assembly would be far greater in the actual combustor.

The geometry of the swirler in the 3D cad model and, therefore, of Models 3 and 4, was also simplified, with the vanes being modelled as straight, rather than the curved profile of the actual combustor. This is not an oversimplification as swirlers may be designed with straight vanes in practice. The difference in the performance

of straight and curved swirler vanes is described in (Lefebvre & Ballal, 2010) as the straight vanes producing a less efficient, but more stable flow (while having the advantage of being simpler and cheaper to produce).

The geometry of the liner was simplified in Models 3 and 4 to not include the cooling holes or secondary holes in order to reduce the complexity of the mesh. The temperature and velocity fields produced by these models will therefore not be an exact representation of the behaviour within the actual Proteus combustor. It was felt that the general nature of the required results did not warrant the increased complexity of including these holes.

The simple turbulence model used in Models 3 and 4 is adequate for the purpose of determining the general temperature and flow fields. If a more detailed analysis is required, a more advance turbulence model would need to be employed. Aspects of the flow that have not been considered due to the level of precision of the flow field include the additional turbulence and vorticity due to vortex shedding of the swirler blades. The $k-\varepsilon$ model is not well suited to the highly rotational flow that is found in the combustion zone (ANSYS, 2013) and a different model would need to be employed for a detailed analysis of the flame.

The design and geometry of the injector in the CFX simulations of Models 3 and 4 was greatly simplified to decrease the complexity of the mesh. The fuel used was taken to be methane gas, instead of the Jet A1 that would be used in the actual engine. This was done both to simplify the CFX computations and as it is likely to be the fuel used in any future test rigs used for experimental validation (as has been used in (Huls, 2006) (Pożarlik, 2010) and (A. P. Dowling, 2003)).

With the exact behaviour of the flame not possible to verify without a test rig, it was felt to be prudent to leave the development of a thermo-acoustic source term for a later project that would have a means of experimental validation. With this in mind, the acoustic excitation was taken to be a 1-Dimensional value of $1m.s^{-1}$ along the axis in all cases for the sake of simplicity.

The inlet to the combustor is assumed to be closed, an assumption which is used in (A. P. Dowling, 2003) and (Huls, 2006) due to the choked state of the flow exiting the compressor making this a reasonable assumption. The geometry of the diffuser itself is greatly simplified in both the CFD and acoustic analysis. In the case of the CFD simulations, the diffuser is modelled as a straight cone, while the real geometry is more of a curved shape. In the ANSYS Acoustic models, the diffuser is

modelled as a straight duct, with no change in area. The simplification in the case of the CFD model is in order to reduce the complexity of the mesh involved, while that of the acoustic model was necessary in order for the 1-Dimensional model to be able to be used for verification purposes.

No modelling has been conducted of the cooling film in the liner, which affects both the temperature of the liner and damps out the acoustic loads experienced by the liner (Polifke, et al., 2001). This would be a significant limitation for a model of the Proteus combustor, but less of an issue for a model of an LPP design which does not make use of these films. As no analysis of the Fluid Structure Interaction (FSI) between the combustion gases and liner was being conducted in this project, the effect of the cooling film on these results was assumed to be negligible.

The temperature profiles produced in Model 4 were sampled at several axial points of interest in the transverse plane at that point. The values of the temperatures on each of these planes was averaged and used as the input for the acoustic and theoretical models. This is a significant simplification as the temperature distribution is far from radially uniform in the combustor. The simplification was necessary in order to make use of the 1-dimensional models. Including the radial distribution in the acoustic models would have led to a more realistic representation of the Acoustic Field in the combustor.

Many of the limitations of the models produced in this project come about through the simplifications necessary for modelling the “burner” components (swirler, injector, acoustic source term from the flame). With the focus of this project on the propagation of the acoustic waves through the combustor, these limitations may be addressed when the model is extended to include a burner source term in the manner of (Dowling & Stow, 2003) (Polifke, et al., 2001).

The assumptions of neglecting the mean flow of the air in the combustor and the modelling of the acoustic wave as behaving in a purely planar fashion were found to be reasonable for the conditions experienced in the combustor.

4. Results

This section discusses the results obtained from the models described in Chapter 3 and listed in Table 1. The intention of this discussion is to give a sense of the progression through the project, culminating in a prediction of the Sound Pressure Level in an open, composite duct with a variable temperature profile. The assumptions upon which the use of the ANSYS Acoustic and 1-Dimensional models are based are validated in the course of the discussion

4.1. Model 1

In Model 1, a harmonic analysis of a simple duct was performed, following the procedure described in section 3.2. A simulation was conducted, using the ANSYS Acoustic FEA package, and the results of this simulation validated by comparing them with those of a theoretical calculation conducted in Matlab. The results for the SPL calculated in both the ANSYS Acoustic simulation and Matlab script are visible in Figure 23.

The Matlab script was verified by comparing the results of the calculations from the final “slice” with the expected results at the end of the duct, using the transfer matrix across the length of the duct. These values were found to agree for several input velocities and frequencies.

In order to determine the ideal mesh configuration for this geometry, multiple simulations were performed using different mesh configurations. These configurations were compared in Figure 23 to see where the best agreement may be found.

The size of the elements is given in terms of elements per wavelength at the maximum frequency of interest. This frequency is taken to be the cut-on frequency of the duct at room temperature, 1200Hz. The calculations themselves were conducted using a frequency of 600Hz, which the frequency used for all the models in this project. The reason for using 600Hz for the calculations was that it is within the range at which the highest degree of noise is produced in a typical gas turbine combustor (Duran, et al., 2014)

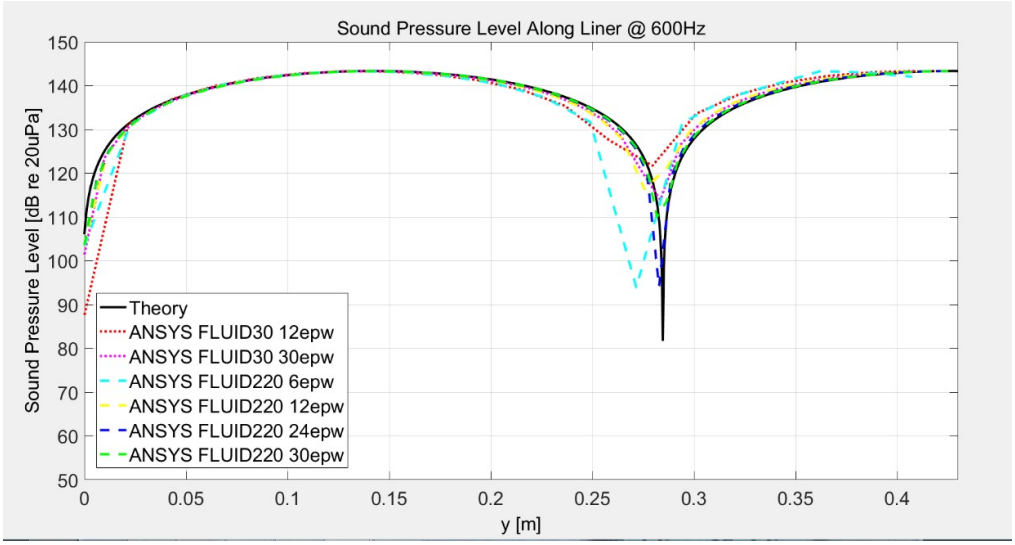


Figure 23: SPL for Model 1, theory vs ANSYS with multiple meshes used

The results from the meshes making use of FLUID30 elements were inferior to those making use of the more detailed FLUID220 elements. The final mesh selected for the model was comprised of FLUID220 elements at a size of 24 Elements per Wavelength at the maximum frequency of interest (1200Hz) at room temperature. Increasing the resolution of the mesh beyond this stage did not improve the level of agreement with the results from the theoretical model. With the emphasis of this project being on the development of the method, rather than the numerical values obtained, the 6epw mesh with FLUID220 elements did produce results of an acceptable accuracy for this simple geometry. The 24 epw mesh was selected as it is to be used for the more complex geometries of Models 2,5,6 and 7, where a finer resolution would be required. These models all introduce their own areas of uncertainty and, therefore, it was decided to have as good an agreement with the theory of the basic duct as possible to use as a base for these later models.

With the mesh size confirmed, the final objective of Model 1 was addressed. This objective was to confirm the validity of the assumption of planar behaviour of the acoustic waves in the duct. A modal analysis of Model 1 was conducted in ANSYS Acoustic, with the first four modes shown in Figure 24. The frequencies and shapes of these modes were validated against theoretical calculations, using Equations 16 and 17 (Howard & Cazzolato, 2014):

$$f_n = \frac{nC_0}{2L} \quad 16$$

$$\psi_n = \cos\frac{n\pi x}{L} \quad 17$$

Where f_n and ψ_n are the mode frequency and shape respectively, n is the mode index and L is the length of the duct. Note that the mode shape is non-dimensional and, as such, the figured produced in ANSYS do not display a legend for the results of a Modal Analysis. In Figure 24 and Figure 26, green is 0, red is maximum and blue is minimum, with the orange and yellow shades lying between maximum and 0 and the lighter shades of blue lying between minimum and 0.

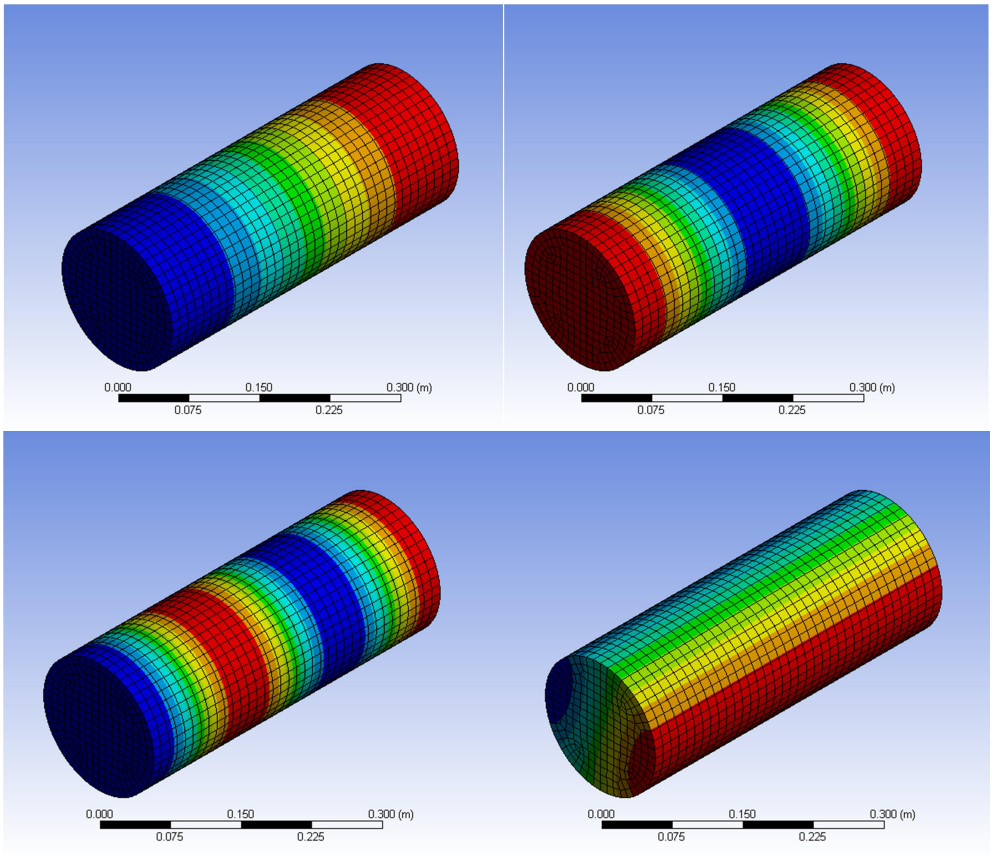


Figure 24: First four modes of simple duct (Clockwise from top left)

The modes progress clockwise from the top left of Figure 24, with frequencies of $400\text{Hz}, 800\text{Hz}$ 1200Hz and 1600Hz respectively. The change to a transverse shape at mode 4 indicates that the cut-on frequency occurs somewhere between 1200Hz and1600Hz. This was in agreement with the calculated cut on frequency of1220Hz. This cut-on frequency is calculated at room temperature, any increase in temperature (as would be experienced in a gas turbine combustor) would result in a higher cut-on and greater range of validity of this assumption.

By confirming that the mode shapes are, in fact, planar below the calculated cut-on frequency, the comparison between the 1 and 3 dimensional models was justified,

allowing for the use of the theoretical Matlab scripts to be used to provide validation of the ANSYS Acoustic simulations.

From Table 1, the purpose of Model 1 is to develop basic ANSYS model and Matlab script, confirm the plane wave assumption and set the mesh element size and type for subsequent models. With these tasks completed, the model was then extended to the more complex geometry of Model 2.

4.2. Model 2 and Model 5

The purpose of Models 2 and 5 was to perform a harmonic analysis on a geometry that more closely approximates that of a gas turbine combustor. This was achieved by building on the procedures and scripts developed in Model 1.

The Matlab script for the theoretical calculations in Model 2 was verified in the same manner as Model 1, but with the values at points -2 to 3 (as shown in Figure 14) being checked. Once again, the results of the two methods of calculating the acoustic properties at these points were in agreement for several input velocities and frequencies.

As may be seen in Figure 25, there was a good agreement between the theoretical values along the liner and those produced by the model in ANSYS. Around the duct representing the swirler (located between z=0 and z=-0.2), however, there was a slight disagreement between the two calculations. This was due to the sudden discontinuity in area that leads to a region of more complex acoustic behaviour than the simple plane wave that was the assumption of the theoretical model.

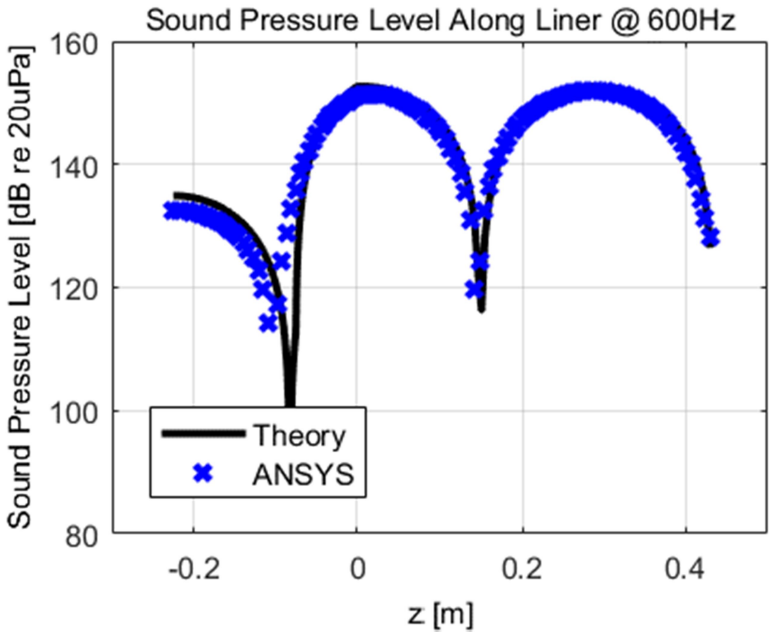


Figure 25: SPL for Model 2, ANSYS vs Theory

The non-planar behaviour of the regions at either end of the Swirler duct may be seen in Figure 26, which depicts the results of a Modal analysis of Model 2 for the fourth mode (occurring at 1130Hz), with shading of the figure ranging from blue to red for the low to high values of the mode respectively. The distortion at the ends of this duct will not be predicted by the theoretical models and explains the difference in the results from the two methods in these regions.

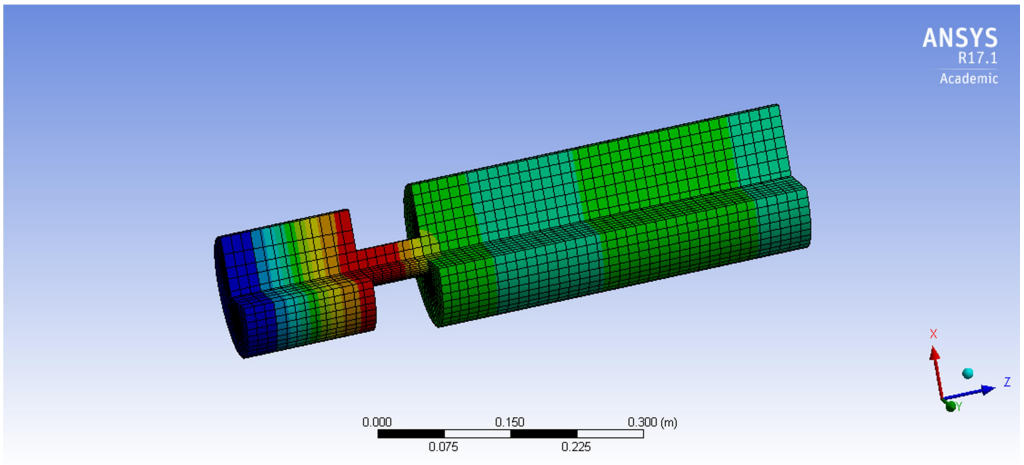


Figure 26: Mode 4 of Model 2 showing non-planar behaviour around swirler

In order to obtain a better agreement between the models, it would be preferable to follow the norm in producing one dimensional models of a combustor of determining

the transfer matrix of the burner (the swirler, injector and flame) experimentally (Polifke, et al., 2001).

Models 2 and 5 show that a harmonic analysis of a composite duct may be performed using both the FEA methods of ANSYS Acoustic and the acoustic multiports employed in the Matlab script. The theoretical models were found to struggle with the sudden changes of area around the swirler. This limitation could be overcome by implementing a transfer function for the burner to serve as a source term for the model.

4.3. Model 3

Model 3 was used to simulate the flow of air through a cold combustor. The aim was to confirm the location of the zone in which combustion will occur and to provide the velocity inputs to be used in the simplified geometry of Model 4. The inlet velocity of the combustor was taken from the stated outlet velocity of $82\mathrm{m.s}^{-1}$of the compressor in the Proteus combustor's manual (Siddeley, 1961). For more information on the specifications of this combustor, see Appendix B.

The mesh of Model 3 was produced as described in section 3.4. The aspect ratio quality of the mesh was above 0.8 within the body of the combustor (comprising of hexagonal mesh elements). The tetrahedral mesh at the walls of the liner and swirler blades, as well as in the annulus, had an aspect ratio quality above 0.3. The Y+ values around these walls was kept at a maximum of 11.06 by the scalable wall function used (ANSYS, 2013).

The velocity vector and field of Model 3 is shown in Figure 27. The function of the swirler is apparent in creating a region of very low velocity/reversed flow in the primary zone of the combustor. This region of flow serves to anchor the flame and, in this project, was used as the location of the source of the acoustic waves in all Matlab and ANSYS Acoustic Models.

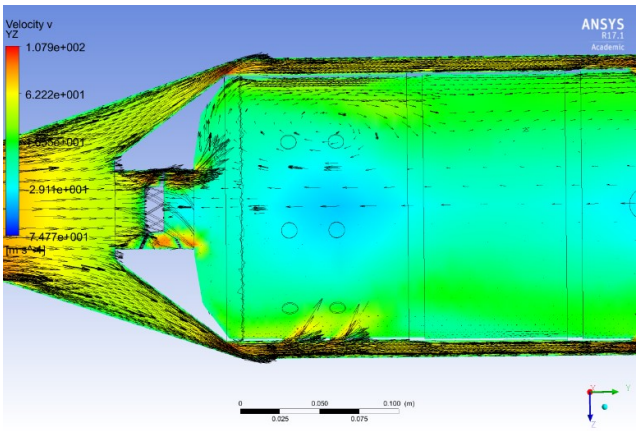


Figure 27: Velocity vector and field at inlet of cold combustor

The aim of Model 3, in addition to illustrating the effects of the combustors' geometry on the flow, was to obtain the input velocities for Model 4. These were obtained in ANSYS CFX Post, with the magnitude of the velocity field of the combustor in the XY plane shown in Figure 28. The velocity field in the YZ plane, as well as the axial component of this velocity field in each of the planes, may be viewed in Appendix C.

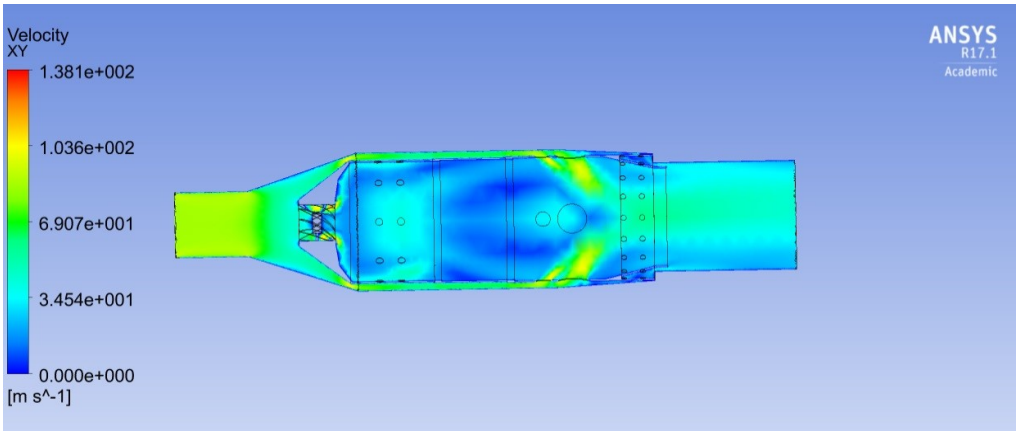


Figure 28: Velocity field in XY plane of Combustor (no flame)

As a means of verifying the model, the mass flow rates at the inlet and outlet of the combustor were compared, with Table 2 showing a difference between the two of $15.8 \times 10^{-3}\%$ which was considered adequate for this qualitative assessment.

Table 2: Verification of results from Model 3

Location	Mass flow rate (kg/s)
Inlet	630×10^{-3}
Outlet	630×10^{-3}
Difference	10×10^{-5}

% error	15.8×10^{-3}

The location of the flame was confirmed as being in line with the primary holes of the combustor, with this plane to be used as the location of the source of the sound in all FEA and Theoretical models.

The purpose of Model 3 was to give a qualitative assessment of cold air flow through the combustor in order to obtain inputs for Model 4. The required precision of the results was not very high and several simplifications were made. The most noticeable limitation of the model is the use of an unstructured mesh in the near wall regions of the model. While this may lead to inaccuracies in the results, it should be noted that the neglecting of the cooling holes in the liner means that the near wall behaviour in the model was never going to be a true representation of that in the actual combustor.

Model 3 also allowed for the procedure for developing a geometry, mesh and simulation to be practiced without the additional complication of the modelling of the combustion. These procedures, mesh refinements and base geometries could then be modified and used to model the combustion in Model 4.

4.4. Model 4

The mesh of Model 4 was produced by modifying the parts used in Model 3 and using the same input values for the definition of the mesh. Once again, the aspect ratio quality of the mesh in the combustion chamber was above 0.8 and the majority of the tetrahedral mesh at the walls of the liner and swirler blades above 0.5. The Y+ values around these walls was kept at a maximum of 11.06 by the scalable wall function used (ANSYS, 2013).

The mesh consisted of 378000 elements, with the hex core elements having a typical side length of $4mm$. The characteristic dimension of the flow is taken as the diameter of the core vortex (ANSYS, 2013). The mesh therefore has 10 elements per characteristic dimension, which was considered to be adequate for the requirements of this simulation.

The velocity inputs for Model 4 are presented in Table 3. The fast run inputs were taken from the results of Model 3.

Table 3: Boundary conditions input to CFX-Pre for Model 4

Input velocities for Model 4

Location	Velocity (m/s)
Inlet	40
Primary holes	100
Secondary holes	80
Dilution holes 1	70
Dilution holes 2	70
Fuel injection	100

As discussed in section 3.4, one of the assumptions in using the Finite Element method employed in ANSYS Acoustic is that the effects of the mean flow may be ignored. This is generally considered to be a valid assumption in the case of flows with a low Mach number (less than 0.3). It may be seen from the results in Figure 29 that the Mach number through the combustor was well below this threshold, making the use of a Finite Element model a reasonable method for this problem.

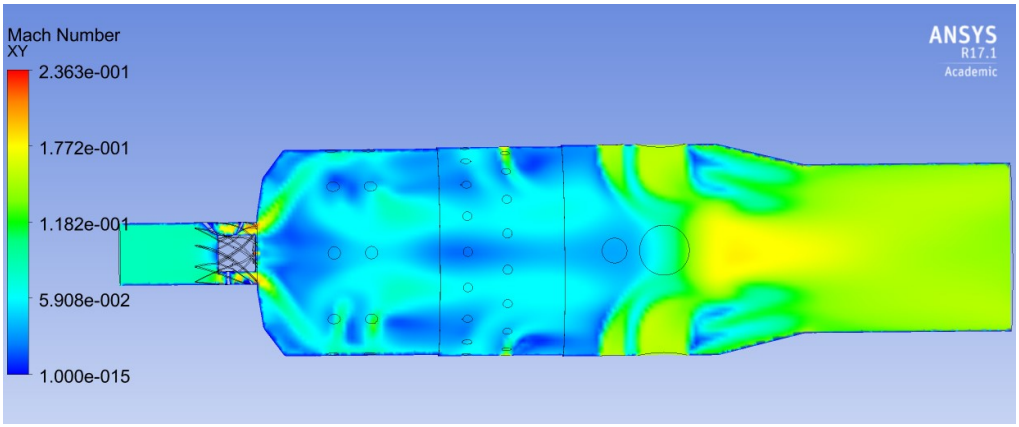


Figure 29: Mach number through fired combustor liner

The temperature field of the fired combustor in Model 4 is shown in Figure 30, with the areas of combustion and dilution clearly visible. The depth of the penetration of the jets, and the pattern factor created at the outlet, was in line with that described in (Lefebvre, 2010). It should be noted that the asymmetry of the result shown in Figure 30, particularly in the primary zone, is due to the alignment of the different cooling holes and the location of the plane of interest. With the cooling holes of the liner ignored, the effect of the cooling film on the walls of the liner is not taken into account in this simulation. The justification for this simplification is given in section 3.7. This temperature field was exported to the ANSYS models of Model 6 and Model 7 in the manner described in section 3.4.

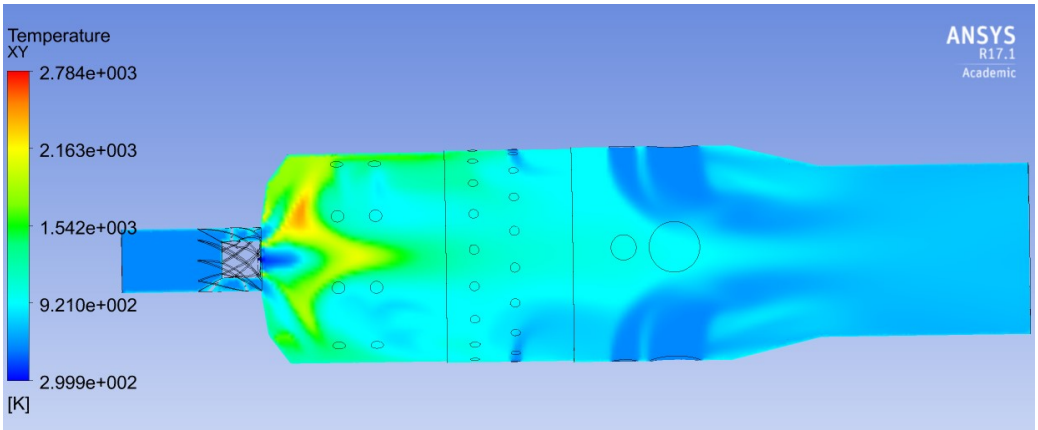


Figure 30: Temperature field, with velocity vector in ZY plane of fired combustor

The average temperature at each of the planes (Figure 31) was calculated in CFX post and the results used as detailed in section 3.5. The temperature profile visible in each of these slices affords an opportunity to visualise the behaviour of the Flame and Flow through a gas turbine combustor. While it was necessary to reduce the temperature profile to 1 dimension, it should be noted that this prevents the radial and circumferential distribution of the temperature to be taken into account.

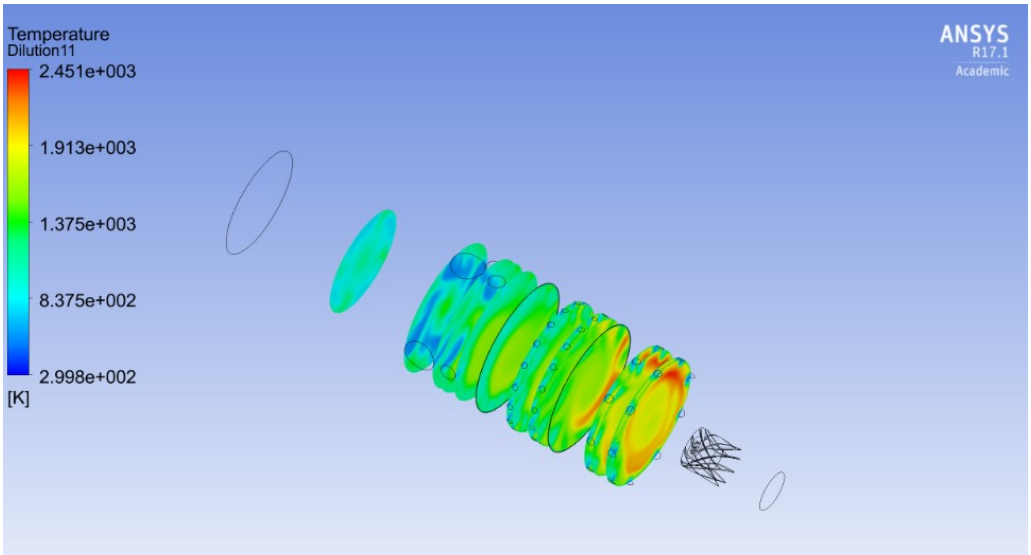


Figure 31: Temperatures at various sample points

The temperature profile obtained from the planes in Figure 31 and used in Model 6 and Model 7 is shown in the graph in Figure 32, which compares this profile with a linear variation between the inlet and outlet of the combustor. The increase in average temperature between $y = 0.05m$ and $y = 0.1m$corresponds to the location

of the flame at the primary holes, within the collapsing vortex produced by the swirler visible in Figure 27

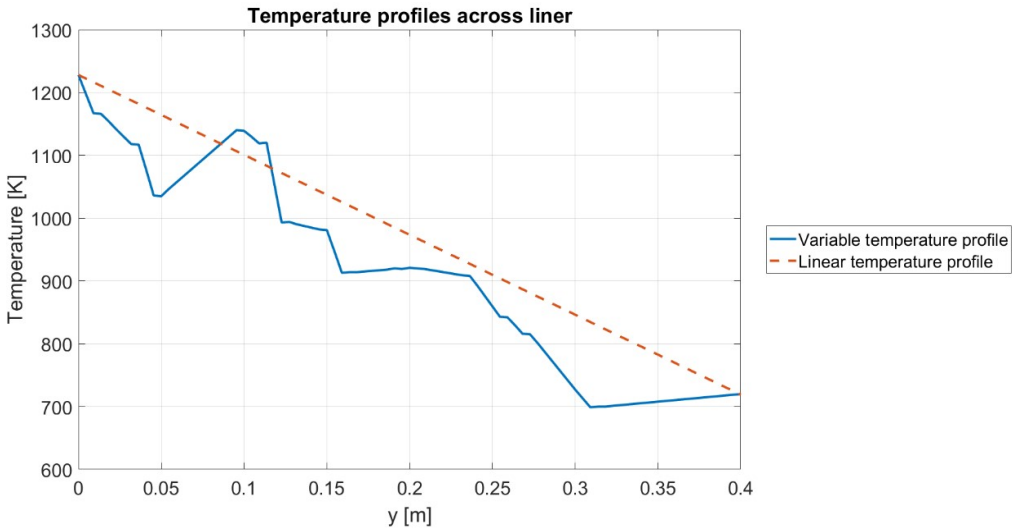


Figure 32: Linear and variable temperature profiles along combustor liner

The simulation was verified by comparing the mass flow rates at the inlets and outlet of the combustor. Table 4 shows the difference between the two of $16.8 \times 10^{-3}\%$ which was considered to be well within the level of precision of the package used.

Table 4: Verification of Model 4

Location	Mass flow (kg/s)
INLET	51.8×10^{-3}
OUTLET	-506×10^{-3}-
Dilution 1	56.2×10^{-3}
Dilution2	225×10^{-3}
Primary	90.5×10^{-3}
Secondary	80.7×10^{-3}
Injection	2.05×10^{-3}
Total	-8.05×10^{-5} -
% error	16.8×10^{-3}

In order to validate the results of Model 4, the calculated outputs were compared with the expected outputs from the manual. This comparison is shown in in Table 5.

Table 5: Validation of Model 4

Validation of Model 4 results			
	Proteus	Model 4	Unit
Peak Combustion Temperature	2500	2450	K
Outlet velocity of combustor	125	107	m/s
Outlet Mach number of combustor	0,35	0,31	-
Outlet temperature of combustor	299	320	K

The peak combustion temperature of Model 4 is very close to that predicted in the Proteus manual, which gives confidence that the temperature field produced here is a good reflection of the profile of a typical combustor. The outlet velocity of Model 4 is lower than that predicted by the manual, which may be explained by the number of simplifications to the geometry and fuel type used in the simulation. A further explanation for this difference could lie with the fact that the velocity calculated for the manual would have been done by hand (the manual being from 1954) and would therefore have had to rely on the macroscopic properties of the flow, compared to the more advanced methods used by the software employed here.

The tasks for Model 4 were to produce a fired simulation of the combustor that produces a quantitative temperature field of a typical gas turbine combustor. The temperature and flow fields have been visualised, with a 1-dimensional temperature profile produced to be used in the FEA and theoretical calculations in Models 6 and 7.

An additional task of this model was to validate the assumption of neglecting the effects of the mean flow in the acoustic analysis of this combustor. The Mach numbers of the flow have been confirmed as being low enough for this to be a reasonable assumption.

4.5. Model 6

Model 6 makes use of the same geometry and methods as Model 1. The purpose of the first part of Model 6 is to validate the procedure for incorporating a change of temperature in both the ANSYS simulation and Matlab script described in Howard and Cazzolato (2014). The second part of Model 6 uses this procedure to incorporate the temperature field produced in Model 4.

The acoustic properties of the mesh in the ANSYS acoustic model were modified by applying the temperature profiles shown in Figure 32 and conducting a thermal analysis using ANSYS Thermal. The first thermal analysis is performed with the

temperatures applied at only the inlet and outlet of the model to produce the linear gradient shown in Figure 32

The result of the thermal analysis of the linear temperature profile is shown in Figure 33. Note that the temperatures are displayed in degrees Celsius, while the inputs to all calculations (in ANSYS and Matlab) must be in degrees Kalvin.

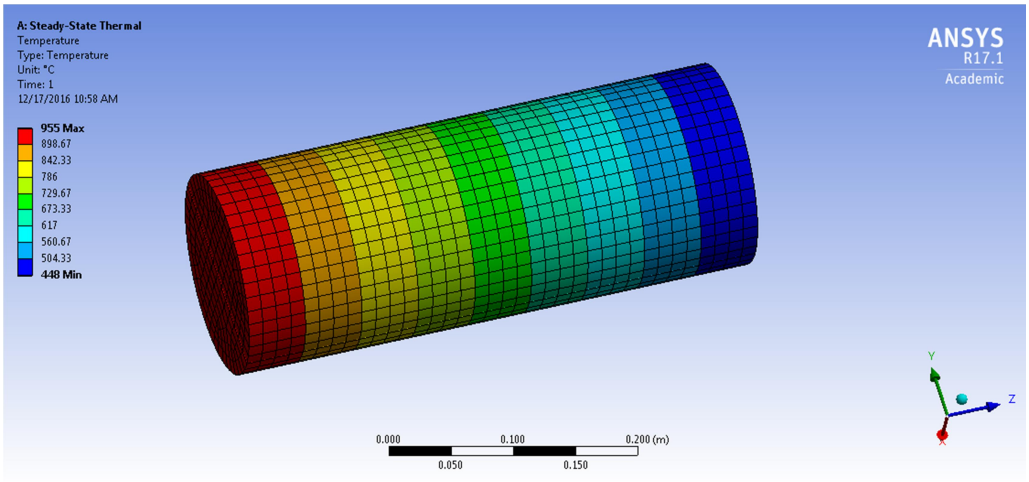


Figure 33: Linearly varying temperature across Model 6

The theoretical calculations were performed using a Matlab script, as in Model 1, but with a new transfer matrix that allows for a temperature gradient to be applied across the duct. The script was verified by making the two temperatures very close in value and comparing the output with the script from Model 1. The results of the calculations by this script were then used to validate those of the ANSYS Model and the comparison may be seen in Figure 34.

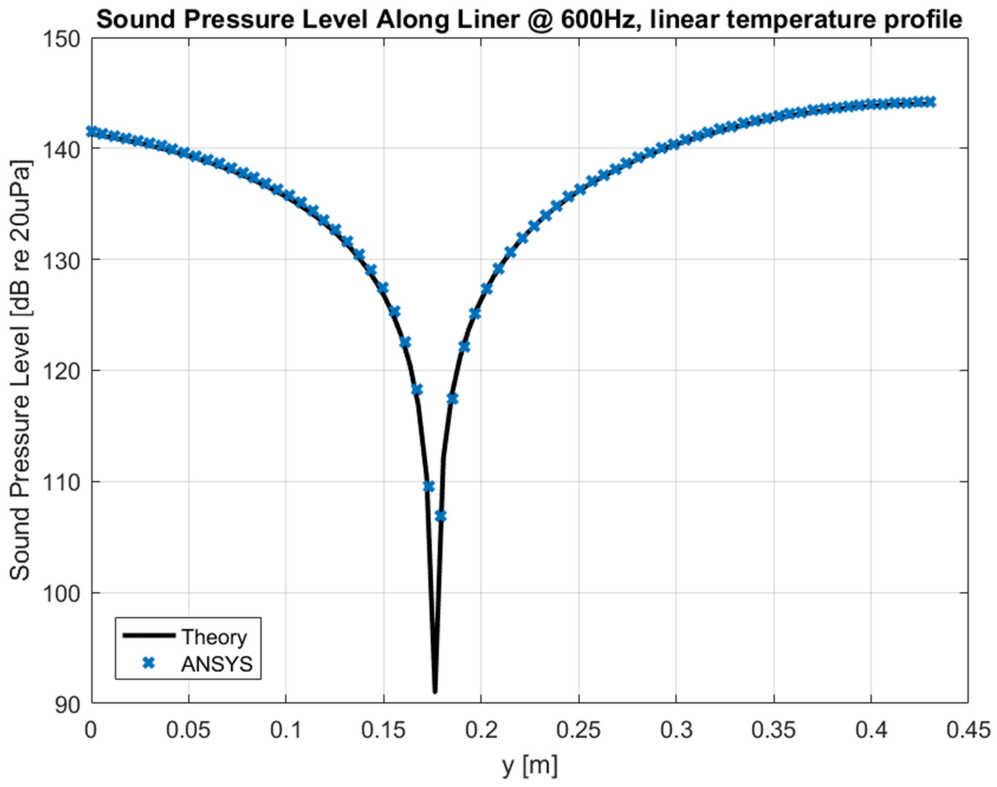


Figure 34: SPL for Model 6a, ANSYS vs Theory

As may be seen, there was good agreement in the two sets of results, giving confidence in the method described in Howard & Cazzolato (2014).

With the calculations of the linear temperature gradient completed, the more complex temperature field was introduced to the model. The temperatures from the planes in Figure 31 were used as the individual values of temperature along the axis of the theoretical model in MATLAB and the results calculated using the same transfer matrix as the first version of Model 6.

The material properties of the model were modified in the same manner as the linear temperature profile, with the result of the thermal analysis shown in Figure 35.

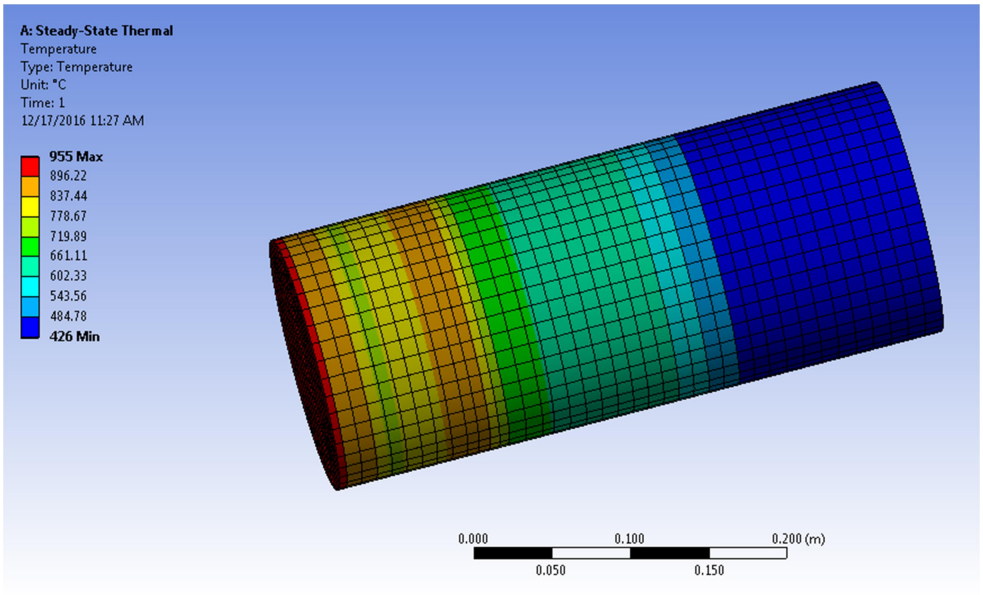


Figure 35: Varying temperature field of Model 6

As with the linear temperature profile, the results of the harmonic of the model after the application of the variable temperature profile were compared with those of the theoretical model in Figure 36.

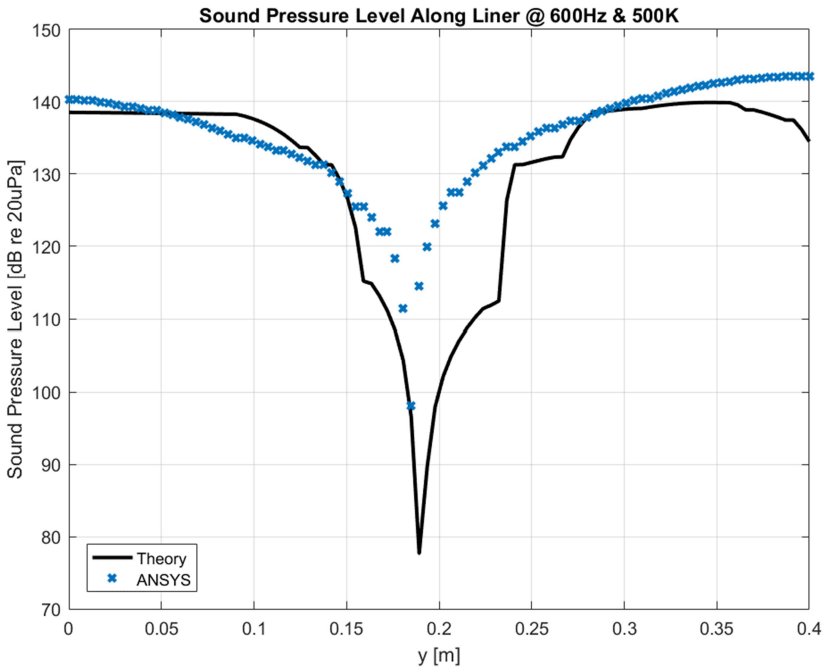


Figure 36: SPL for Model 6b, ANSYS vs Theory

While theoretical and ANSYS models agreed in the general form of the graph, it is clear from Figure 36 that the theoretical model does not handle the sudden changes

in temperature gradient very well. This is likely due to an insufficient number of samples taken from the CFD results of Model 4. A smoother temperature profile would improve the suitability of the theoretical model for validation of the results from the ANSYS Acoustic model.

The results for the ANSYS simulation shown in Figure 36 have several irregularities on the curve. These are produced by the nodes at each plane being displayed twice in the output of the results from ANSYS to excel. These duplicate values were not picked up in the manual sorting of the data described in section 3.3 around Figure 15.

The purpose of Model 6 was to validate and practice the methods for changing the properties of an ANSYS acoustic simulation to take a variation in temperature into account. This was performed for both a linear temperature profile and the profile produced by Model 4. The validation of these simulations was conducted, as with Model 1, by comparing their outputs with those of the theoretical calculations of a verified Matlab script. The linear temperature profile showed excellent agreement between the ANSYS and Matlab results while the validation of the variable temperature profile was limited by the low resolution of the temperature samples taken in Model 4.

4.6. Model 7

Model 7 makes use of the geometry of Model 5 and uses the procedure developed Model 6. This temperature in the liner was made to vary, first linearly and then in accordance with the temperature profile of Figure 32. The temperatures in the diffuser, swirler and outlet were kept constant at the average values of these areas in Model 4.

The results of the SPL along the liner of Model 7, for both the ANSYS and Matlab calculations, are shown in Figure 37. The results show the same level of agreement as the linear profile of Model 6, but with the offset in the shape of the graph the same as that experienced in Models 2 and 5, due to the difficulties experienced by the theoretical model in handling the complex geometry of, and flow through, the swirler.

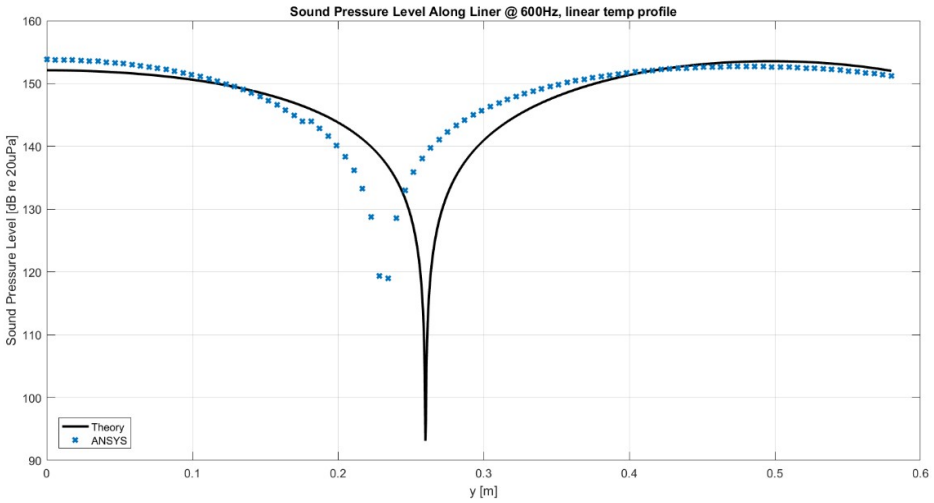


Figure 37: SPL for Model 7a, ANSYS vs Theory

The results of the calculations of the liner of Model 7 with the varying temperature profile are shown in Figure 38. In addition to the offset experienced by Models 2 and 5, the difficulties of the theoretical model in handling the changing temperature gradients in the liner are apparent. In both Figure 37 and Figure 38, the irregularities in the output of the ANSYS simulations discussed in section 4.5 are visible, again displaying the limitations of the methods used to export this data.

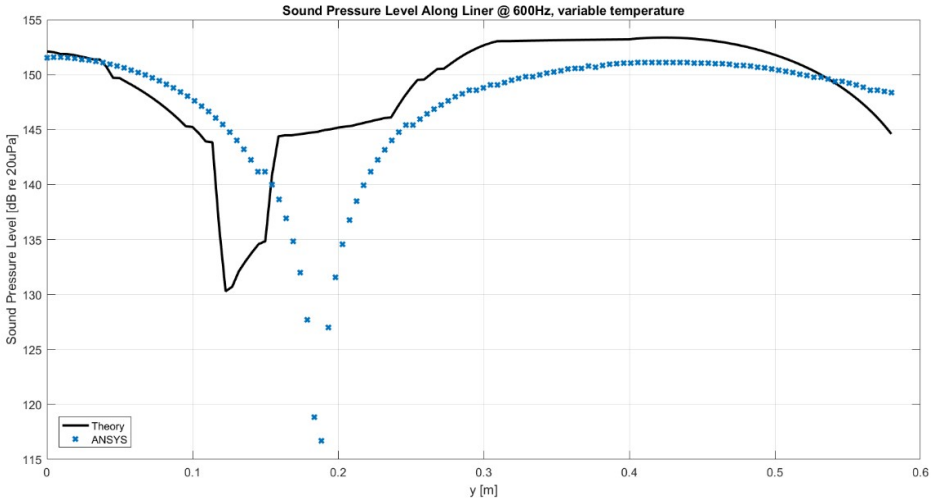


Figure 38: SPL for Model 7b, ANSYS vs Theory

The differences in the results of the ANSYS and theoretical results for Model 7 were a combination of those of Models 2, 5 and 6. This is not surprising as these are the elements used to construct this model. These discrepancies have been explained in

each of the earlier, simple models and there are no further disagreements between the theoretical and ANSYS results of Model 7.

With the limitations in the validation of the ANSYS models all coming from difficulties with the theoretical models in handling sudden changes in duct diameter and temperature, it is expected that a refinement of these theoretical models will lead to a reduction in the degree of these limitations.

The final model of the project is that of an open, composite duct with a variable temperature profile applied to one of the ducts. The results of the SPL of the harmonic analysis of this model in ANSYS Acoustic are shown in Figure 39. The processes used in producing this model have been built up and validated in a step by step fashion described in the previous sections of this chapter.

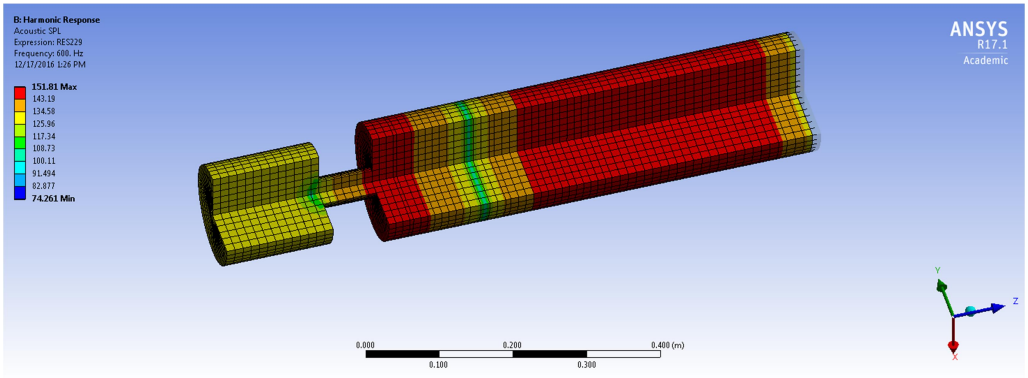


Figure 39: SPL of Model 7b, open duct

The model predicts that the propagation of an acoustic wave through a composite duct geometry and in conditions that approximate those of a gas turbine combustor will be in the form of a planar wave along the axis of the duct. The effects of mean flow of the gas through this combustor are predicted to be negligible and there is expected to be a region of non-planar behaviour around the swirler of the combustor, as shown in Figure 39. The distribution of the SPL at 600Hz along the duct is predicted to be of the general shape of the results shown in Figure 38, with a sudden dip around a third of the way along the length of the combustor.

5. Conclusions

The objective of this project was to develop a numerical model of the acoustic field within a gas turbine combustor. This objective was broken down into three desired outcomes which were in turn broken down into tasks that informed the purposes of each model. The models were developed in a sequential format that allowed for practice in, and validation of, the techniques required for the final simulation.

Model 1 was used to conduct a harmonic analysis of a simple duct. This allowed for the development of the ANSYS Acoustic model and mesh, as well as the Matlab scripts that were used in the more complex models later in the project. The validity of the plane wave assumption that forms the basis of the theoretical models of the Matlab scripts was confirmed at this stage of the project. Various mesh configurations were tested, with a Mesh of 24epw, consisting of FLUID 220 elements, was selected as the basis for the ANSYS models.

Models 2 and 5 were used to extend the geometry of Model 1, in both the ANSYS models and Matlab scripts, to that of a composite duct. The dimensions of this duct were based on those of the Proteus combustor described in section 3.1 and Appendix B. The theoretical model used in the Matlab scripts was found to have a limitation in not being able to deal with the non-planar behaviour around the duct representing the swirler.

In the course of setting up the Matlab scripts used in validating the ANSYS results, a quirk of the standard 4-pole transfer matrix was noticed. If the nomenclature of the ends of the duct and directions of the incident and reflected waves were not kept constant, the transfer matrix was effectively replaced with its inverse. This confusion is easy to occur due to the conventions for fluid mechanics (left to right) and acoustics (right to left) being in opposite directions. This error can be especially confusing because of the relationship between the matrix and its inverse, which gives rise to results that were identical, but with the values of the acoustic pressure multiplied by -1 (reflected about the axis on the graphs produced by the Matlab scripts). The derivation of this matrix and the relationship with its inverse is examined in Appendix E.

When exporting the values calculated along the axis of the ANSYS acoustic models, it was noted that the default format of the export is to list the values in order of node number of the mesh, which does not proceed along the axis. This means

that the standard export of values along the axis is effectively “scrambled”. The order of the nodes along the axis was manually entered into the exported spreadsheet and then sorted to get the nodes (and corresponding values) in order along the axis of the duct. While this method was effective, there were one or two cases where a duplicated node was missed in the sorting process. This lead to the irregularities in the ANSYS results displayed in Figure 37 and Figure 38.

Models 3 and 4 were produced in ANSYS CFX to simulate the behaviour of the gas flowing through the combustor. The velocity and temperature profiles produced in these models give the context in which the acoustic field acts. The neglecting of the effects of mean flow on the acoustics within the combustor was found to be a reasonable assumption at this stage.

A typical temperature profile of a gas turbine combustor was the primary output of Models 3 and 4. As the requirements of this output were very general, several simplifications were made to the model. The simplifications used in the geometry, where the cooling film and secondary holes were removed from the model, were made with the knowledge that these features would not be present in any future work done on designs that make use of a LPP combustor design.

The means of exporting the temperature of Model 4 to the 1 dimensional format required by the theoretical models in the Matlab scripts was to take the average temperature at several planes of interest. It was noted that the 1 dimensional nature of this temperature profile does not allow the radial and circumferential variations in the temperature within the combustor.

Models 6 and 7 took the procedures used in developing Models 1, 2 and 5 and applied the temperatures of Model 4 to produce conditions more akin to those likely to be experienced in a gas turbine combustor. The theoretical model used to validate the ANSYS simulations of these models was very effective when a linear temperature was applied, but less so when the temperature was made to vary in accordance to the temperature profile of Model 4. This was likely due to an insufficient number of sample points taken as a representation of this profile. It is anticipated that an increase in the resolution of this profile would resolve this issue.

The hardware and software used was found to be more than adequate for the simulations undertaken. The time taken to run the Matlab scripts was typically in the order of 10-30s (depending on the amount of results to be retrieved from other sources, such as the spreadsheets of ANSYS results). The ANSYS Acoustic

simulations typically took in the region of 1-5mins and the CFX simulations 3-6hrs to run.

The final model of the project is that of an open, composite duct with a variable temperature profile applied to one of the ducts. The conditions applied to the mesh of the model are a good approximation of what may be expected within a gas turbine combustor. The methods and procedures used in creating this model may be used as a starting point for the analysis of the acoustic behaviour within a combustor of this nature.

6. Recommendations

The recommendations that stem from this project may be divided into two parts. Firstly, there are those that come from the lessons learnt from the mistakes made in this process and what could have been done differently. Secondly there are those that pertain to the future direction of this investigation. Recommendations are given as to the order of projects needed to achieve the goal of determining if the life cycle prediction of a gas turbine combustor may be improved by modelling the contribution of acoustic loads experienced by the liner.

6.1. Lessons Learned

The most challenging aspect of this project was the necessity of using multiple software packages and integrating the results thereof. While the tutorials available for the various ANSYS packages were very useful in isolation, there was little instruction given in the integration between the different aspects of the same project paths (such as Design Modeller to ICEM to CFX), let alone on integration between physics packages that are not conventionally related. An example of this sort of integration is the exporting of the temperature field from CFX to ANSYS Acoustic.

The key to this integration of physics packages is the use of the background language in ANSYS, ADPL (ANSYS Parametric Design Language). Many of the more complicated models in Howard & Cazzolato (2014) are developed through this language and the use of a few well-crafted APDL scripts would have greatly reduced the difficulties encountered in integrating the temperature field with the acoustic analysis and with exporting the results of the Acoustic models to their theoretical counterparts.

To reduce the amount of time required to gain the necessary proficiency with these programs, it is recommended that the first step of any future projects be to undergo formal training and familiarisation with the software to be used before the actual work of the project commences. The development of tutorials on the more unique aspects of the use of these software programs in this area of research is recommended and described in more detail in section 6.2.2.

One of the difficulties encountered with the software was in making changes to the geometry of a specific model. In most cases, any attempt to modify the geometry by changing the 3D model and attempting to integrate it with an existing ICEM geometry resulted in incompatibilities between the two. These changes should be

avoided as far as possible through the careful selection of the initial geometry in the knowledge that any changes made will invariably result in a having to repeat the entire process of setting up the mesh.

When making changes to the geometry, it should be noted that changing the name of any part of a Solid Edge assembly will result in that assembly failing to load correctly. Similarly, when making adjustments to any part of a workbench file, it is good practice to make a copy of the entire workbench project first.

On completion of the project, it was noted that the mass balance approach to verifying the models produced in CFX (Models 3 and 4) was of limited value to a model of a reacting flow. The use of an energy balance to complement the mass balance approach would give assurance that the heat flow through the models, particularly Model 4, was realistic.

6.2. Future work

The scope of the work required to solve the initial problem of quantifying the effects of the acoustic field within a gas turbine combustor on its liner life requires the breakdown of the research into distinct projects. This section describes the recommended sequence of projects to be taken to build upon the work done here.

The large scope of work mentioned above comes with an additionally broad skillset required. The development of a series of tutorials to assist with an accelerated acquisition of these skills is included in this section.

6.2.1. Suggested further projects

It is advised that any further work should be based on a Lean Premixed Pre-vaporised combustor design. While the use of the Proteus design was worthwhile for this study, an LPP is more in line with modern design trends and will produce results that are more relevant to industry. Incidentally, these designs will be significantly easier to analyse from an acoustic perspective than those of traditional designs as they have fewer perforations in the liner. LPP combustors are associated with having a higher acoustic load, making the impact of this load on the liner of greater relevance to this type of design than the traditional design used in the Proteus engine.

The two difficulties in validating the ANSYS Acoustic models produced in this project, the acoustic behaviour around the swirler and the resolution of the temperature field, may be addressed by extending the research in two directions.

The resolution of the temperature field may be addressed by improving the method used in exporting the temperature from the CFD model of the combustor. This may be done through the use of an APDL script that maps the temperature at a given coordinate of the CFD model to the corresponding coordinate in an acoustic FEA model.

A fired test rig to investigate the combustion dynamics of a LPP combustor would facilitate the validation of any CFD models produced. When the geometry of the rig to be used as the base of this research is known, a more complete simulation of the combustor should be completed than what was undertaken in this project.

To address the issue of the non-planar behaviour around the swirler, a source term needs to be found for the burner. The data required to produce this source term may be obtained either directly from the experimental rig or through a numerical model of the rig. This source term may be used to excite ANSYS Acoustic models as well as 1-dimensional analytical models. At this stage, the difficulties encountered in the use of the transfer matrices for a varying temperature profile will need to be addressed, perhaps through the use of several iteration loops in the code.

With the source term of the flame noise established, further investigation may be conducted into the thermoacoustic feedback within the combustor. This investigation may be performed using the ANSYS Acoustic and analytical models described above. Validation of the results of the investigation, however, will require a slightly different experimental setup to that of the fired combustor rig described earlier.

The design of the rig concerned with the Acoustic behaviour of the combustor must have a means of producing a source of sound (i.e. a speaker) in the same location as that of the flame and a means of measuring this sound at various locations within the rig. More advanced projects would then find a means of adding heat and a mean flow to the rig.

The investigations described in this section may be performed either on one multi-purpose rig or by using two dedicated rigs of the same general geometry. This geometry should be kept as simple as possible, especially at first while expertise and confidence in the computational modelling is being built. The preferred geometry for test rigs of this nature appears to be that of a square tube, with (Huls, 2006) (Pożarlik, 2010) and (A. P. Dowling, 2003) making use of this configuration.

Both of the directions of research recommended here may be extended to include an FSI component as both ANSYS CFX and Acoustic are capable of performing this type of analysis. It is recommended that a project be done on the FSI of simpler application, such as an exhaust muffler or HVAC duct, before attempting to integrate this aspect of the research with the acoustic behaviour of a gas turbine combustor.

The initial aim of the experiments conducted on the test rigs should be to start small and focus on validating the models to be used in the tutorials described above. At this stage, the rig(s) should be kept simple and low cost, with the possibility of evolving as the research progresses. In the case of both research streams, the methods described in this project and the lessons learnt in their application will be beneficial.

6.2.2. Software Tutorials

While a formal course may be sufficient to produce this level of general competence, a specific tutorial may be more useful as an introduction to the methods that are pertinent to this problem. These tutorials could be in the form of those provided with ANSYS CFX and ICEM, and developed in house to be tailor made for this area of research. As an example, the tutorial for the CFD aspects of this area of research would follow the steps shown in Figure 40 and could be produced for whichever software package is chosen.

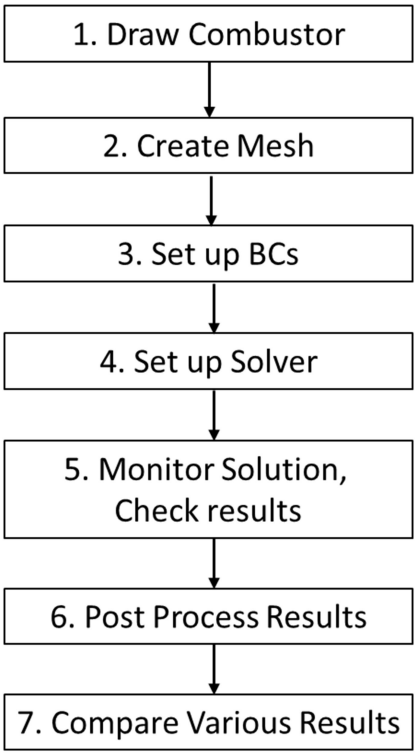


Figure 40: Steps of suggested tutorial on CFD modelling of combustor

The geometry of the combustor to be drawn should be based as closely as possible on any test rig used as the basis for this research. The tutorial should include an explanation of how to import the model into the next step, the creation of the mesh.

In creating the mesh to be used, several meshes should be formed and the simulation run on each of these in order to illustrate the effects of mesh size and quality on the results of the simulation. A simple explanation of the numerical methods used in this software would be useful at this stage. An explanation of the tools and criteria for checking and improving the quality of the mesh should also be included. In this project, a great deal of difficulty was encountered in modifying the geometry upon which the mesh was based and the little tricks and advice for effecting these modifications would be possible to convey at this stage of the tutorial.

As with the geometry, the procedures for transferring the mesh to the next stage of the process, the setup of the boundary conditions of the simulation, should be described in detail in the tutorial. The theory behind the combustion and turbulence models could be covered here and the reasons for selecting particular

methods explained. Several different simulations could be run in order to illustrate the characteristics of these different models.

The setup of the solver would be the next step in this process, with the timescales and precision of the simulation set up and explained. The simulation would then be run and the solution monitored for convergence, with the time for computation and precision and accuracy of the result monitored and recorded.

A series of exercises in the post processing of the results could follow, focussing on the format of the results to be presented in any final reports as well as the methods to be used in exporting these results to other programs.

Once these results have been collected for all simulations, the results could be compared amongst themselves and, if available, with experimental data. This experimental data could either be collected from a test rig as part of the tutorial or the results of past experiments could be used. In this manner, the complete process of using the chosen software for creating a basic model of the combustor could be used, a familiarity of the theory behind the calculations would be gained, along with an understanding of the test rig design and performance.

The results of this tutorial could be used as the base for further simulations, much as those of the combustor tutorial in (ANSYS, 2013) and the exercises in (Howard & Cazzolato, 2014) were used in this project. An example of this would be to conduct experiments making use of the acoustic package of the CFD software in question, with the possible development of a further tutorial that would allow the knowledge of this topic to be shared.

The suggested medium of delivery of this tutorial would be for the background theory to be in document format and for the procedures in the use of the software to be recorded as videos, to ensure that all details of the procedure are captured.

In a similar fashion, the use of the ANSYS FEA Acoustic extension could be used in conjunction with an experimental rig as a tutorial in the use of this software.

References

A. P. Dowling, S. R. S., 2003. Acoustic Analysis of Gas Turbine Combustors. *JOURNAL OF PROPULSION AND POWER,* 19(5), pp. 751-764.

ANSYS, 2013. *ANSYS CFX Reference Guide.* Canonsburg, PA: ANSYS, Inc. .

ANSYS, 2013. *ANSYS CFX-Solver Modeling Guide,* Canonsburg, PA : ANSYS inc.

ANSYS, 2013. Chapter 8: CFX Best Practices Guide for Combustion. In: *ANSYS CFX Reference Guide.* Canonsburg, PA : ANSYS Inc, pp. 110-111.

ANSYS, 2013. Gas Turbine Combustors. In: *ANSYS CFX Reference Guide.* Canonsburg, PA: ANSYS Inc, p. 109.

ANSYS, 2013. Meshing Requirements. In: *ANSYS CFX Reference Guide.* Canonsburg, PA : ANSYS Inc, p. 155.

ANSYS, 2013. Solver Yplus and Yplus. In: *ANSYS CFX Solver Theory Guide .* Canonsburg, PA : ANSYS Inc, p. 123.

ANSYS, 2013. The K-Epsilon Model. In: *ANSYS Solver Modelling Guide.* Canonsburg, PA : ANSYS Inc, p. 141.

Bake, F. et al., 2005. *Indirect Combustion Noise Generation.* Monterey, California, American Institute of Aeronautics and Astronautics.

Ballal, D. & Lefebvre, A., 1974. Turbulence Effects on Enclosed Flames. *Acta Astronautica,* Volume 1, pp. 471-83.

Baskharone, E. A., 2006. *Principles of Turbomachinery in Air-Breathing Engines.* 1st ed. Cambridge: Cambridge University Press.

Bathe, K., 1998. Fluid Structure Interactions. *MECHANICAL ENGINEERING*, April, pp. 66-68.

Bodony, D., 2017. *Univeristy of Illanois - Aeroacoustics.* [Online]
Available at: http://acoustics.ae.illinois.edu/
[Accessed 19 May 2017].

Boudier, G., 2007. *Investigating the Thermo-Acoustic Stability of a Real Gas Turbine Combustion Chamber Using Large-Eddy Simulations.* Lisbon, CERFACS.

Boyce, M., 2012. Combustors. In: *Gas Turbine Engineering Handbook.* Oxford: Elsevier, pp. 427-487.

Boyce, M. P., 2012. Aircraft-Derivative Gas Turbines. In: *Gas Turbine Engineering Handbook.* Oxford: Butterworth-Heinemann, pp. 39-31.

Bragg, S., 1963. Combustion Noise. *Journal of the Institute of Fuel*, January, pp. 12-16.

Chen, G., Tang, K. & Jin, T., 2004. Advances in thermoacoustic engine and its application to pulse tube refrigeration. *Chin. Sci. Bull.,* 49(13), pp. 19-28.

COMSOL, 2017. *Multiphysics Cyclopedia.* [Online]
Available at: https://www.comsol.com/multiphysics/aeroacoustics
[Accessed 19 05 2017].

Culick, E. C. & Yang, V., 1995. Overview of Combustion Instabilities. In: V. Young, ed. *Liquid Rocket Engine Combustion Instability.* Pasadena: AIAA, pp. 3-31.

D.C. Mathews, N. R., 1977. Prediction and Measurement of Direct Combustion Noise in. *Journal of Aircraft,* 14(9), pp. 850-859.

Dowling, A. P. & Stow, S. R., 2003. Acoustic Analysis of Gas Turbine Combustors. *JOURNAL OF PROPULSION AND POWER,* 19(5), pp. 751-764.

Dowling, A. P. & Stow, S. R., 2003. Acoustic Analysis of Gas Turbine Combustors. *JOURNAL OF PROPULSION AND POWER,* 19(5), pp. 751-764.

Dowling, A. & Stow, S., 2003. Acoustic Analysis of Gas Turbine Combustors. *JOURNAL OF PROPULSION AND POWER,* 19(5), pp. 751-764.

Duran, I., Moreau, S., Nicoud, F. & Livebardon, T., 2014. Combustion Noise in Modern Aero-Engines. *Aerospace Lab Journal,* Issue 7, pp. 1-11.

E. C. Culick, V. Y., 1995. Overview of Combustion Instabilities. In: V. Young, ed. *Liquid Rocket Engine Combustion Instability.* Pasadena: AIAA, pp. 3-31.

EEA, 2016. *EEA - Nitrogen oxides.* [Online]
Available at: http://www.eea.europa.eu/data-and-maps/indicators/eea-32-nitrogen-oxides-nox-emissions-1/assessment.2010-08-19.0140149032-3
[Accessed 24 April 2016].

EPA, 2016. *EPA - Nitrogen Dioxide.* [Online]
Available at: https://www3.epa.gov/airquality/nitrogenoxides/index.html
[Accessed 24 April 2016].

Epperlein, J., Bamieh, B. & ÅSTRÖM, K., 2015. Thermoacoustics and the Rijke Tube: Experiments, Identification and Modeling. *IEEE CONTROL SYSTEMS MAGAZINE* , 17 March, pp. 57-77.

F. Biagioli, e. A., 2007. Combustion dynamics linked to flame behaviour in a partially premixed swirled industrial burner. *Experimental Thermal and Fluid Science,* Volume 32, pp. 1344-1353.

Fahy, F. & Thompson, D., 2015. *FUndamentals of Sound and VIbration.* 2nd ed. Boca Raton: CRC Press.

FLIGHT, 1954. *Flightglobal.* [Online]
Available at: https://www.flightglobal.com/pdfarchive/view/1954/1954%20-%200985.html
[Accessed 24 April 2017].

Garrett, S., Adeff, J. & Hofler, T., 1993. Thermoacoustic Refrigerator for Space Applications. *Journal of Thermophysics and Heat transfer,* 7(4), pp. 595-601.

Hirschberg, A. & Rienstra, S., 2004. *An introduction to aeroacoustics,* Eindhoven: Eindhoven University of Technology.

Ho, P. & Doyle, V., 1979. *Combustion Noise Prediction Update,* s.l.: AIAA Paper 79-0588.

Hossaini, M. K. e., 2013. Review of the New Combustion Technologies in Modern Gas Turbines. In: *Progress in Gas Turbine Performance.* s.l.:InTech, p. 147.

Howard, C. & Cazzolato, B., 2014. Natural Frequencies. In: *Acoustic Analyses Using Matlab® and Ansys®.* Boca Raton: CRC Press, p. 102.

Howard, C. Q., 2013. The Corrected Expressions for the Four-Pole Transmission Matrix for a Duct with a Linear Temperature Gradient and an Exponential Temperature Profile. *Open Journal of Acoustics,* Volume 3, pp. 62-66.

Howard, C. Q. & Cazzolato, B. S., 2014. *Acoustic Analysis using ANSYS and MATLAB.* 1 ed. Boca Raton: CRC Press.

Howard, C. Q. & Cazzolato, B. S., 2014. Example of a circular duct. In: *Acoustic Analysis using ANSYS and MATLAB.* Boca Raton: CRC Press, p. 147.

Huls, R., 2006. *ACOUSTO-ELASTIC INTERACTION IN COMBUSTION CHAMBERS,* Enschede: University of Twente.

Hultgren, L. S., 2012. *A Comparison of Combustor-Noise Models,* Cleveland: NASA.

Kinser, L. E., Frey, A. R., Coppens, A. B. & Sanders, J. V., 2012. *Fundamentals of Acoustics.* 4th ed. Hoboken: John Wiley & Sons, Inc..

Kok, J. B., Alemela, R., Roman, J. & Kapucu, M., 2010. *Combustion Dynamics in Gas Turbine Engines,* Cairo: University of Twente.

Lefebvre, A. H. & Ballal, D. R., 2010. *Gas Turbine Combustion: Alternative Fuels and Emmissions.* 3rd ed. Boca Raton: CRC Press.

Lefebvre, B., 2003. Aerodynamics. In: *Gas Turbine Combustion.* Boca Raton: CRC Press, pp. 113-149.

Lefebvre, B., 2003. Basic Considerations. In: *Gas Turbine Combustion.* Boca Raton: CRC Press, pp. 10-33.

Lefebvre, B., 2003. Heat transfer. In: *Gas Turbine Combustion.* Boca Raton: CRC, pp. 315-355.

Lefebvre, B., 2010. 7. Combustion Noise. In: *Gas Turbine Combustion.* Boca Raton: CRC Press, pp. 293-313.

Lefebvre, B., 2010. Emmissions, regulations. In: *Gas Turbine Combustion.* Boca Raton: CRC Press, pp. 362-364.

Lefebvre & Ballal, 2010. 7. Combustion Noise. In: *Gas Turbine Combustion.* Boca Raton: CRC Press, pp. 293-313.

Lefebvre & Ballal, 2010. Emmissions, regulations. In: *Gas Turbine Combustion.* Boca Raton: CRC Press, pp. 362-364.

Lefrancois, E. & Boufflet, J.-P., 2010. An Introduction to Fluid-Structure Interaction: Application to the Piston Problem. *Society for Industrial and Applied Mathematics Review,* 52(4), pp. 747-767.

Lighthill, M., 1952. On sound generated aerodynamically. I. general theory.. *Royal Society of London Proceedings Series A,* Volume 211, p. 564–587.

Mathews, D. C. & Rekos, N. F., 1977. Prediction and Measurement of Direct Combustion Noise in. *Journal of Aircraft,* 14(9), pp. 850-859.

Nakamura, T. & Kaneko, S., 2008. 6. Acoustic Vibration and Noise Caused by Heat. In: *Flow Induced Vibrations: Classifications and Lessons from Practical Experiences.* Amsterdam: Elsevier, pp. 247-277.

P.Y. Ho, V. D., 1979. *Combustion Noise Prediction Update,* s.l.: AIAA Paper 79-0588.

Polifke, w., Poncet, A., Pascherette, C. & Dobbeling, K., 2001. Reconstruction of Acoustic Transfer Matices By Instationary Computational Fluid Dynamics. *Journal of Sound and Vibration,* 245(3), pp. 483-510.

Polifke, w., Poncet, A., Pascherette, C. & Dobbeling, K., 2001. Reconstruction of Acoustic Transfer Matices By Instationary Computational Fluid Dynamics. *Journal of Sound and Vibration,* 245(3), pp. 483-510.

Pożarlik, A., 2010. *VIBRO-ACOUSTICAL INSTABILITIES INDUCED BY COMBUSTION DYNAMICS IN GAS TURBINE COMBUSTORS,* Enschede: University of Twente.

Rayleigh, J., 1896. *The Theory of Sound.* London: Macmillan.

Richards, G., 1996. *Gas Turbine Combustion Instability.* St Louis, Spring Technical Meeting of the Central States Section of the Combustion Institute.

Sandberg, G., Wernberg, P.-A. & Davidsson, P., 2009. *Fundamentals of Fluid-Structure Interaction,* Lund: CISM.

Shivashankara, B. & Crouch, R., 1977. Noise Characteristics of a Can-Type Combustor. *Journal of Aircraft,* 14(8), pp. 751-6.

Siddeley, B., 1961. *Proteus 765 Series Engine.* Bristol: Bristol Siddeley Engines Limited.

Singh, S., Hansen, C. H. & (2, C. Q. H., 2008. *A detailed tutorial for evaluating in-duct net acoustic power transmission in a circular duct with an attached cylindrical Helmholtz resonator using transfer matrix method.* Geelong, The University of Adelaide.

Soucek, O., 2012. *Charles University, Applied Mathematics, Geophysics.* [Online]
Available at: http://geo.mff.cuni.cz/jednooci_slepym/os-FSI-intro.pdf
[Accessed 12 May 2017].

T. Nakamura, S. K., 2008. 6. Acoustic Vibration and Noise Caused by Heat. In: *Flow Induced Vibrations: Classifications and Lessons from Practical Experiences.* Amsterdam: Elsevier, pp. 247-277.

Tinga, T., 2006. Gas Turbine Combustor Liner Life Assessment Using a Combined Fluid/Structural Approach. *Journal of Engineering for Gas Turbines and Power,* pp. 69-79.

Topiwala, J., Mistry, G., Patel, S. & Umrigar, P., 2016. Fluid Structure Interaction: Fundamentals and Application - A Review. *The International Journal of Research in Mechanical Engineering and Technology ((IJRMET),* 6(2), pp. 65-68.

TutorVista, 2015. *Gas Turbine Generator.* [Online]
Available at: http://www.tutorvista.com/physics/gas-turbine-generator

Appendix

A - Gas Turbine Combustor Design

Appendix A Contents

Appendix A Contents ..... Aii
Appendix A Figures ..... Aiii
A1. Introduction A1
A2. Gas Turbines A2
A3. Combustor development A4
A4. Combustor arrangement A7
A5. Combustor components A8
A.5.1 Fuel Atomiser A9
A.5.2 Ignition A11
A.5.3 Diffuser A13
A.5.4 Flame Stabilisation A14
A.5.5 Liner design A14

Appendix A Figures

Figure A1: Brayton cycle T-S diagram A2
Figure A2: Turbine components and energy flow A3
Figure A3: Axial flow gas turbine with 9 compressor stages and 4 turbine stages (TutorVista, 2015) .. A3
Figure A4: Simplest form of combustor A4
Figure A5: Simple combustor with diffuser A5
Figure A6: Simple combustor with diffuser and swirler A5
Figure A7: Temperature profile of combustor output as a function of the radius of the turbine blade A6
Figure A8: Simple design of a typical combustor A6
Figure A9: Combustion zones and components of typical combustor (Hossaini, 2013) A7
Figure A10: Can, Can Annular and Annular combustor arrangements A7
Figure A11: Faired (top) and Dump (bottom) Diffusers (Lefebvre, 2003) A13
Figure A12: Wigglestrip film cooling (Lefebvre, 2003) A17
Figure A13: Stacked Ring film cooling (Lefebvre, 2003) A17
Figure A14: Splash Cooling film cooling (Lefebvre, 2003) A18
Figure A15: Machined Ring film cooling (Lefebvre, 2003) A18
Figure A16: Two forms of Rolled Ring film cooling (Lefebvre, 2003) A18
Figure A17: Z-Ring film cooling (Lefebvre, 2003) A19

A1. Introduction

This Appendix serves to summarise the literature reviewed in undertaking this investigation into the effects of the acoustic loading of a gas turbine combustor liner. The review is presenting in a sequential format, first focussing on the equipment being studied and progressing to the theoretical aspects of the study before citing previous attempts to integrate these aspects.

Throughout the literature, the multi-disciplinary nature of the multi physics problems that need to be solved in order to conduct this investigation are emphasised. The difficulties that these present and the skills required to overcome these difficulties are repeatedly noted, not just in the overall analysis, but in the various fields of study that need to be mastered before integrating them into a coherent whole.

The discussion of the design of gas turbines and, in particular, the components and configuration of combustors, is the first of these areas to be mastered. It is considered to be particularly relevant to this project as it informs which aspects of the design are essential to the various models and what limitations will arise by the necessary simplifications made therein. It also serves as a reminder that every aspect of the design of a combustor constitutes an entire field in its own right, and a solid grounding in these areas is necessary in order to complete a project with the integrative nature of this one.

After a detailed review of the construction of a typical, can type combustor, the noise produced in this combustor is briefly discussed. The nature of this noise is then examined and the fields of Thermoacoustics and Aeroacoustics are introduced as the sources of this noise. Several interesting applications and areas of interest of are described in order to get a sense of the scope of these fields.

From the treatment of the noise, attention is then turned to the study of Fluid Structure Interaction, which is the study of the effect of the fluid on a mechanical structure and vice versa. Again, the areas of application of this field of study are described in order to get a sense of the scope and as an indication on where further reading and sources of upskilling may be found for future efforts in this project.

Finally, previous works around the specific aim of this project, the investigation into the effects of acoustic loads on the liners of gas turbine combustors is examined. While some interesting points are noted as to the strategies undertaken to integrate

the various theoretical aspects of this problem, the emphasis of this review is on the individual components of the problem and of the theory behind the design of the technology that is the source of the questions behind this research.

A2. Gas Turbines

A gas turbine is a thermal engine that uses the Brayton Cycle to convert thermal energy into a useful mechanical output. The thermal energy is produced through the combustion of a fuel (which may be liquid or gas, the name gas turbine refers to the working medium, heated air, compared to steam) and the mechanical work produced may be transmitted either through an output shaft or in the form of an accelerated airflow for propulsive purposes. The different stages of an ideal, air standard, Brayton Cycle (shown in **Figure A1**) consist of; Isentropic compression (1-2), Isobaric heat addition (2-3) and Isentropic expansion back to atmospheric pressure (3-4). As the exhaust gas cools back to atmospheric temperature, it returns to state 1, although this obviously does not take place in the machine itself

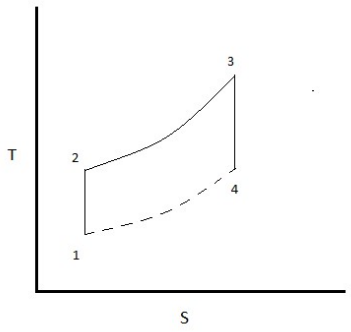


Figure A1: Brayton cycle T-S diagram

The turbine may be thought of as having three basic components that combine to create the above process. The Compressor draws in a quantity of air at state 1 and raises it to the pressure of state 2. The air reacts with the burning fuel, raising its temperature at a constant pressure. This high energy air expands through the turbine, which extracts enough energy to run the compressor and drive the output shaft, for turbo shaft engines (as in **Figure A2**) or, in the case of a turbo-jet engines, the hot gas is directed through a nozzle, providing propulsive power.

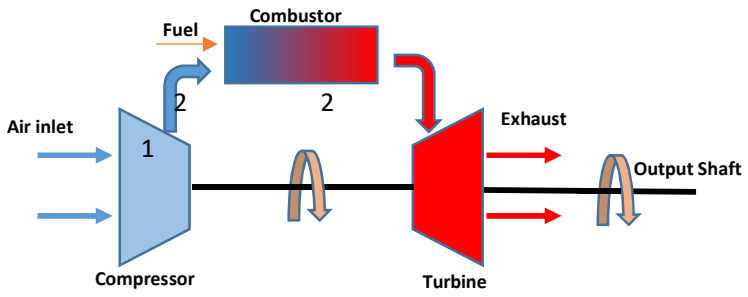


Figure A2: Turbine components and energy flow

These components may be arranged in various configurations, depending on the application. The first distinction to be made is whether the flow through the rotating components (compressor and turbine) remains constantly axial (parallel with the shaft) or if it changes between radial and axial. These components are termed axial compressors and turbines, for the axial flow, and centrifugal compressors and radial turbines for radial/axial flow. As a rule of thumb, radial components are better suited to medium head and medium flow situations and may tolerate a wider operating range. Axial components are more suited to high flow, low head situations and have a fairly narrow operating range.

The amount of shaft work required will typically necessitate a division of the rotating components over a series of stages. The reason for this is that the larger the pressure gradient across a stage, the higher the associated losses. This effect is more pronounced for the compressor than the turbine, and it is therefore usual to see more compressor than turbine stages (as in Figure A3). Axial components lend themselves to multi-staging better than their radial counterparts, making them a superior choice for propulsive aero applications as well as larger industrial power generating applications.

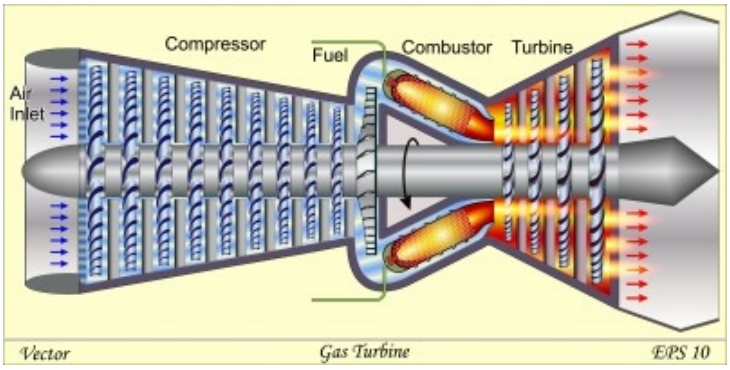


Figure A3: Axial flow gas turbine with 9 compressor stages and 4 turbine stages (TutorVista, 2015)

The work produced by the gas turbine may be in the form of propulsive power or in work transferred to a shaft. Propulsive, jet engines are found in aircraft applications, with aerodynamics dictating the necessity of a small cross sectional area and as good a power to weight ratio as possible. In ground based, turboshaft applications however, there is more tolerance for weight and size of components, with reliability and maintainability, along with operational efficiency, the primary design requirements, making radial designs more attractive.

The rotating components of a turboshaft machine may operate on a common shaft, if the load and speed are expected to be reasonably constant. For loads and speeds that are expected to vary considerably, a better option is to fit a second, low pressure turbine after the high pressure turbine that drives the compressor, with the two turbines on separate shafts. The superior response to varying load has made the use of aero-derivative gas turbines (where the design for a turbojet turbine is used, with the low pressure turbine replacing the exhaust nozzle) very popular in electricity generation applications (Boyce, 2012).

A3. Combustor development

The function of the combustor is to provide the heat addition section of the Brayton Cycle described in section A2 and achieves this through the burning of fuel. The simplest possible form of combustor is shown in Figure A4, with fuel injected into an airstream in a straight walled combustion chamber. When this fuel is ignited (ignition source not shown), the resulting flame would, in theory, provide the heat required to run the turbine.

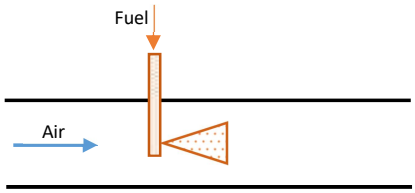


Figure A4: Simplest form of combustor

The pressure loss of the flow through the combustor (ΔP_{hot}) may be described by:

$$\Delta P_{hot} = \frac{1}{2}\rho V^2 \left[\frac{T_4}{T_3} - 1\right] \text{ (Lefebvre, 2003)} \qquad \text{A- 1}$$

Where T_3 and T_4 are the inlet and outlet temperatures of the combustor respectively, V is the velocity of the air through the combustor and ρ is the density of the air.

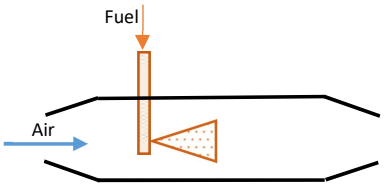


Figure A5: Simple combustor with diffuser

With air velocities from the compressor typically in the region of $170 m.s^{-1}$, the pressure related losses would be unacceptably high in the simple combustor shown in Figure A4. Reducing this flow to the maximum allowable velocity in the combustor of around $15 m.s^{-1}$ is the function of the diffuser, shown in Figure A5.

Unfortunately, the straight through arrangements shown in Figure A4 and Figure A5 do not provide a secure enough "anchor" for the flame and it is necessary to provide an area of low velocity, with a high degree of swirl to ensure that the flame is held in place and provides a stable heat source. One way of achieving this is through the use of a "swirler", as shown in Figure A6, which causes the incoming air to rotate, creating a vortex that collapses in on itself and giving the flame a region of slightly reversed flow in which to be anchored.

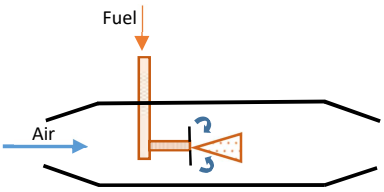


Figure A6: Simple combustor with diffuser and swirler

The air not used in creating this vortex is typically diverted around the combustion liner to be added to the flow further downstream (Lefebvre, 2003). Additional air for combustion is added via a set of primary and then a set of secondary holes in the liner walls. The remaining air is used to dilute and cool the combustion products before they come into contact with the combustor blades.

The root of the turbine blade is particularly susceptible to fatigue failure, while the tip is difficult to cool effectively, meaning that it is desirable for the output profile of the combustor to vary as a function of the radius of the turbine blade (Baskharone, 2006), as per the graph in Figure A7.

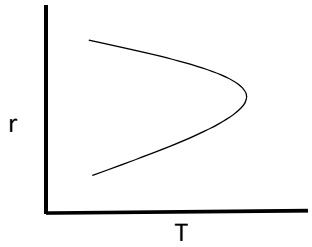


Figure A7: Temperature profile of combustor output as a function of the radius of the turbine blade

The diverted air flow around the combustor flow acts as a cooling mechanism for the liner and is added to the flow within the liner so as to provide an output temperature profile that is acceptable for the turbine blades.

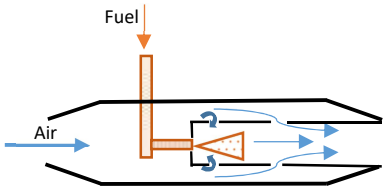


Figure A8: Simple design of a typical combustor

For the typical, diffusor type combustor described above, the airflow through the combustor may be divided into 3 zones of distinct behaviour. The first of these is the primary zone, where the air entering the combustor is deliberately swirled to create a vortex that allows for fuel and air to mix as well as anchoring the flame in place. The second is the intermediate zone, where additional air is provided to the flow to ensure 100% combustion takes place. The third and final zone before exiting the combustor is the dilution zone that adds the remaining air to the flow, lowering the temperature and altering the temperature distribution of the combustor outlet. The length of the dilution zone is typically 55 – 65 % of the combustor. Figure A9 shows a typical combustor, with the discussed zones and components annotated.

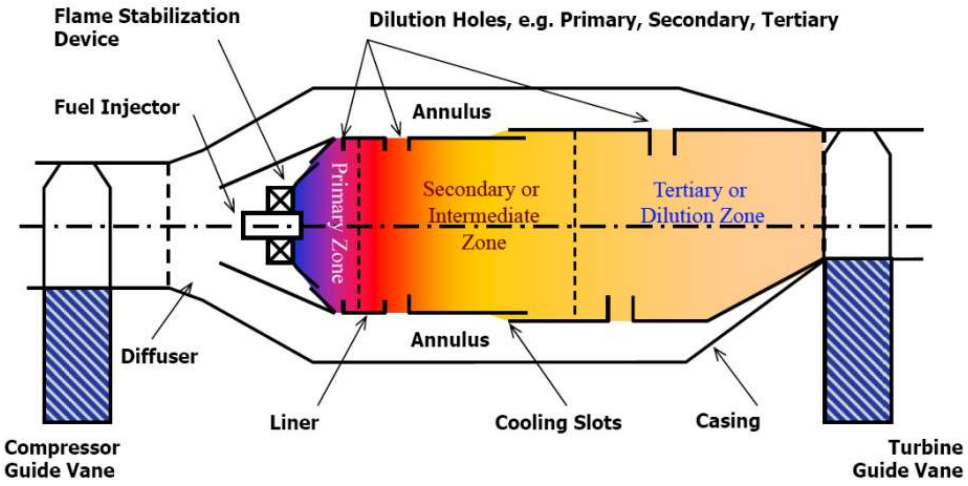


Figure A9: Combustion zones and components of typical combustor (Hossaini, 2013)

A4. Combustor arrangement

Combustors are typically arranged on the gas turbine in one of three ways; Can, Can-Annular or Annular. The three options are shown respectively in Figure A10.

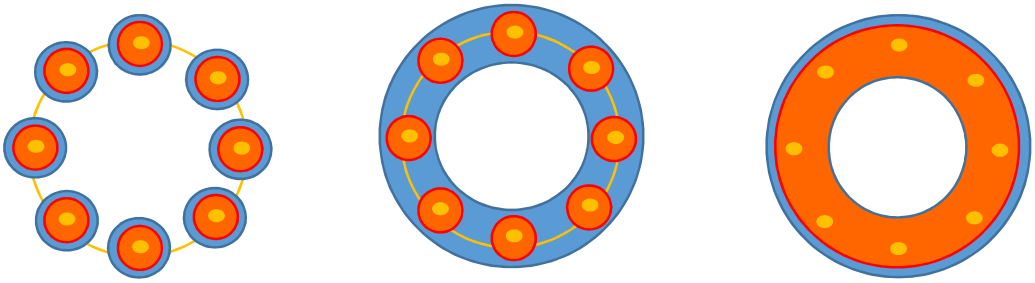


Figure A10: Can, Can Annular and Annular combustor arrangements

Can combustors consist of individual, independent combustors with each combustor having its own casing, liner and burner. They are relatively simple and inexpensive to develop and construct and provide very good access for maintenance. Their disadvantage is that they are typically larger and heavier than their annular counterparts. Can combustors may be mounted concentrically around the turbine shaft or, in the case of industrial applications, alongside in a “silo” arrangement.

Can annular combustors consist of several, cylindrical, combustors arranged circumferentially around the shaft of the gas turbine. The difference between this arrangement and a concentric arrangement of can combustors is that, in this case, the liners are located in a common casing, providing a common annulus. This common annulus gives better flow characteristics than the individual casings of can combustors and are more compact, with a disadvantage of making access to individual burners more difficult.

Can and Can-annular combustors do come with the drawback of having relatively high pressure losses and poor airflow characteristics. The cans are typically linked via flame tubes that allow for easy re-ignition of one can, should its flame blow out.

Annular combustors offer the best performance characteristics of the three arrangements, but are the most costly and difficult to develop. The annular combustor is an annular space with multiple burners, which gives more volume for mixing and less surface area to cool than its can type counterpart.

Regardless of the arrangement, the desired performance characteristics of the combustor are (Boyce, 2012):

- There must be total combustion of the fuel
- The ignition of the fuel must be reliable and smooth
- The flame must be reliable
- There must be low pressure losses (this is proportional to the square of the velocity through the combustor) and minimal pressure pulses and oscillations
- The outlet gas must have an even temperature distribution so as not to cause hot spots on the turbine blades
- The combustor must be durable and maintainable
- Minimal cost and size
- The combustion process must conform to environmental regulations, with minimal soot, smoke and, in particular, NO_x production.

A5. Combustor components

The individual components of the combustor described above are specifically designed to achieve the performance requirements.

A.5.1 Fuel Atomiser

The first of these components deals with the core function of the combustor; heat addition to the air from the compressor outlet, which corresponds to the first stage of combustor development, described in Figure A4.

In order to provide the energy required, fuel needs to be injected to the space in a manner that supports combustion. The fuel to the combustor is atomised to achieve the most efficient combustion possible. In general, the smaller the drops of fuel, the more efficient the combustion as there is more surface area per unit volume to both absorb energy and mix with the air of combustion.

The forces at play in the atomisation of fuel are (Boyce, 2012);

- The disruptive force of the air on the fuel stream
- The surface tension of the fuel, which holds the stream in shape and pulls it into a spherical shape once the stream is disturbed
- The viscosity of the fuel, which resists the deformation of the stream caused by the disruptive forces

The classic mechanism of the atomisation of a jet may be divided into four broad categories, depending of the velocity of the jet relative to the air stream.

Firstly, for low relative velocities, the Reyleigh mechanism is prevalent. In this mechanism, the disruptive force of the air on the jet produce axi-symmetric oscillations that culminate in the stream breaking into drops of roughly equal size (about twice that of the jet diameter).

As the velocity increases, the mechanism of break up remains the same, but with the increased velocity producing oscillations of shorter wavelength that culminate in smaller drops of fuel (roughly the same diameter as that of the jet).

When the relative velocity between the two fluids reaches a sufficient level, the unsteady surface oscillations on the fuel jet become the primary mechanism of disintegration of the flow, producing droplets that are much smaller than the initial jet diameter

Finally, for very high jet velocities, the atomization occurs almost instantaneously after the jet exits the orifice, with no wave propagation and resulting droplets in the order of 80μm. This process is termed “prompt atomization”.

There are several types of design of fuel atomizer, the most simple of which is the “plain orifice” type, which is essentially a hole at the end of a tube that relies on the pressure differential across the orifice of at least 150kPa to produce a thin jet of fuel that is rapidly atomised in contact with the surrounding air.

With the spray pattern produced by the plain orifice atomizer too narrow for practical applications, an improvement of the design is to run the fuel through a swirl chamber before exiting through the orifice. This type of atomiser is termed a “Simplex” atomiser. The swirl chamber imparts a rotating component to the velocity of the fuel and results in the spray pattern forming a hollow cone with a far greater spray angle than that produced by the plain orifice type.

The main disadvantage of this method of fuel atomisation is that the flow rate is proportional to the square of the fuel pressure. This means that a tenfold increase in fuel flow would require a 100fold increase in fuel pressure, which would place an unrealistic demand on the fuel pump.

As a means of reducing the effects of this drawback, the atomiser may be designed with two simplex orifices operating in series, allowing for an increase in flow and response to changes in load to be achieved without too great a change of fuel pressure required.

A further means of reducing the demands on the fuel pump is to use air to augment the pressure differential across the orifice of the atomiser. This is achieved by either air assist or air style atomisers.

With air assist atomisers, the impingement of the augmenting air may be immediately upstream or downstream of the orifice. This way, the injector may be designed for full load conditions and, as the required flow is reduced, air may be added to the jet to maintain pressure. Air assist atomisers have several advantages over their pressure fed equivalents in that they require a smaller fuel pump and use less power, provide better atomization and better mixing of the fuel droplets and the air.

Airblast type atomisers use a similar mechanism to air assist atomisers in that they both make use of the kinetic energy of the air added to the fuel stream to break the fuel up into smaller droplets. Airblast types, however, use significantly more air than air assist types.

An example of an airblast type atomiser is the prefilming atomiser, where the fuel is dispersed in the form of a film that is ensconced between two, counter-rotating

airstreams that impinge on the film of fuel and break it up, while producing the type of hollow cone spray pattern seen in simplex atomisers.

A final method of atomisation is to add the air directly to the bulk flow of the fuel, producing an effervescent mixture that atomises very well once sprayed through the orifice. Unfortunately, the injected air would have to be at the same pressure as that of the fuel stream, necessitating a separate compressor and rendering this method unsuitable for aircraft applications, where the additional weight would be unacceptable.

A.5.2 Ignition

Once the fuel has been atomised, combustion will only be initiated if there is some source of external energy. The process of ignition has been well studied and may be thought of as having three primary phases.

For the first phase of ignition, a spark ignites a small portion of fuel that produces a small kernel of flame that has enough energy to propagate through the primary zone.

The kernel produced in phase 1 then ignites the surrounding air-fuel mixture in the primary zone, leading to sustained combustion.

In the case of can or can-annular combustor arrangements, the flame is finally passed to the surrounding combustor cans through the flame tubes.

The performance of the ignition system of the gas turbine (its ability to ignite the air/fuel mixture in a given situation) is an important requirement in terms of the overall design of the gas turbine, especially in the case of aircraft engines, where re-ignition of a flame that has been extinguished in mid-flight is an obvious safety concern. The ignition needs to be possible in a wide range of ambient conditions, reliable and fast.

Ignition performance is improved with an increase in the amount of energy provided by the ignition system, the as well as the temperature and pressure of the air/fuel mixture. The performance is decreased with an increase in air velocity, fuel drop size and turbulence of the air/fuel mixture.

The most common form of ignition system used in gas turbines is the spark ignition system, much like the use of a spark plug in an internal combustion engine. The

spark ignition system allows for a controllable discharge of very high temperature in a very small area, which is perfect for igniting the kernel of flame in phase 1 of the ignition process.

The design considerations of a spark ignition system are, firstly, its location. The spark must be located in the primary zone and in contact with the spray from the injector in order to have the best effect. The rule of thumb is that the further the igniter protrudes into the combustion chamber, the better the ignition performance and the shorter the igniter's lifespan. For industrial applications, where the re-lighting performance is not as crucial a consideration, the igniter is frequently made to be retractable so as to give the best performance and not affect the lifespan of the igniter.

The performance of the ignitor is directly affected by the energy of the spark and is improved with an increase in the length of path that the spark has to travel. This is due to the increase in resistance of the path, leading to more heat being generated by the spark itself. Increasing the gap width of the igniter, the pressure of the air/fuel mixture or the velocity thereof all have the effect of increasing the spark length and, therefore, the energy output of the igniter.

The duration of the spark is another key performance parameter in determining the amount of energy discharged by the igniter. The optimum duration is regarded to be around 100μs. A duration that is too short leads to the electrical and radiation losses of the system being too high and an excessive duration leads to the energy of the spark being dispersed over too large a volume of air/fuel mixture, rendering it ineffective.

Related to the spark duration is the spark rate, the time taken between sparks. On start-up, as the engine is cranking over, the fuel and air flow rates will vary considerably from optimum operating conditions. Ignition will only take place within the flammability limits of the air/fuel mixture and it may take several tries for this to occur.

The life of the ignitor is affected by the service interval employed, the energy output of each spark, the temperature and oxidising nature of the environment within the combustor and the materials employed in its construction. Plug life may be extended by increasing its diameter, which increases the amount of arcing material (which is eroded slightly on each sparking attempt).

The two primary designs of spark type igniters are flush mounted and sunken. Flush mounted igniters are more costly, mechanically weaker and more difficult to manufacture than recessed ignitors. However, they do provide superior spark energy and igniter life span. Flush mounted igniters are less susceptible to fuel wetting, which makes their re-ignition characteristics more reliable.

A.5.3 Diffuser

The necessity of the reduction in velocity from the compressor outlet to the combustor inlet has already been discussed in Section A3, with diffusion the method used to achieve this in a traditional combustor design.

The diffusor may be faired, giving gradual changes in pressure and velocity and low associated losses. Unfortunately, this gradual flow happens over a significant length, which isn't always available for the given size constraints of the overall combustor design. In addition, faired diffusers are susceptible to input fluctuations from the upstream compressor and their long length renders them more susceptible to thermal distortion and manufacturing fluctuations (Lefebvre, 2003)

In order to avoid these disadvantages, the angle of divergence of the diffuser may be widened and "dump" the airflow into the combustor. These dump diffusers are smaller and lighter than the faired style escribed above. The resulting turbulent flow is less susceptible to upstream fluctuations in the flow, thermal distortion or manufacturer deviations. The downside is that they do carry a heavier penalty in the form of pressure losses.

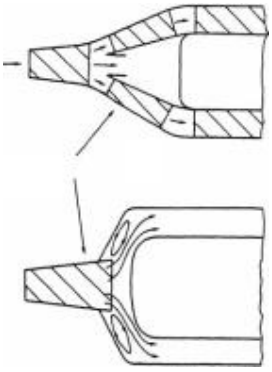


Figure A11: Faired (top) and Dump (bottom) Diffusers (Lefebvre, 2003)

A.5.4 Flame Stabilisation

As discussed around Figure A6: Simple combustor with diffuser and swirlerigniting the fuel/air mixture is of little use in a stream of air flowing at around 25m/s without some form of flame stabilisation, a way of “anchoring” the flame in place. This is achieved through the creation of the primary zone of airflow through the combustor, reverses the flow of the air to make an area of recirculation that entrains the flame and prevents it from being blown out.

This toroidal shaped flow zone is created through the use of swirler vanes around the fuel injector as well as a single row of holes located circumferentially around the liner. As a rule of thumb, a smaller number of larger holes in the liner has the effect of maximising the stability of the flame in the primary zone.

The swirler vanes serve to provide a cone shaped vortex that, when given a sufficiently high degree of rotation, breaks down and recirculates the flow through its core due to a drop in the static pressure within this core. This method has the added advantage of providing excellent mixing characteristics due to the high degree of turbulence produced. The flow through the swirler may be axial or radial, with axial being the more common and better understood.

The amount of flow imparted by an axial swirler is characterised by the non-dimensional “swirl number” (S_n), governed by the axial momentum and thrust of the flow related to the swirler’s diameter. For S_n values less that 0.4, the swirl is said to be weak, with no recirculation taking place. There is a transition period between S_n values of 0.4 and 0.6, after which the swirl may be said to be strong and produces good recirculation.

The design of the vanes of the swirler contribute directly to the size of the recirculation zone produced. This may be increased by increasing the vane angle, increasing the number of vanes, decreasing the vane aspect ratio or changing from flat to curved vanes. Curved vanes are more efficient and create a higher degree of swirl. Flat vanes, however, are cheaper to produce and the stall regions produced after each vane contribute to greater flame stabilisation and reduction in combustion noise.

A.5.5 Liner design

The production of the three zones of flow within the combustor is a function of the combustion liner. In addition, the liner must be able to operate in the hostile environment of the combustion zone and handle the temperatures and pressures produced. The design of the liner reflects these functions.

The flow zones are created through the injection of air from the annulus between the casing and liner, through perforations around the circumference of the liner, designed to produce the desired airflow. The flow of the jets of air through these perforations has been well studied as to their depth of penetration into the main flow of the liner, their mixing characteristics and the discharge coefficient of the perforations (Lefebvre, 2003).

The penetration of the jet into the main flow stream is dependent on several factors: the diameter of the perforation, the relative velocities and densities of the two streams, the number of perforations in the plane and whether or not they are directly opposed and, finally, the angle of penetration of the jet.

This angle of penetration may be described by the equation:

$$(\sin\theta)^2 = \frac{C_D}{C_{D\infty}}$$ (Lefebvre, 2003) A-1

Where C_D is the discharge coefficient of the jet and $C_{D\infty}$ is the maximum discharge coefficient of the hole in question. A shallower angle has the effect of reducing the radial component of the flow as well as the effective diameter of the hole, both of which lead to less penetration of the jet into the flow.

The discharge coefficient (C_D) is a measure of the efficiency of the flow through the hole, with a higher C_D giving a more stable flow, but coming with the cost of an increase in size. The value of C_D is dependent on the type, shape and spacing of the hole, the pressure drop through the liner and its static pressure as well as the swirl and velocity profiles of the flows.

The ability of the injected air to mix with the gases already present in the liner is important in all three of the zones. The primary zone uses the flow to creating the flame stabilization flow vortices as well as to provide oxygen for continued combustion. The intermediate zone requires good mixing to ensure complete combustion of the remaining combustion products. The dilution zone has specific mixing requirements to produce the desired pattern factor at the combustor outlet.

The ability of the jet to mix with the liner flow is dependent on the following factors; the size and shape of the hole, the number of holes and penetration factor, the length of the liner and the relative temperatures and velocities of the two flows. An additional factor to be considered is the momentum flux ratio, typically denoted as J.

The flow through the annulus of the combustor provides the source of the air injected through the liner holes. It has been found that a slower flow leads to better performance as it is more steady, gives a constant pressure along the liner, better C_D values for the holes (and, therefore, steeper angles of penetration) and fewer losses.

As mentioned above, the design of the liner wall needs to allow it to be able to handle the temperatures and pressures arising from the combustion process. For the case of an uncooled liner wall, the sum of the heat transferred to the inner wall of the liner by radiation and convection will be equal to the heat conducted through the liner which, in turn, is equal to the sum of the heat transmitted via radiation and convection from the outer wall of the liner to the annulus airflow. The temperatures produced in this uncooled wall would typically be in the region of 2100ºC, far beyond the melting point of the materials used in the construction of the liner.

These temperatures motivate the use of cooling methods for the liner wall to promote mechanical integrity and durability. The norm is to make use of the annulus air flow to create a thin film of cooling air over the inner wall of the liner to prevent the convective heat addition and to remove some of the heat absorbed through radiation. This film is created through the use of circumferential rings, giving the liner the appearance of an extended telescope.

The rings may be formed through several methods, the most simple of which is through the use of wigglestrips (Figure A12). The wavy wigglestrips are used to join the segments of the liner to allow a portion of the annulus flow to be diverted to the inner wall of the liner. Wigglestrips provide very good mechanical strength, but have the disadvantage of producing poor airflow characteristics.

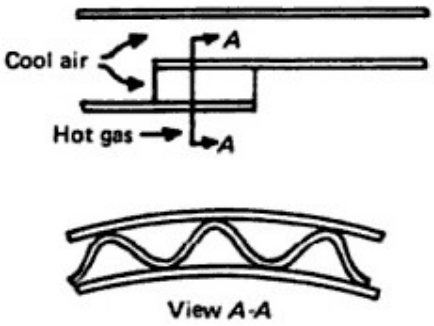


Figure A12: Wigglestrip film cooling (Lefebvre, 2003)

A method that provides superior airflow to that of wigglestrips is a stacked ring (Figure A13), which replaces the wigglestrips with a bend in the mating surface of the liner segments and machining holes to provide the cooling film. Stacked rings lack the rigidity of wigglestrips, but the precise nature of the machined holes allows for very accurate airflows and velocities to be produced.

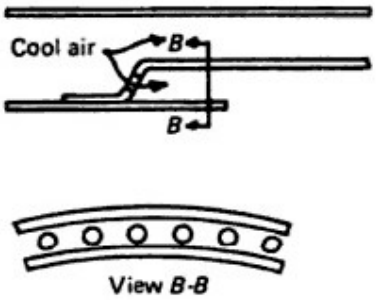


Figure A13: Stacked Ring film cooling (Lefebvre, 2003)

Instead of making use of the total pressure drop across the liner, it is possible to only make use of the static pressure drop through the use of the splash cooling method (Figure A14). In this case, the liner annulus is constant, with a lip brazed to the inner surface of the liner and holes machined in the liner to provide the cooling air flow. The length of the lip is typically four times the diameter of the holes.

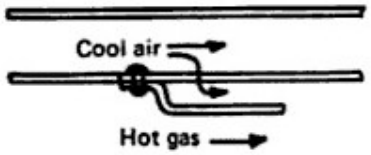


Figure A14: Splash Cooling film cooling (Lefebvre, 2003)

An obvious point of concern for the splash cooling method is the strength and durability of the brazed joint that attaches the lip to the liner. One means of overcoming this concern is to machine the liner to include the lips (Figure A15), obviating the need for the brazed joint. This method of producing the cooling film is termed Machined Ring and has an additional advantage in that the inlet holes may be machined to make use of the total pressure or static pressure drops across the liner, or a combination of both.

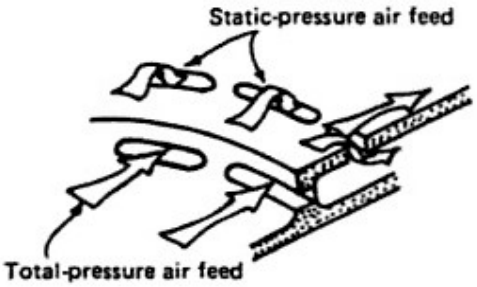


Figure A15: Machined Ring film cooling (Lefebvre, 2003)

A problem that arises with both machined and splash cooling methods is the production of hot spots in the lips that threaten the mechanical integrity of the design. In order to combat this, use is made of a double pass method known as Rolled Ring film cooling (Figure A16).



Figure A16: Two forms of Rolled Ring film cooling (Lefebvre, 2003)

Instead of using of a lip to make use of the static pressure drop to provide the cooling film, it is possible to have a raised portion of the liner in which many, very small, holes are drilled (Z-Ring, Figure A17). The resulting structure is mechanically simple, with few separate parts, but comes at a high cost of manufacture.

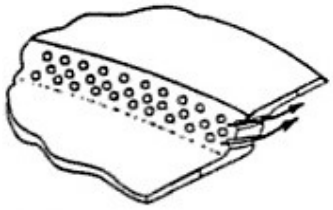


Figure A17: Z-Ring film cooling (Lefebvre, 2003)

In general, the disadvantage found in the use of film cooling methods on liner walls is that the cooling effect is not constant. The cooling effect is naturally higher closer to the inlet of the cooling air, where the temperature is lowest, and decreases as the film grows further from the inlet.

A way to provide uniform cooling over the length of the liner would be to allow for some sort of transpiration of the cooling air through the liner. This may be achieved through the use of porous or laminated materials to construct the liner or through effusion techniques similar to that used in the Z-ring film cooling technique. The transpiration methods here have an advantage in that the cooling effect occurs not only across the entire length of the liner, but through the entire wall thickness as well, allowing for good cooling efficiency. The drawbacks of these methods are that they required a high mass flow rate of air through the annulus, may lead to difficulties in maintenance and (for angled effusion in particular) require 20% thicker liner walls to be used.

In addition to the methods listed above, the cool side of the liner wall may be augmented, through the use of roughening, fins, ribs or wire, to provide a greater conductive cooling effect through the width of the liner wall.

The materials used in the construction of the liner have an effect on the amount of cooling required and, while not a cooling method per say, the use of reflective thermal barriers and tiles on the inner walls of the liners reduce the amount of heat absorbed. The use of tiles obviously carries a weight penalty, rendering them of more interest to stationary industrial applications than aircraft propulsion.

Some desired properties of the materials used in liner construction are;

- High strength under high temperatures
- Resistance to thermal expansion and fatigue
- Inexpensive and easy to fabricate
- Resistant to oxidation
- Low thermal conductivity
- Low density
- High Young's modulus

In order to meet these requirements, as well as the required service life of 15 000hr for Marine, 25 000 flights for Aero and 100 000hr for industrial applications; Metal alloys Nimonic 75, 203 and 83 and Hastelloy HSS Haynes 188 are commonly used in the fabrication of gas turbine liners (Lefebvre, 2003).

Appendix

B - Proteus Combustor

Appendix B Contents

Appendix B Contents ..... Bii
Appendix B Figures ..... Biii
Appendix B Tables ..... Biii
B1. Introduction B1
B2. Proteus engine B1
B3. Proteus Engine Combustor B3
B4. 3D Model of Proteus Combustor B10

Appendix B Figures

Figure B1: Bristol Proteus 790 series engine B1
Figure B2: Schematic of Proteus Engine B2
Figure B3: Design of Proteus Combustor (Siddeley, 1961) B3
Figure B4: Combustor on Proteus gas turbine engine B4
Figure B5: Layout of combustor liner design B5
Figure B6: Soot pattern around swirler B6
Figure B7: Soot pattern around secondary holes and cooling strip. B7
Figure B8: Dilution holes B7
Figure B9: Diffuser and burner B8
Figure B10: Schematic of Proteus Combustor Burner (Siddeley, 1961) B9
Figure B11: Nozzle and swirl chamber of fuel injector B9
Figure B12: Outlet of combustor. B10
Figure B13: 3D Model of Proteus Combustor used as the basis for the models developed in this project B11

Appendix B Tables

Table B1: Information from Gas flow diagram of Proteus Engine B2
Table B2: Information from Gas flow diagram of Proteus Engine (SI) B3
Table B3: Proteus combustor components B4

B1. Introduction

This Appendix serves to describe the engine used to obtain the geometry and boundary conditions for the models of this project. These inputs to the models are taken from the example of a Bristol Proteus Gas Turbine engine that resides in the Aerospace Laboratory at the University of the Witwatersrand (Figure B1).

B2. Proteus engine

The engine used as the basis for the geometry and boundary conditions of the models throughout this project is a Bristol Proteus Mark 790 (serial number: 79087). The Proteus was first put into production in 1947 (FLIGHT, 1954), with this particular engine manufactured in 1954 and has a rated output of $3000\mathrm{kW}$ at $12000\mathrm{rpm}$ and fuel consumption of $1241\mathrm{l.h^{-1}}$.



Figure B1: Bristol Proteus 790 series engine

The engine is a makes use of a 12 stage axial compressor, followed by a single radial stage that uses $5740\mathrm{kW}$ to achieve a compression ratio of 7.2:1. The diagram in Figure B2 shows the layout of the compressor, which is driven by the external spool of the shaft, which is in turn powered by the first two stages of the turbine.

The reverse flow arrangement of the gas is also visible as it passes through the compressor, then turns and runs back through the combustor and turbine.

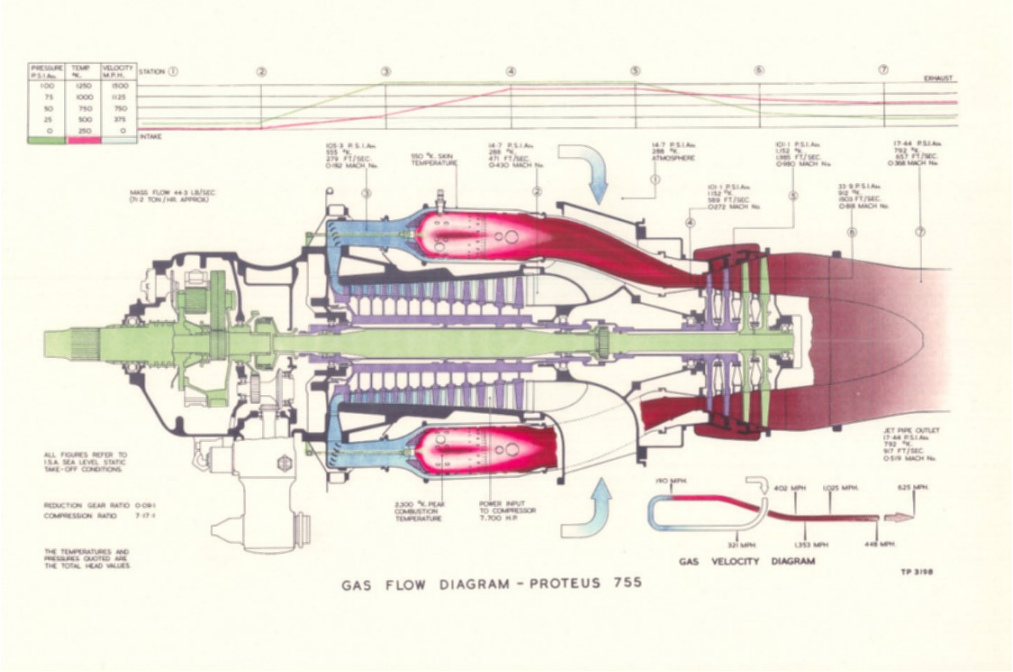


Figure B2: Schematic of Proteus Engine

The physical properties of the gas at various stages of the process are also depicted in Figure B1 and are consolodated in Table B1.

Table B1: Information from Gas flow diagram of Proteus Engine

Total Mass Flow	44,3	lb/s
Power input to compressor	7700	hp
Output pressure of compressor	102	psi
Outlet velocity of compressor	270	ft/s
Outlet Mach number of compressor	0,182	-
Outlet temperature of compressor	555	K
Peak Combustion Temperature	2500	K
Skin temperature of combustor	550	K
Output pressure of compressor	14,7	psi
Outlet velocity of compressor	421	ft/s
Outlet Mach number of compressor	0,35	-
Outlet temperature of compressor	299	K

These values are converted to SI units to be used as inputs to the CFD models produced in ANSYS CFX and described in Appendix C.

Table B2: Information from Gas flow diagram of Proteus Engine (SI)

Total Mass Flow	20	kg/s
Power input to compressor	5741	kW
Output pressure of compressor	7,24	bar
Outlet velocity of compressor	82	m/s
Outlet Mach number of compressor	0,182	-
Outlet temperature of compressor	555	K
Peak Combustion Temperature	2500	K
Skin temperature of combustor	550	K
Output pressure of compressor	1	Bar
Outlet velocity of compressor	123	m/s
Outlet Mach number of compressor	0,35	-
Outlet temperature of compressor	299	K

B3. Proteus Engine Combustor

The combustors of the Proteus engine are arranged in a can annular format, with the design of an individual combustor shown in Figure B4.

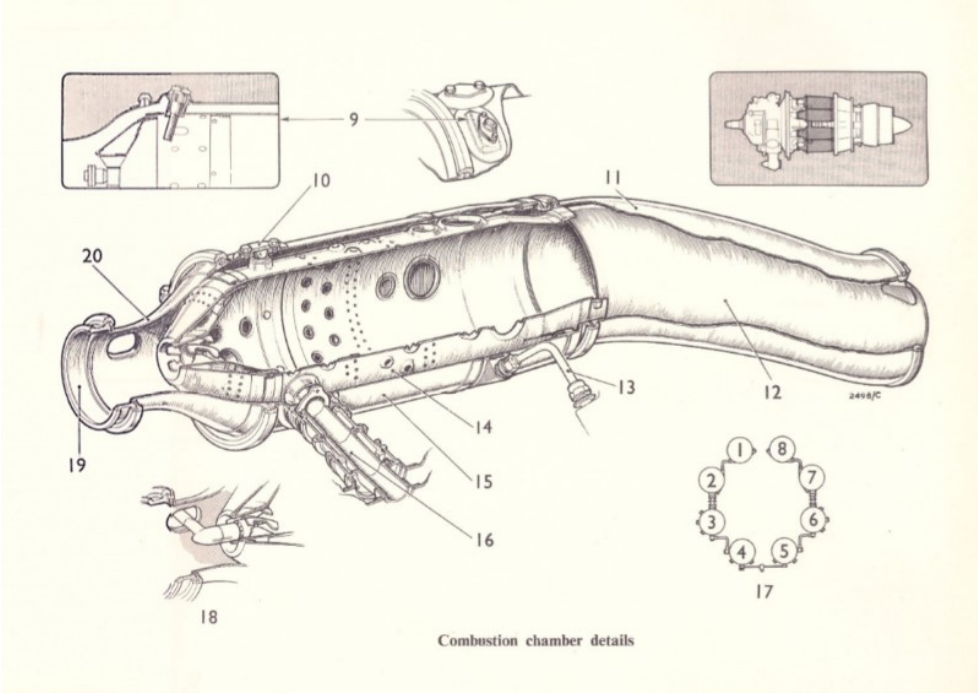


Figure B3: Design of Proteus Combustor (Siddeley, 1961)

The labels for the numbered components in Figure B3 are given in Table B3, with the function of these components discussed in Appendix A of this report.

Table B3: Proteus combustor components

1	Combustion Chamber	11	Air Casing
2	Combustion Chamber	12	Liner
3	Combustion Chamber	13	Drain Pipe
4	Combustion Chamber	14	Flame Tube
5	Combustion Chamber	15	Outer Casing
6	Combustion Chamber	16	Interconnector
7	Combustion Chamber	17	Combustion Chamber Drain System
8	Combustion Chamber	18	Burner Location
9	Glow Plug Location	19	Sleeve
10	Locating Plug	20	Expansion Chamber (Diffuser)

This combustor was removed from the engine and its dimensions measured and used to create the 3D model in Solid Edge, the geometry upon which all other models in this project were based.



Figure B4: Combustor on Proteus gas turbine engine

The layout of the holes in the combustion liner, with the swirler, cooling slots, primary and secondary holes and dilution holes all clearly visible, is shown in Figure B5. The radial and axial distribution of each feature was measured, along with the diameters of the holes and angle of the swirler blades. The overall layout is in close

agreement with the principles of gas turbine combustor design described in (Lefebvre & Ballal, 2010).



Figure B5: Layout of combustor liner design

In Figure B5, the soot patterns give an insight into the flow patterns that have been experienced in this particular liner. The effect of the cooling slots is especially visible here.

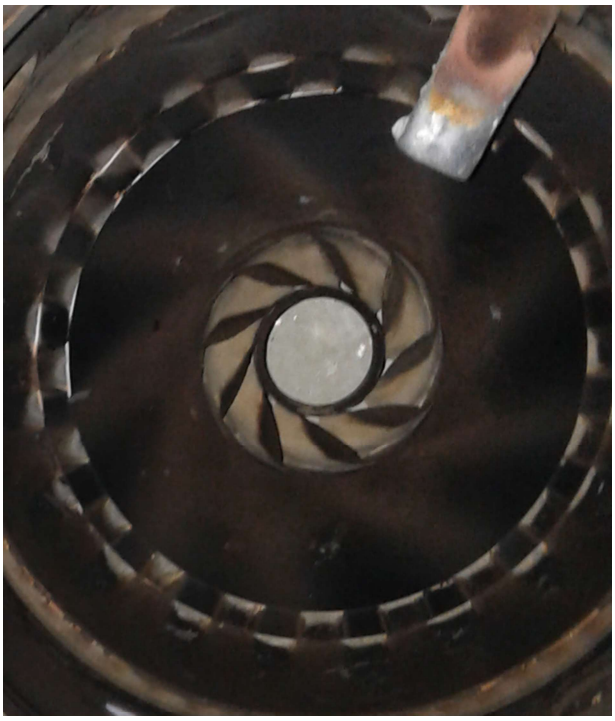


Figure B6: Soot pattern around swirler

Figure B6 shows that there is a strongly radial aspect to the flow out of the swirler, which is often ignored in discussions on swirler design as the emphasis is usually placed on the tangential aspect of the flow (which is what produces the vortex breakdown that serves to anchor the flame).

The soot patterns around the secondary air injection holes and second cooling strip are shown in Figure B7. In this figure, the main flow would be from left to right, and it can be clearly seen that the secondary holes have a lip that forces the angle of penetration of the jets back into the flow, creating the lighter segment of the soot pattern around the upstream sides of the holes. The exact same patterns are visible around the primary holes and cooling slots and are not shown here.

The effect of the cooling strip is illustrated by the contrast in the coloration before and after the cooling film is introduced to this section of the liner, with the area of the liner immediately after the strip appearing almost untouched by soot and flame and the preceding area heavily darkened.



Figure B7: Soot pattern around secondary holes and cooling strip.

As with the secondary holes, it is apparent from Figure B8 that the dilution holes also use a slight lip to direct the angle of their jets, though not to as pronounced a degree as the secondary holes.

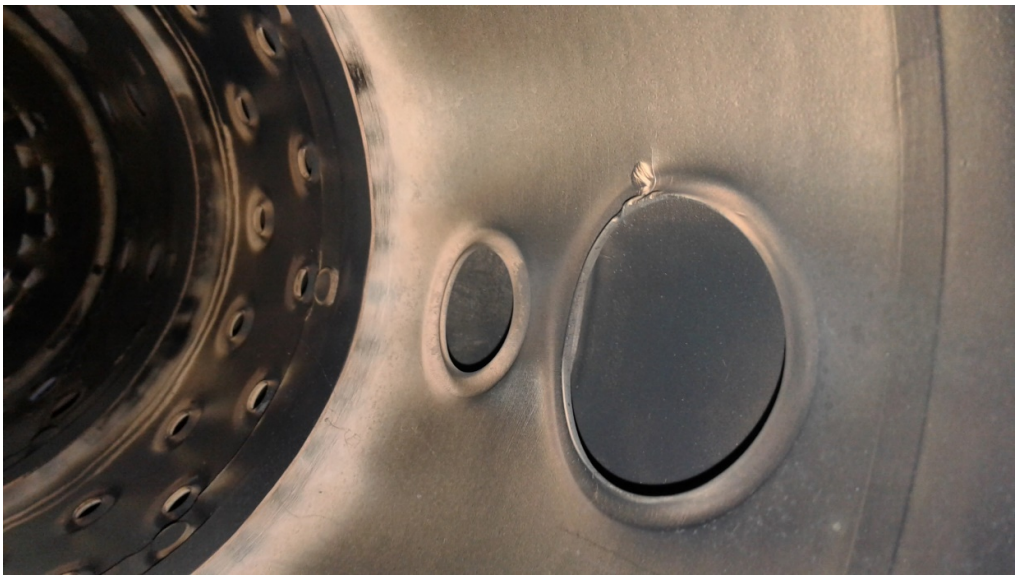


Figure B8: Dilution holes

The air from the dilution has the effect of greatly reducing the temperature of the gas coming from the combustion zone, which accounts for the lighter colouring of the liner in this area. The relative size and spacing of these holes is as predicted by theory in (Lefebvre & Ballal, 2010) and (Baskharone, 2006) in order produce the desired outlet pattern factor to the turbine.

The diffuser (refered to as the “expansion chamber” in the manual) and burner are shown in Figure B9. While the actual diffuser has a distinctly curved shape, this was modelled as a linear cone to simplify the geometry and subsequent meshing of the CFD models.



Figure B9: Diffuser and burner

The mounting arrangement of the burner is shown in Figure B9, with the burner inserted into the hole in the middle of the swirler, visible in Figure B6. Figure B10 describes the internal layout and function of the burner.

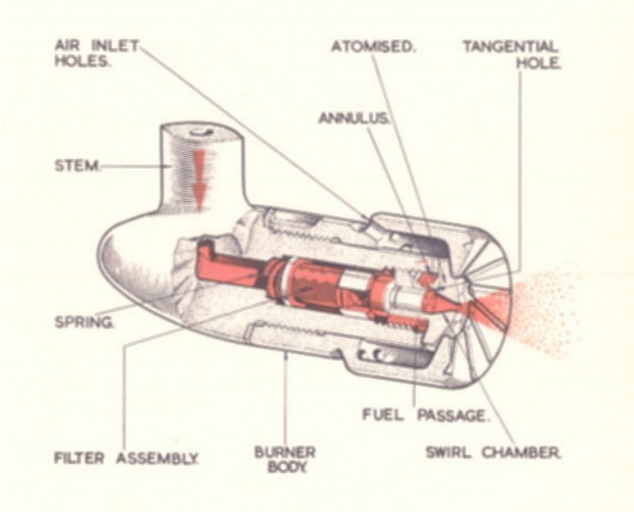


Figure B10: Schematic of Proteus Combustor Burner (Siddeley, 1961)

The nozzle and swirl chamber of the burner are shown in Figure B11. Instead of modelling the entire burner, the hole in the swirler was made solid and the injector simplified to a single hole on this surface.



Figure B11: Nozzle and swirl chamber of fuel injector

Finally, the outlet of the combustor to the first stage of the tubine is shown in Figure B12. This was initially assumed to be of constant diameter (and was modelled as such), but was then discovered to be in the form of a nozzle, which increases the velocity of the gas reaching the turbine blades.



Figure B12: Outlet of combustor.

The configuration of the outlet of the combustor is of interest in the context of an acoustic analysis of the liner, as it will determine the impendence characteristics of the duct. While it was initially thought that the liner would behave as an open ended duct with an outlet impedance, this configuration indicates that it may be possible to assume this boundary to be sufficiently hard to make the assumption of a closed duct a valid one.

B4. 3D Model of Proteus Combustor

With the dimensions and simplifications described above, a 3D model of the combustor was produced in Solid Works and exported to ANSYS Design Modeller (DM) as the first step in an ANSYS Workbench project. The final model in ANSYS DM is shown in Figure B13, with the addition of inlet and outlet transition pieces to assist with the modelling in ANSYS CFX, described in Appendix C.

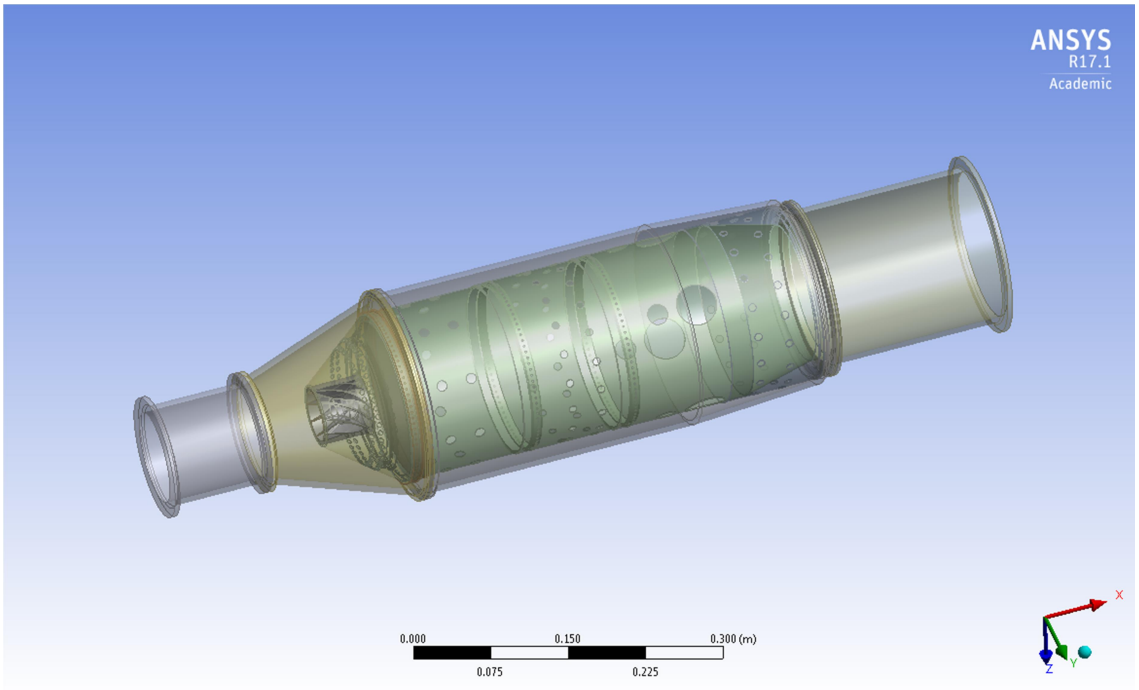


Figure B13: 3D Model of Proteus Combustor used as the basis for the models developed in this project

Appendix

C - ANSYS CFX Models

Appendix C Contents

Appendix C Contents Cii
Appendix C Figures Ciii
Appendix C Tables Civ
C1. Introduction C1
C2. Model 3 ..... C1
C2.1. Geometry, Mesh and Boundary conditions C1
C2.2. Velocity flow fields C2
C2.3. Pressure field C6
C2.4. Verification C7
C3. Model 4 ..... C7
C3.1. Geometry, Mesh and Boundary conditions C7
C3.2. Velocity flow fields (fast model) C9
C3.3. Temperature fields C14
C3.4. Validation C18

Appendix C Figures

Figure C1: Boundary conditions in CFX Pre for Model 3 ..... C2
Figure C2: Velocity vector at inlet of cold combustor C3
Figure C3: Velocity vector and field at inlet of cold combustor C3
Figure C4: Axial velocity in XY plane of Combustor (no flame) C4
Figure C5: Axial velocity in YZ plane of Combustor (no flame) C4
Figure C6: Velocity vector at outlet of cold combustor C5
Figure C7: Velocity field in XY plane of Combustor (no flame) C5
Figure C8: Velocity field in YZ plane of Combustor (no flame) C6
Figure C9: Pressure in combustor (no flame) C6
Figure C10: Mesh used for Model 4 ..... C7
Figure C11: Cross section of mesh used in Model 4 ..... C8
Figure C12: Boundary conditions in CFX-Pre for Models 4 ..... C8
Figure C13: Mach number through fired combustor liner (fast) C10
Figure C14: Mach number through fired combustor liner (slow) C10
Figure C15: Velocity field in ZY plane of fired combustor liner (fast) C11
Figure C16: Velocity field in XY plane of fired combustor liner (fast) C11
Figure C17: Axial velocity field in ZY plane of fired combustor liner (fast) C11
Figure C18: Axial velocity field in XY plane of fired combustor liner (fast) C12
Figure C19: Velocity vector at inlet of fired combustor (slow) C12
Figure C20: Velocity field in XY plane of fired combustor (slow) C13
Figure C21: Velocity field in XY plane of fired combustor (slow) C13
Figure C22: Axial velocity field in XY plane of fired combustor (slow) C13
Figure C23: Axial velocity field in XY plane of fired combustor (slow) C14
Figure C24: Pressure through fired combustor liner (fast) C14
Figure C25: Temperature field in XY plane of fired combustor liner (fast) C15
Figure C26: Temperature field in ZY plane of fired combustor liner (fast) C15
Figure C27: Temperature field, with velocity vector in ZY plane of fired combustor (slow) C16
Figure C28: Temperature field in ZY plane of fired combustor (Slow) C16
Figure C 29: Temperature field in XY plane of fired combustor C17
Figure C30: Planes for sampling temperatures through fired combustor C17
Figure C31: Temperatures at various sample points (slow) C18

Appendix C Tables

Table C1: Verification of results from Model 3 ..... C7

Table C2: Boundary conditions input to CFX-Pre for Model 4 ..... C9

Table C3: Validation of fast run of Model 4 ..... C18

Table C4: Verification of slow run of Model 4 ..... C19

C1. Introduction

This Appendix serves to describe the process and results of the CFD simulation of the air flow and combustion through the combustor of a Proteus gas turbine. This is achieved through two models that are run through a simulation in ANSYS CFX. The first model (Model 3) is purely of the air flow through the combustor, without any combustion occurring. The results of this simulation are used as inputs to a simplified geometry that simulates the full combustion process in Model 4. The input variables of the combustor are then adjusted to give the final temperature field that is used in later acoustic and theoretical models.

While none of the results here are experimentally validated, they are verified by comparing the mass flows in and out of the model. A weak validation is completed by comparing the results of the model to the expected behaviour of the flow within the combustor, both according to theory found in (Lefebvre, 2010) and the service manual of the Proteus engine (Siddeley, 1961)

C2. Model 3

C2.1. Geometry, Mesh and Boundary conditions

The geometry developed in Solid Edge, described in Appendix B, was used in creating the mesh for Model 3 in ANSYS ICEM as part of an ANSYS workbench project. This geometry includes the combustor liner, swirler, diffuser and casing. The small gap between the combustor casing and liner, along with the thin walls of the liner itself made the correct sizing of the mesh in these regions especially crucial.

In order to reduce the complexity of the geometry and associated mesh, the cooling film holes and secondary air holes are not included in this model.

To improve the mesh quality, the interior of the liner was filled with hexagonal mesh elements, creating a more uniform pattern and reducing the work required for calculations in these regions.

Once the mesh was developed and smoothed, it was exported to ANSYS CFX-Pre (**Figure 17:** Boundary conditions in CFX Pre for Model 3Figure C1) to set up the boundary conditions for the calculations. For this model, all walls were set to the "no friction" condition, with the surface at the inlet to the diffuser set as an inlet with a normal velocity of $85\mathrm{m.s^{-1}}$. The outlet of the model was set as an outlet with a reference pressure of $0\mathrm{kPa}$.

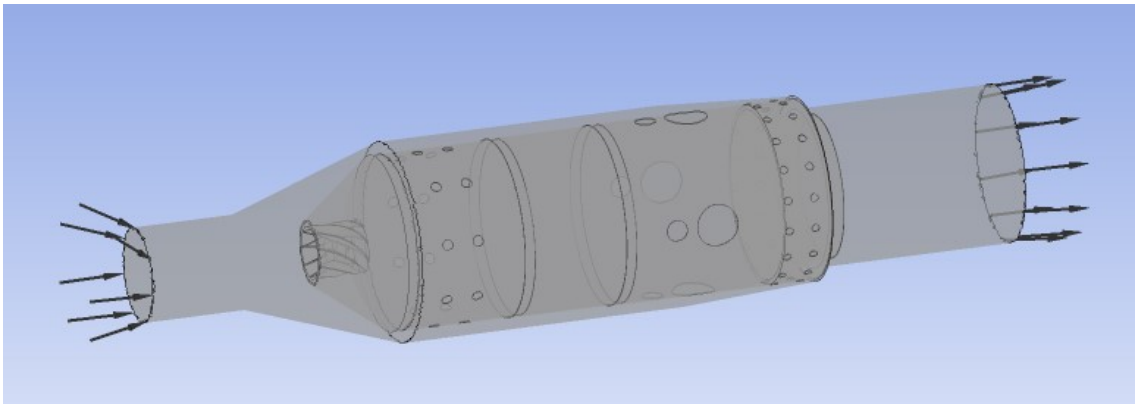


Figure C1: Boundary conditions in CFX Pre for Model 3

C2.2. Velocity flow fields

The first reason for conducting the simulations associated with Model 3 was to confirm that the geometry obtained from the measurements of the Proteus combustor described in Appendix B will give a realistic representation of the flow through a gas turbine combustor. One of the expected characteristics of this flow is the Lucas flow pattern described in (Lefebvre & Ballal, 2010), where the collapsing vortex created by the swirler creates a region of very low (even reversed) velocity flow. This region is vital to ensuring a stable flame in the combustor.

The vector field in **Figure C2** confirms that this circulation of flow does occur for the geometry and input velocity used and shows that the model does give a realistic representation of the flow in a gas turbine combustor.

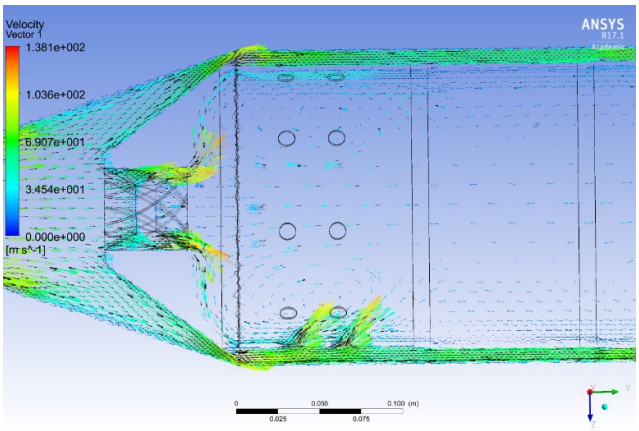


Figure C2: Velocity vector at inlet of cold combustor

An alternative view of this field, shown in Figure C3 shows the region of low velocity in which the flame is anchored. It is this region that is modelled as the “Flame Zone” in the acoustic and theoretical models described in Appendices D and F.

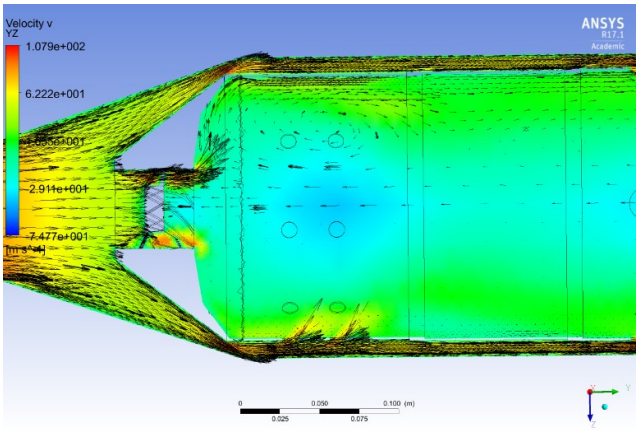


Figure C3: Velocity vector and field at inlet of cold combustor

The axial flow velocities of the entire model in the XY and YX planes are shown in Figure C4 and Figure C5 respectively and show the increase in velocity of the flow once the air from the dilution holes is added.

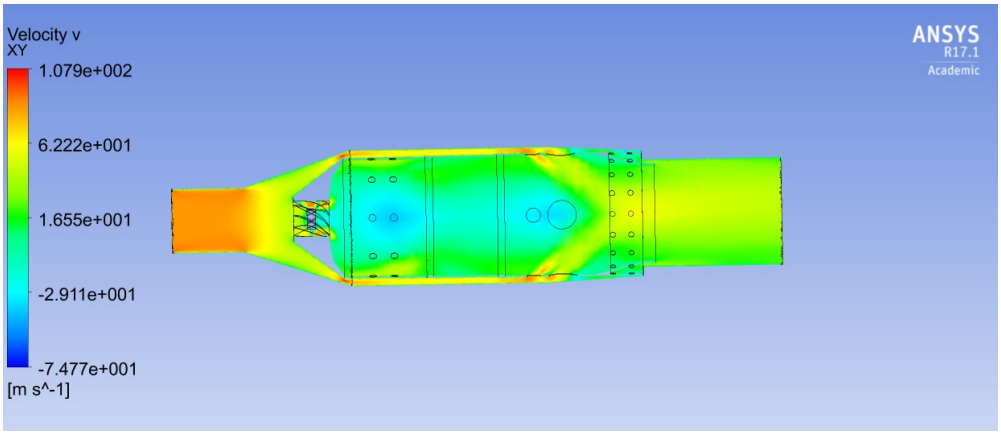


Figure C4: Axial velocity in XY plane of Combustor (no flame)

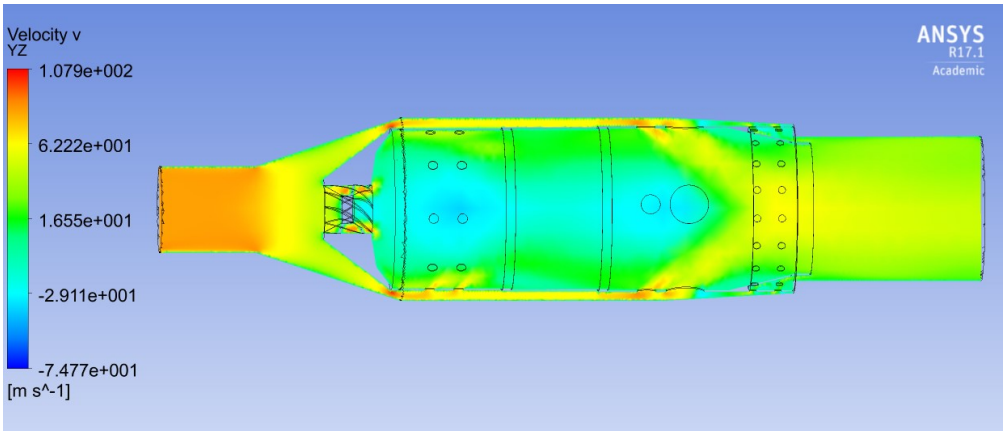


Figure C5: Axial velocity in YZ plane of Combustor (no flame)

The second reason for conducting this simulation is to get an indication of the velocities likely to be encountered at the liner holes. These velocities are then used as inputs for the fired combustor simulated in Model 4. Having these velocities as inputs to Model 4 eliminates the need for the annular flow modelled here, greatly reducing the size and complexity of the mesh required.

The nature of the flow at the dilution holes at the end of the combustor may be seen in Figure C6. It should be noted that the angle of penetration of these jets into the main flow of the combustor is shown here is slightly different to what would be expected in the Proteus combustor. This is due to the fact that the dilution holes of the actual combustor have a lip that diverts the flow from the holes backwards into the main flow stream. This feature was not noticed until after the simulations had been completed. With the effect of these lips taken into account, it is expected that the angle of projection of the jets in the actual combustor would be very close to perpendicular to the main flow.

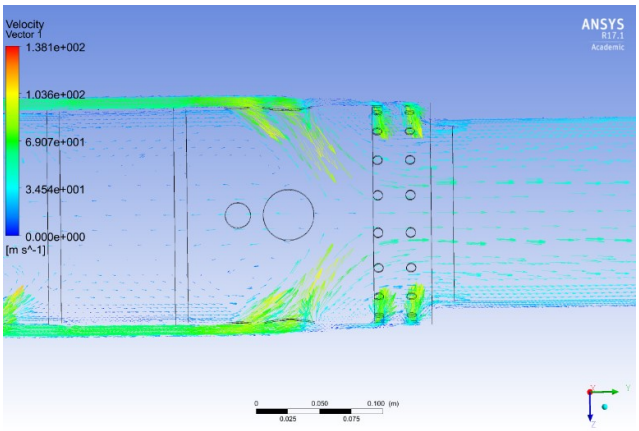


Figure C6: Velocity vector at outlet of cold combustor

A qualitative idea of the magnitudes of the velocities of the air coming through each of the liner holes may be gained by viewing Figure C7 and (in particular) Figure C8. The non-symmetric arrangement of the liner holes about its axis makes it necessary to view the results of the simulation from several angles in order to get a complete view of the distribution of the flow through the combustor

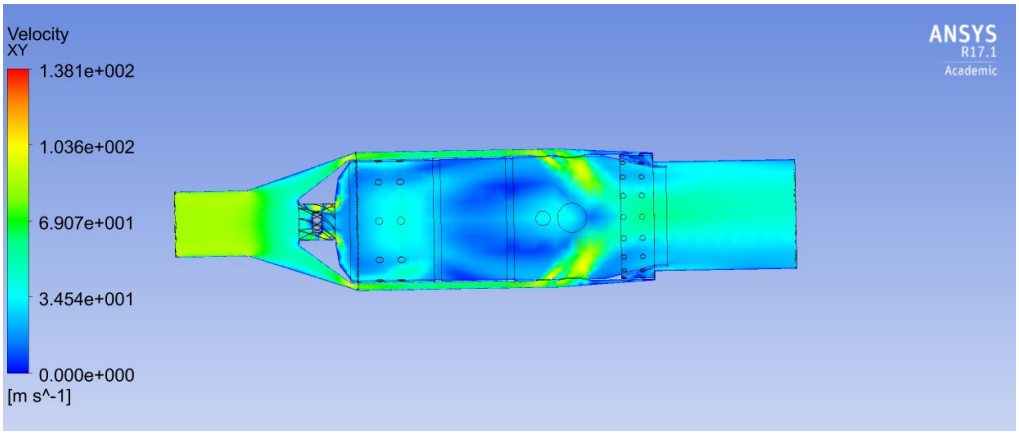


Figure C7: Velocity field in XY plane of Combustor (no flame)

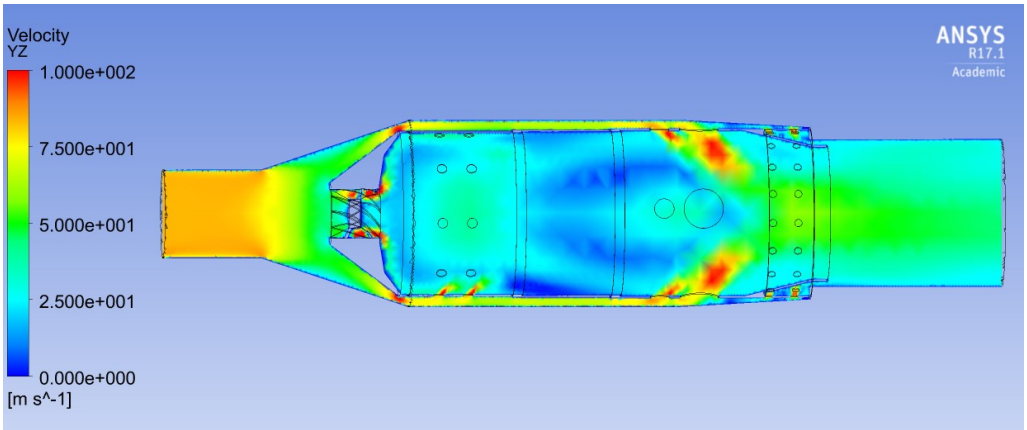


Figure C8: Velocity field in YZ plane of Combustor (no flame)

C2.3. Pressure field

In the acoustic and theoretical models of this project, it is assumed that there is a negligible degree of variation in the mean pressure through the combustor. This is in line with the Brayton cycle on which the gas turbine operates, in which the heat of combustion is added through an isobaric process. Figure C9 shows that there is some variation in the pressure around the primary and dilution holes. The variation is considered to be small enough for the assumption of constant pressure to be reasonable in the context of this project.

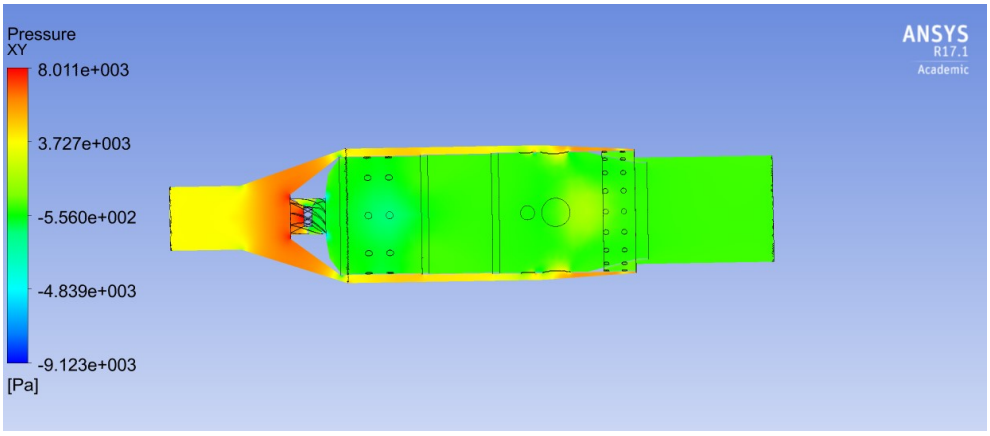


Figure C9: Pressure in combustor (no flame)

C2.4. Verification

As a means of verifying the model, the mass flow rates at the inlet and outlet of the combustor were compared, with Table C1 showing a difference between the two of merely 0.01579% which was considered adequate for this qualitative assessment.

Table C1: Verification of results from Model 3

Location	Mass flow rate (kg/s)
Inlet	630×10^{-3}
Outlet	630×10^{-3}
Difference	10×10^{-5}
% error	15.8×10^{-3}

C3. Model 4

C3.1. Geometry, Mesh and Boundary conditions

The geometry from Model 3 is simplified to that of model 4 by removing the diffuser and casing and defining the various liner holes as inputs in CFX pre. The overview of this mesh is shown in Figure C10.

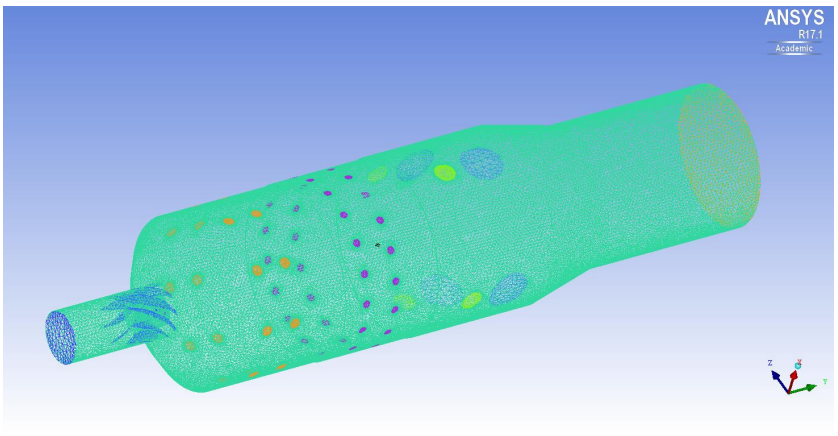


Figure C10: Mesh used for Model 4

A cross section of this mesh may be seen in Figure C11. To improve the quality of the mesh, the uniform geometry of the interior of the liner was filled with hexagonal mesh elements, creating a more uniform pattern and reducing the work required for calculations in these regions.

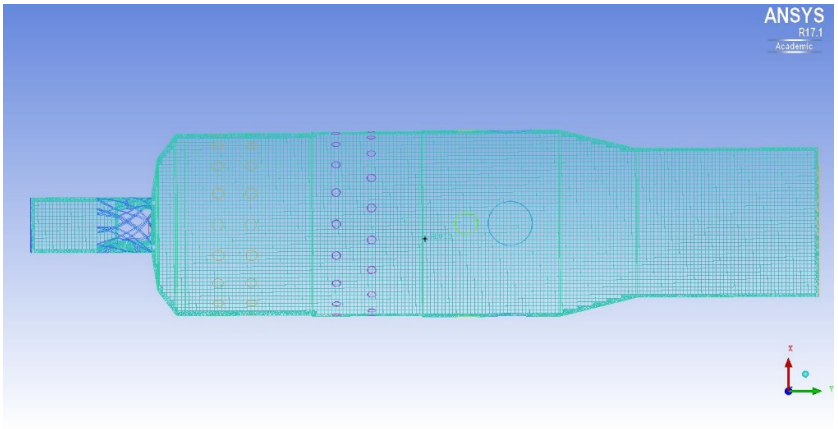


Figure C11: Cross section of mesh used in Model 4

The results of the normal velocities through the holes in the liner and entering the swirler from Model 3 were used as inputs in Model 4, with the graphic from CFX Pre shown in Figure C12. As the secondary air holes were not calculated in Model 3, the velocity through these was estimated as being an average of the values in the primary and dilution holes.

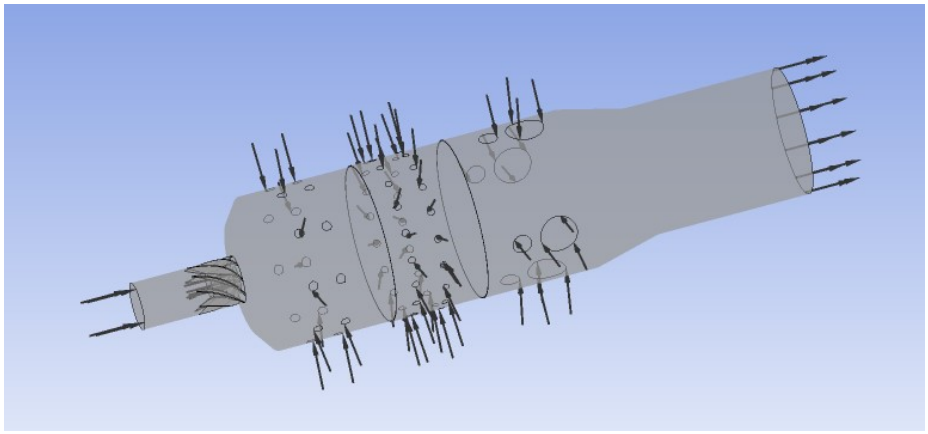


Figure C12: Boundary conditions in CFX-Pre for Models 4

Two runs were completed of model 4, first with the high velocity inputs (known as the “fast run”) from Model 3. These produced flows and temperatures that could be

compared to the expected values from the Proteus service manual of (Siddeley, 1961).

Once these results were confirmed, a slower set of inputs was used that are more in line with what might be found in a test rig for future development.

The input conditions for each run may be viewed in Table C2.

Table C2: Boundary conditions input to CFX-Pre for Model 4

Input velocities for Model 4		
Location	Fast runl (m/s)	Slow run (m/s)
Inlet	40	20
Primary holes	100	6
Secondary holes	80	8
Dilution holes 1	70	20
Dilution holes 2	70	15
Fuel injection	100	60

The chemical reaction between the fuel and air was based on the input conditions of the Combustor tutorial in (ANSYS, 2013). A PDF flamelet model was used in accordance with the suggested practice of combustion modelling in (ANSYS, 2013). The fuel used was methane, as in the tutorial. While this may not be a realistic fuel for the Proteus combustor, it was felt that the need for a realistic fuel source was outweighed by the simplicity of the chemical reaction of the methane with the air. Additionally, Methane is a common source of fuel in combustor test rigs such as that used in (Dowling & Stow, 2003) and (Pożarlik, 2010). What the use of methane as the fuel did necessitate, however, was a particularly high velocity through the nozzle modelled on that of the Proteus in order to get the correct mass flow rate of fuel for a realistic simulation of the flame in the combustor.

C3.2. Velocity flow fields (fast model)

One of the main reasons for using the slower flow rate is that the plane wave assumption, necessary for the theoretical models used to validate the acoustic models later in the project, is only valid for flows that have low Mach numbers.

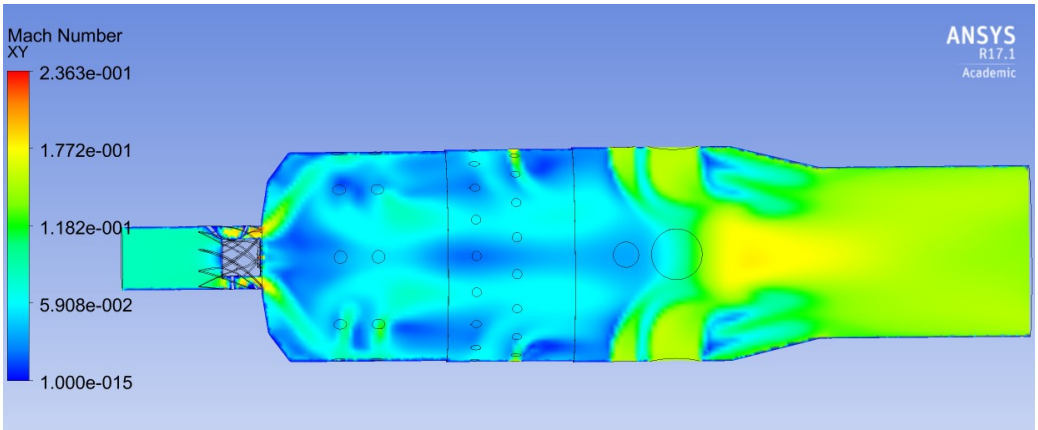


Figure C13: Mach number through fired combustor liner (fast)

While the values of the faster run are still mostly within the range for this assumption to be valid (Figure C13), the extremely low values of the slower run (Figure C14) allow a greater degree of certainty in the use of the plane wave assumption.

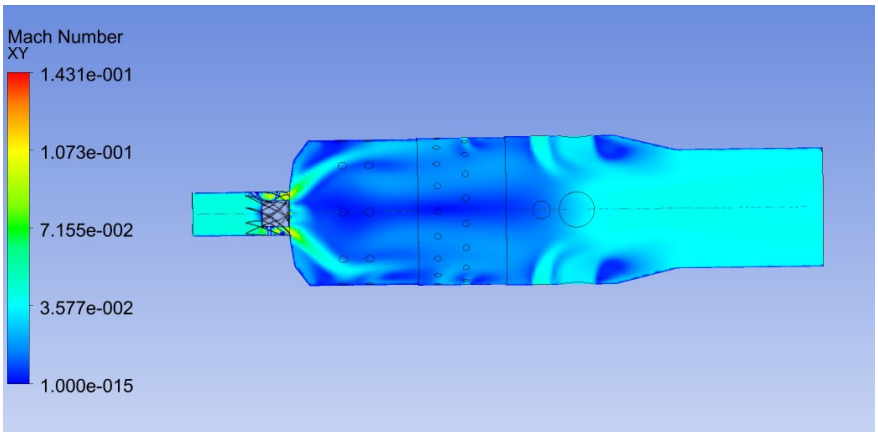


Figure C14: Mach number through fired combustor liner (slow)

As with Model 3, the results of the velocity flow through Model 4, for both models, are shown in the XY and YZ planes. This is done for both the axial and total velocity values. The results for the fast run are presented in Figure C15 to Figure C18. From these results, it appears that the use of the high injection velocity has resulted in a high degree on penetration of the fuel through the length of the combustor, while the air does follow the expected Lucas profile.

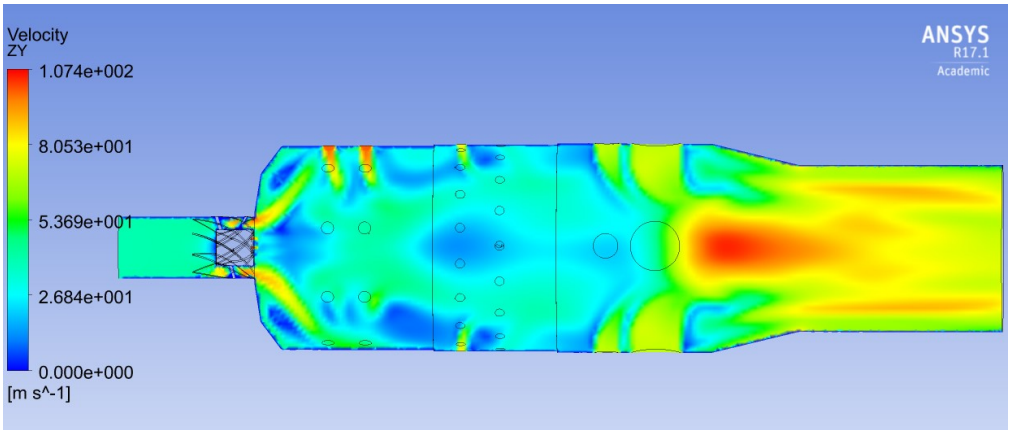


Figure C15: Velocity field in ZY plane of fired combustor liner (fast)

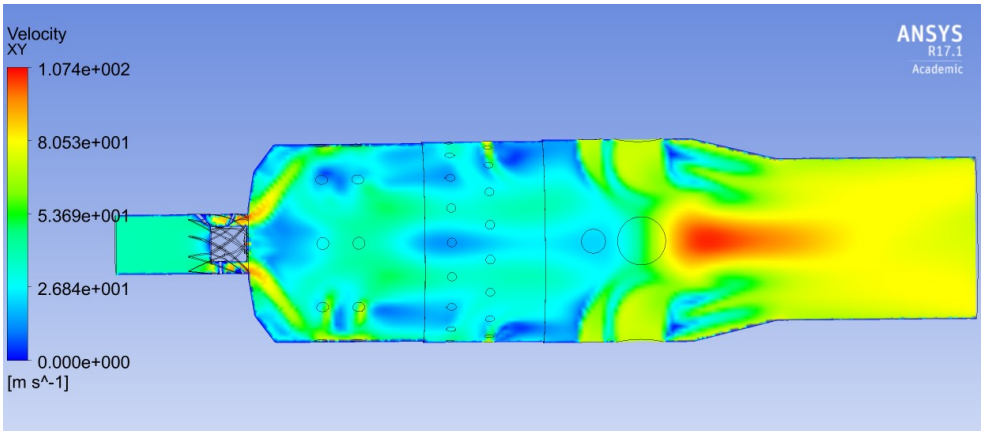


Figure C16: Velocity field in XY plane of fired combustor liner (fast)

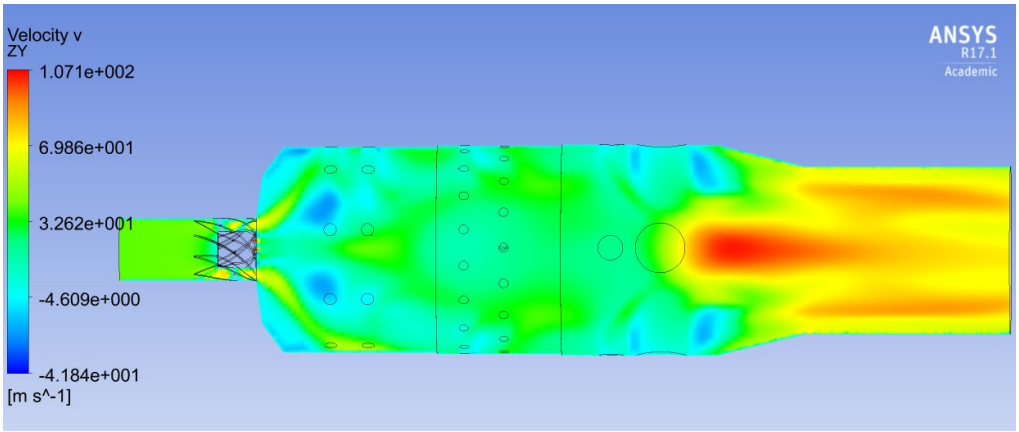


Figure C17: Axial velocity field in ZY plane of fired combustor liner (fast)

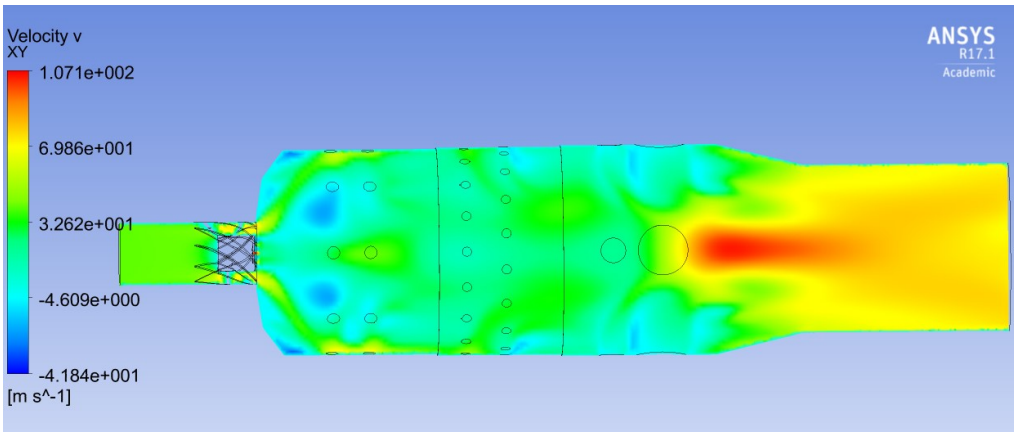


Figure C18: Axial velocity field in XY plane of fired combustor liner (fast)

The results of the slow run are presented in Figure C19 to Figure C23. It is interesting to note that the areas of zero velocity along the axis of Figure C20 and Figure C21 are strikingly similar to the flame profile illustrated in (Siddeley, 1961). Figure C19, Figure C22 and Figure C23, give a more distinctly visible “flame zone” and defined degree of penetration of the fuel that support the divisions of the geometry used in the acoustic and theoretical models.

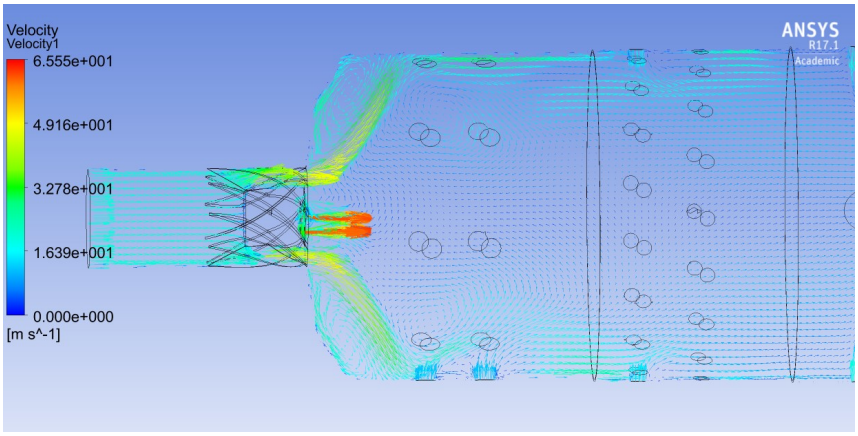


Figure C19: Velocity vector at inlet of fired combustor (slow)

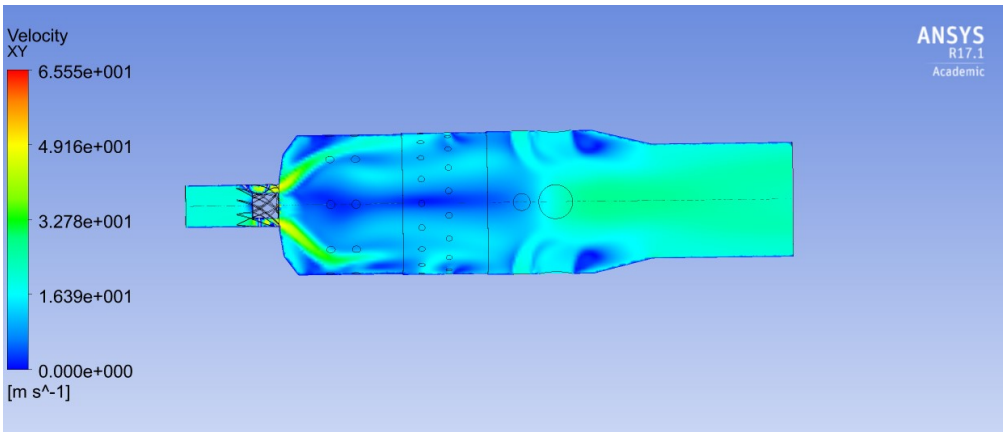


Figure C20: Velocity field in XY plane of fired combustor (slow)

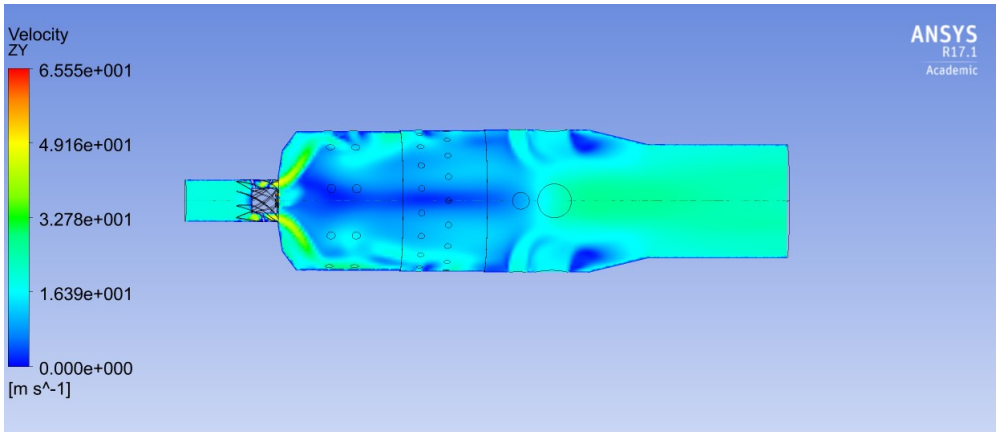


Figure C21: Velocity field in XY plane of fired combustor (slow)

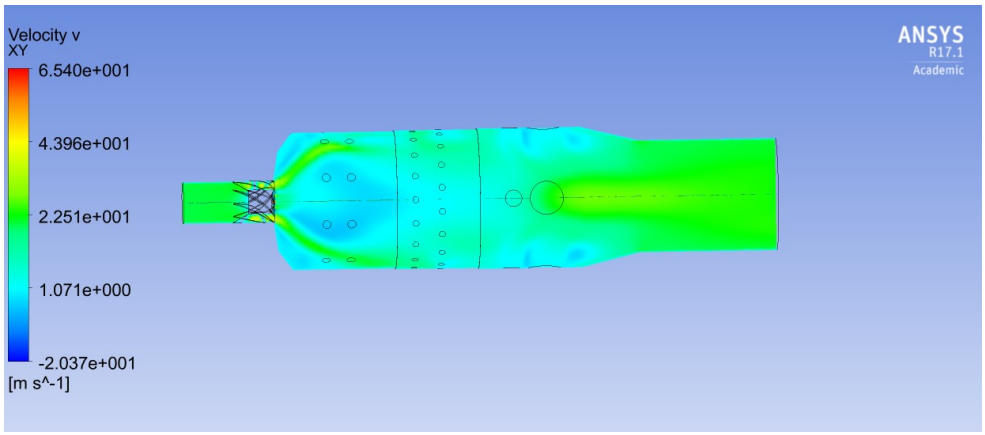


Figure C22: Axial velocity field in XY plane of fired combustor (slow)

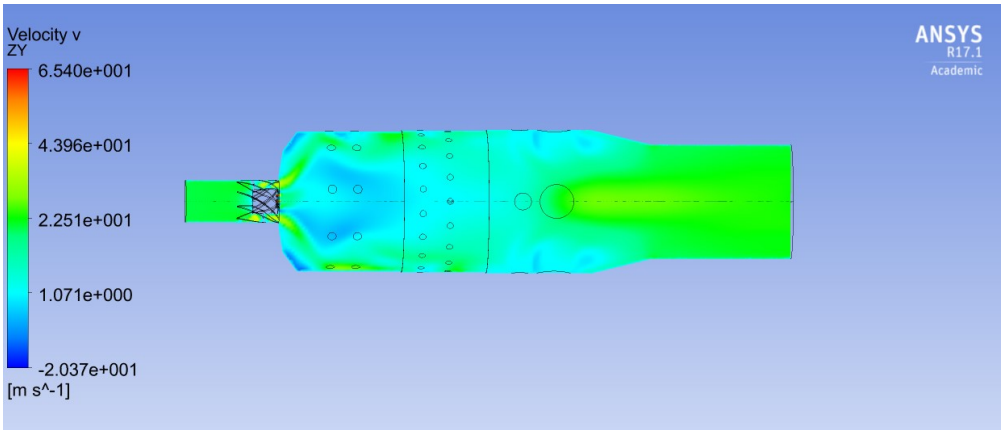


Figure C23: Axial velocity field in XY plane of fired combustor (slow)

C3.3. Temperature fields

As with Model 3, the pressure field of the model is presented to ensure that the constant pressure assumption is valid.

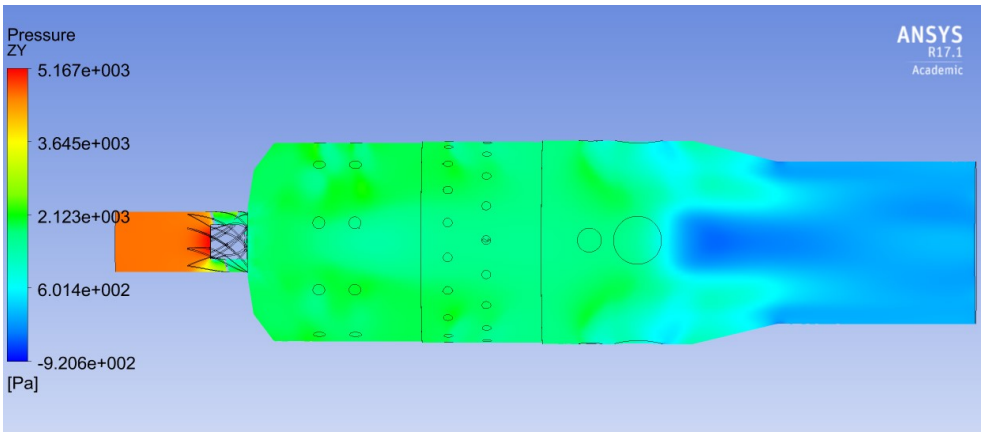


Figure C24: Pressure through fired combustor liner (fast)

The temperature field produced by the fast run of Model 4 is presented in the XY and YZ planes of the Model by Figure C25 and Figure C26. The radial arms of the high temperature zone and the axial component conform to the burn patterns of the actual combustor and the flame illustration in (Siddeley, 1961). As with the flow patterns of Model 3, it is expected that the angle of projection of the air from the secondary and dilution holes would be angled further back into the flow in the actual combustor, due to the lips on the holes that alter the angle of projection of the jets.

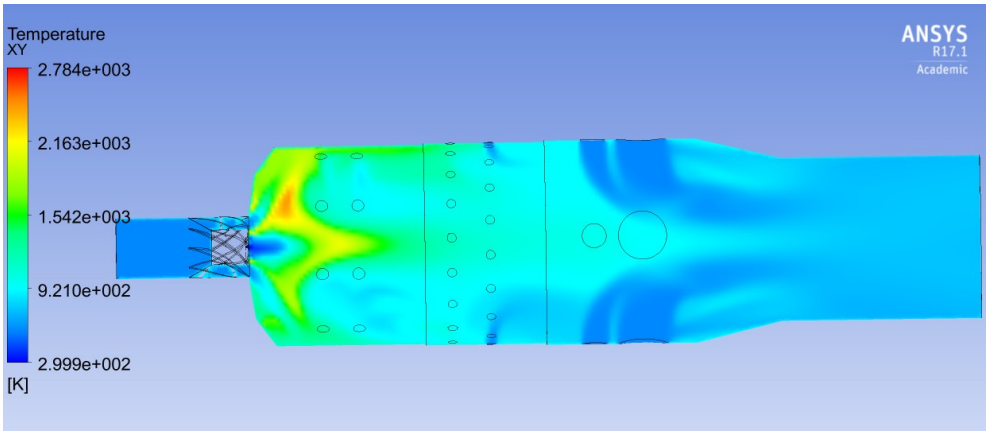


Figure C25: Temperature field in XY plane of fired combustor liner (fast)

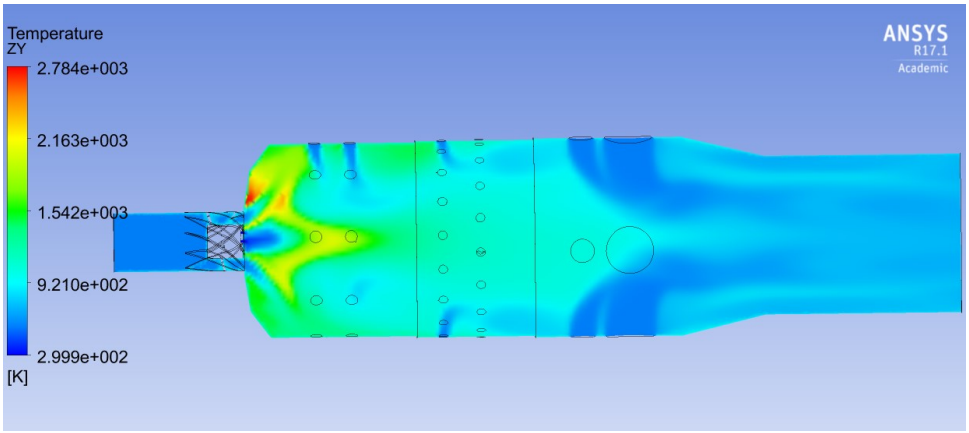


Figure C26: Temperature field in ZY plane of fired combustor liner (fast)

A combination of the flow velocity vector and temperature field of the slow model is shown in Figure C27. In this model, the effect of the dilution holes is more pronounced, with a classic temperature pattern factor, as described in (Baskharone, 2006) visible at the exit of the combustor to the outlet transition piece.

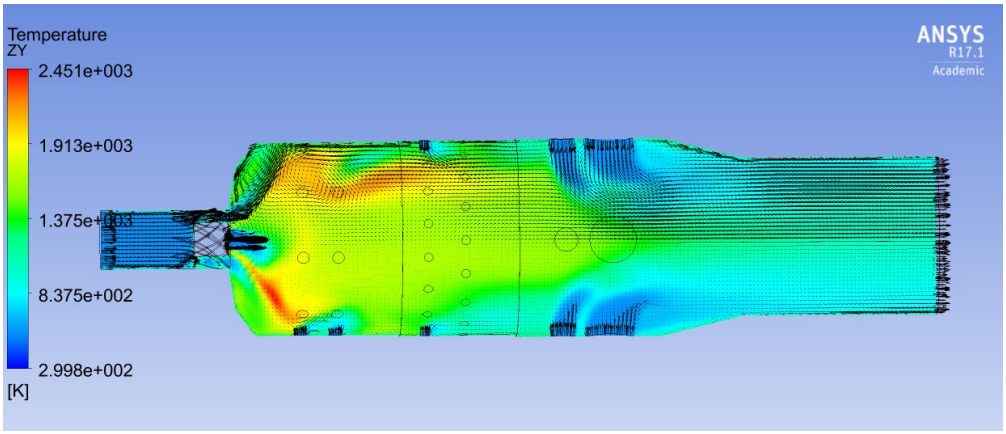


Figure C27: Temperature field, with velocity vector in ZY plane of fired combustor (slow)

The temperature field of Model 4 with the slow run is shown in the XY and YZ planes of the model in Figure C28 and Figure C **29**. These models show the location of the highest temperatures in the "Flame Zone", as well as the non-symmetrical nature of the flame about the axis of the model.

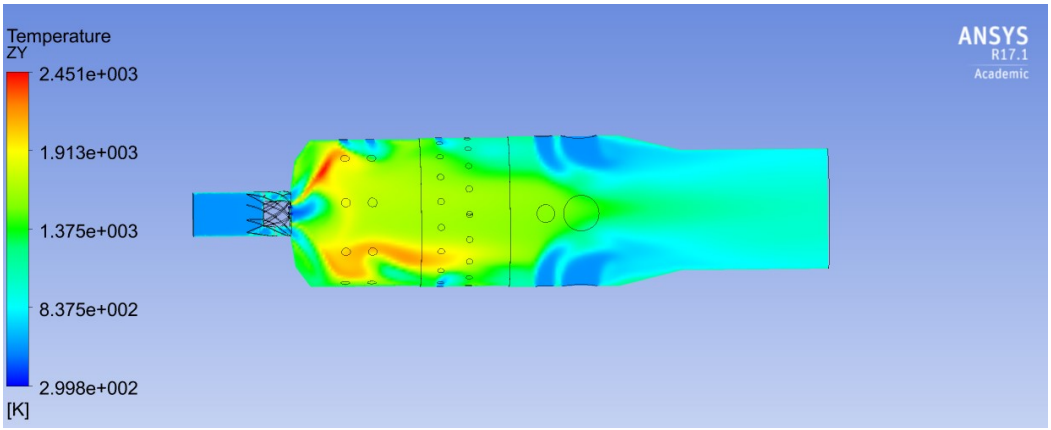


Figure C28: Temperature field in ZY plane of fired combustor (Slow)

Once again, the pattern factor of the outlet of this simulation is clearly illustrated. The radial arms of the flame agree with the soot patterns visible in the physical specimen of the Proteus combustor and the maximum temperature of 2451K is close to that of the engine's manual of 2500K (Siddeley, 1961)

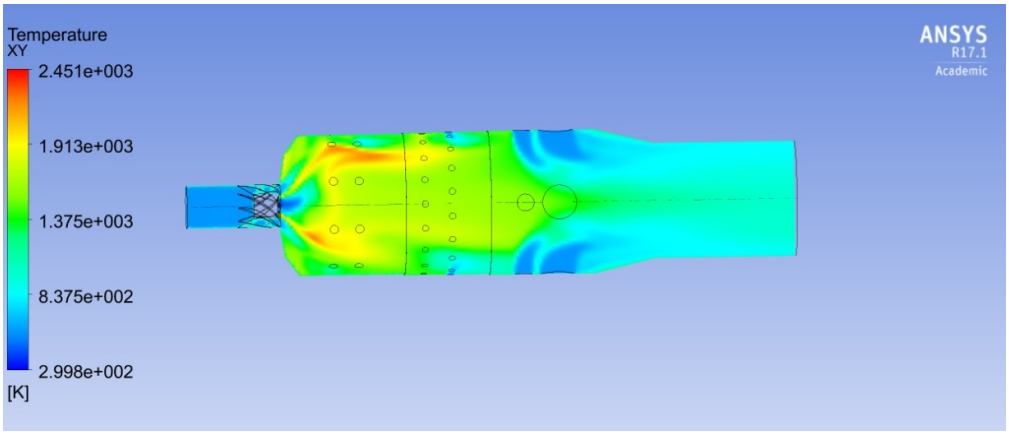


Figure C 29: Temperature field in XY plane of fired combustor

In order to make use of this temperature field, in the Acoustic models, it must be mapped from ANSYS CFX to an equivalent model in ANSYS mechanical. While it would have been preferable to export these values directly, the skill set to do so was not attainable in the time available for this project.

Instead of exporting the entire temperature field, several planes (shown in Figure C30) were created at various points of interest; such as at the axis of each set of liner holes, where the temperature could be expected to make any significant changes.

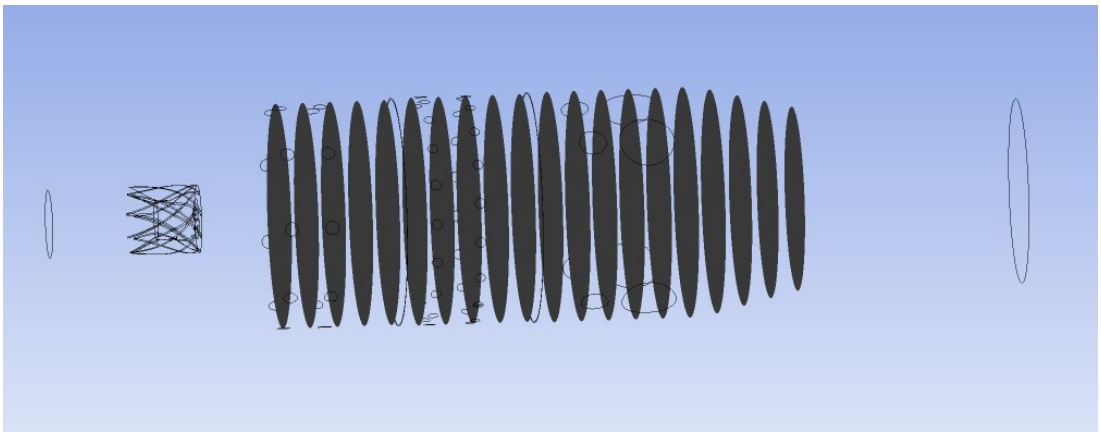


Figure C30: Planes for sampling temperatures through fired combustor

The average temperature at each of the planes (Figure C31) was calculated in CFX post and the results used as detailed in Appendix D. Once again, the temperature

profile visible in each of these slices affords an opportunity to visualise the behaviour of the Flame and Flow through a gas turbine combustor.

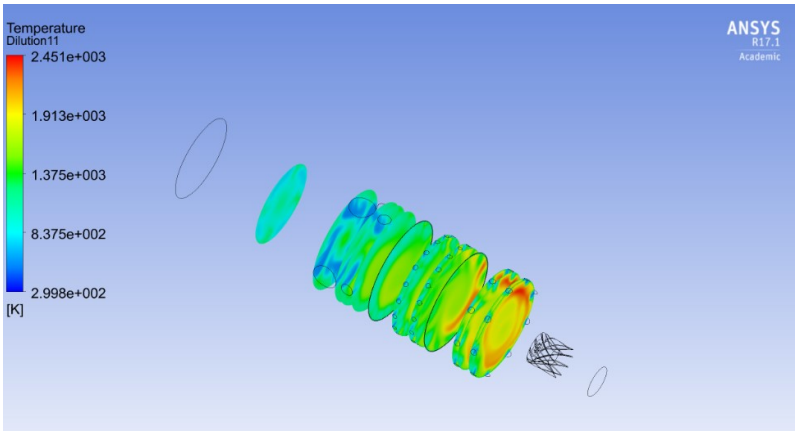


Figure C31: Temperatures at various sample points (slow)

While the method for exporting the temperature field detailed here may not be the most elegant solution, it does allow the same set of results to be used in the theoretical models described in Appendix D, which allows for direct comparison of the results obtained through the theoretical and Acoustic models.

C3.4. Validation

As the inputs of the fast run have been taken from the operating manual of the combustor, the calculated outputs may be compared with the expected outputs from the manual, as has been done in Table C3.

Table C3: Validation of fast run of Model 4

Verification of Model 4 results			
	Proteus	Model 4 (fast)	Unit
Peak Combustion Temperature	2500	2700	K
Outlet velocity of combustor	125	107	m/s
Outlet Mach number of combustor	0,35	0,31	-
Outlet temperature of combustor	299	280	K

As the values from the slower run to not reflect the operating conditions of the combustor, an alternate means of at least verifying the results was required. The mass flow rates at the inlets and outlet of the combustor were compared for the slow run, with Table C4 showing a difference between the two of merely 0.0168% which was considered adequate for this qualitative assessment.

Table C4: Verification of slow run of Model 4

Location	Mass flow (kg/s)
INLET	51.8×10^{-3}
OUTLET	-506×10^{-3}
Dilution 1	56.1×10^{-3}
Dilution2	249×10^{-3}
Primary	90.5×10^{-3}
Secondary	80.7×10^{-3}
Injection	2.05×10^{-3}
Total	8.5×10^{-5}
Error	0.0168%

Appendix

D - ANSYS FEA Acoustic Models

Appendix D Contents

Appendix D Contents ..... Dii
Appendix D Figures ..... Diii
D1. Introduction D1
D2. Model 1 ..... D2
D2.1. Mesh size D2
D2.2. Confirmation of Plane wave assumption D3
D2.3. Harmonic Analysis D4
D3. Model 2 ..... D6
D4. Model 5 ..... D8
D5. Model 6 ..... D9
D6. Model 7 ..... D12
D7. Exporting data from ANSYS to MATLAB D17

Appendix D Figures

Figure D1: Mesh and geometry of Model 1 (24epw) D2
Figure D2: SPL along Model 1 for various element sizes and types D3
Figure D3: First four modes of simple duct in Model 1 (Clockwise from top left) D4
Figure D4: Results for harmonic analysis of Model 1 ..... D5
Figure D5: Model 2 geometry and mesh D6
Figure D6: Modes 2 and 3 of Model 2 ..... D6
Figure D7: Results for harmonic analysis of Model 2 ..... D7
Figure D8: Results for harmonic analysis of Model 5, closed end D8
Figure D9: Results for harmonic analysis of Model 5, open end D8
Figure D10: Linearly varying temperature across duct D9
Figure D11: Results for harmonic analysis of Model 6 with linearly varying temperature D10
Figure D12: Mesh with multiple planes D10
Figure D13: Varying temperature field of Model 6 ..... D11
Figure D14: Results for harmonic analysis of Model 6 with variable temperature field D11
Figure D15: Geometry and Mesh of Model 7 ..... D12
Figure D16: Linear temperature field of Model 7 ..... D12
Figure D17: Results for harmonic analysis of Model 7 with linearly varying temperature, closed duct D13
Figure D18: Results for harmonic analysis of Model 7 with linearly varying temperature, open duct D14
Figure D19: Temperature inputs for variable temperature field of Model 7 ..... D14
Figure D20: Variable temperature field of Model 7 ..... D14
Figure D21: Results for harmonic analysis of Model 7 with variable temperature, closed duct D15
Figure D22: Results for harmonic analysis of Model 7 with variable temperature, open duct D16
Figure D23: Nodes along axis of ANSYS Model D17

D1. Introduction

This Appendix serves to describe the development of the ANSYS Acoustic Finite Element Analysis models developed in this project, starting from the simple duct of Model 1 and building to the final Model 7, which incorporates variable geometry and temperature fields. A visual representation of the results of each model is presented, compared to the graphical format produced by the MATLAB programs described in Appendix F. The results for the imaginary component of the acoustic velocity and the real component of the acoustic pressure are omitted as these are equal to zero in all of the models.

D2. Model 1

The first model produced in the acoustics package of ANSYS Mechanical was that of a simple duct, as found in the examples in Howard & Cazzolato (2014).

D2.1. Mesh size

The size and type of mesh to be used throughout the project was determined by running simulations of various configurations, starting with the minimum theoretical size of 6 elements per wavelength (epw) for the maximum frequency to be examined, 1200Hz.

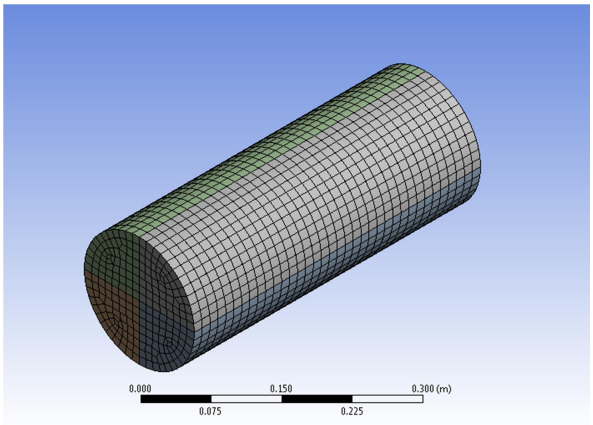


Figure D1: Mesh and geometry of Model 1 (24epw)

The choice of elements to be used was between FLUID220 and FLUID30, with the FLUID220 elements having additional nodes at the midpoints of their vertices, making them more detailed for a given element size.

Figure D1 shows the final mesh selected, after the comparisons detailed in Appendix F and shown in Figure D2, of 24epw for a frequency of 1200Hz, using FLUID220 elements. This mesh type and density was used for all subsequent acoustic models in the project and corresponds to an element size of 12mm.

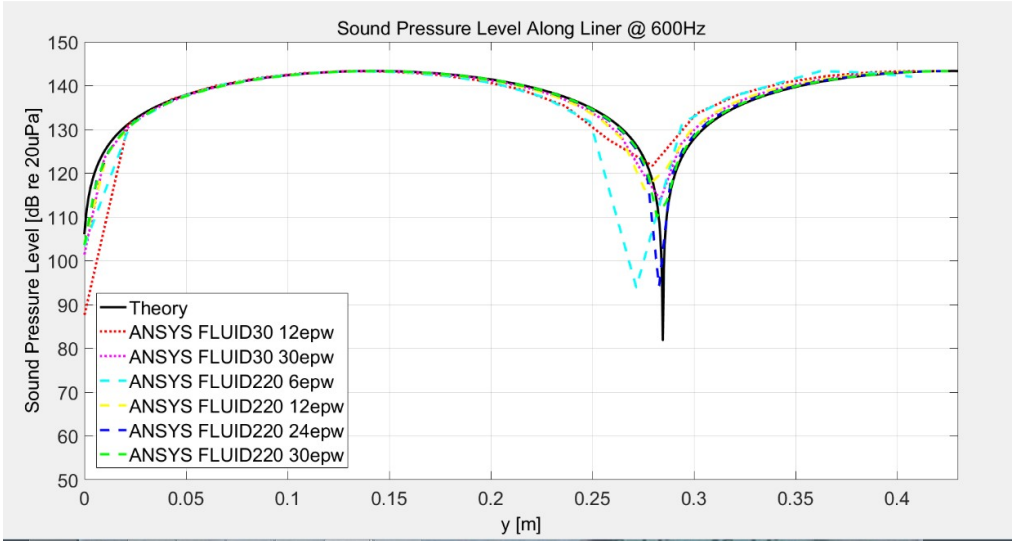


Figure D2: SPL along Model 1 for various element sizes and types

D2.2. Confirmation of Plane wave assumption

In order for the one dimensional equations used to construct the theoretical models in MATLAB to be valid, it was necessary to make the assumptions that the acoustic pressures and velocity in the duct will propagate in the form of planar waves along the axis of the duct. The maximum theoretical frequency at which this will occur is found by:

$$f_c = \frac{1.8412 C_0}{2\pi a}$$ (Singh, et al., 2008) **D-1**

For the geometry of the combustor, at room temperature, the cut on frequency, up to which the plane wave assumption is valid, is 1218Hz. To verify this assumption, a modal analysis of the geometry of Model 1 was conducted, with the results presented in Figure D3.

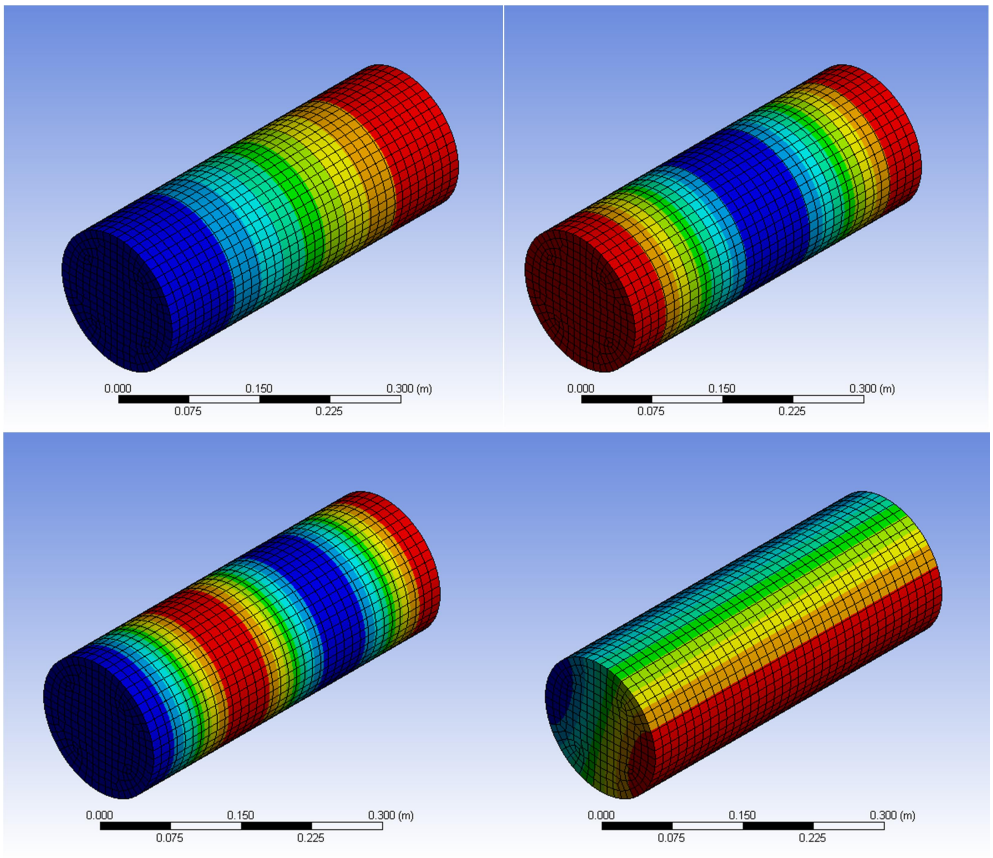


Figure D3: First four modes of simple duct in Model 1 (Clockwise from top left)

D2.3. Harmonic Analysis

A harmonic analysis of Model 1 was conducted by placing an acoustic excitation of $1\mathrm{m.s^{-1}}$ at the driving end. The results for the acoustic velocities and pressures were obtained from this analysis, along with those of the Sound Pressure Level throughout the duct. Note that the real and imaginary results for the velocity and pressure values are displayed separately and, as noted at the introduction to this Appendix, the real pressure values and imaginary velocity values are consistently zero throughout this project. The results for the imaginary component of the acoustic pressure, the real component of the acoustic velocity and the total value of the SPL of Model 1, at $600\mathrm{Hz}.$ with an excitation of $1\mathrm{m.s^{-1}}$ are presented in Figure D4. These results were exported to a table in Microsoft Excel and used in comparison with the theoretical models developed in MATLAB and detailed in Appendix D

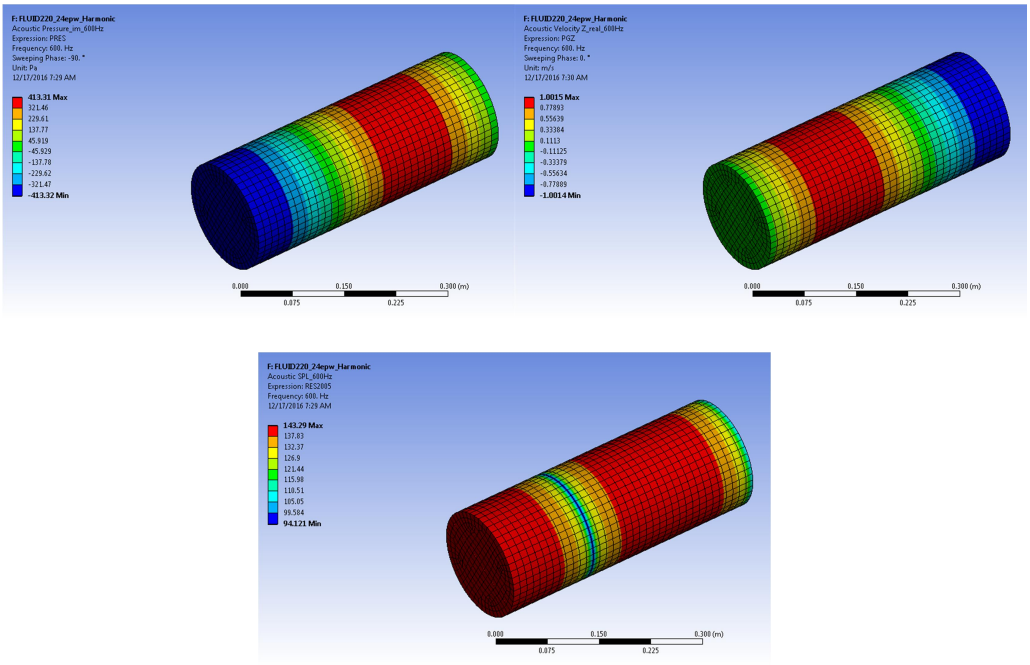


Figure D4: Results for harmonic analysis of Model 1

D3. Model 2

After confirming the validity of the plane wave assumption and settling on the element size and type to be used in the subsequent models, the geometry of Model 1 was extended to more closely approximate that found in a gas turbine combustor assembly. The extended geometry consists of additional ducts, based on the dimensions of the diffuser, swirler, flame zone and liner of the Proteus combustor, described in Appendix B, and may be seen in Figure D5.

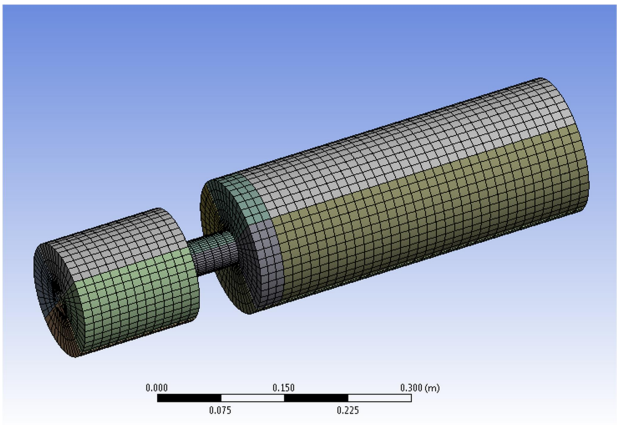


Figure D5: Model 2 geometry and mesh

To ensure that the plane wave assumption is still valid for this more complex geometry, a modal analysis was conducted of Model 2. A cutaway view of modes 2 and 3 (occurring at frequencies of 410Hz and 800Hz respectively) may be seen in Figure D6

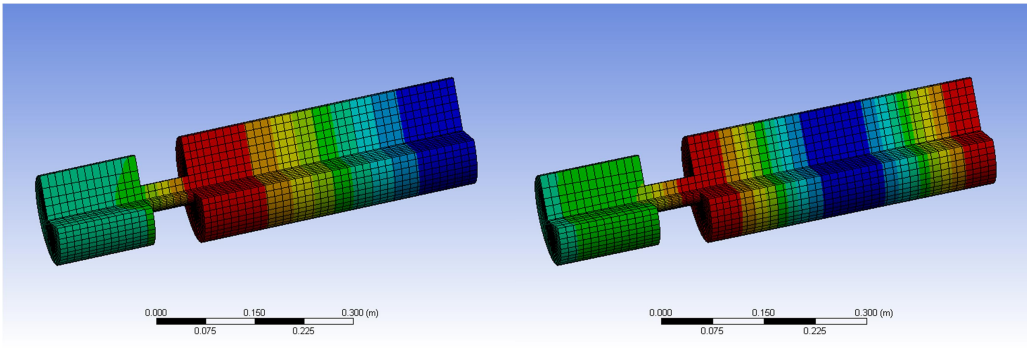


Figure D6: Modes 2 and 3 of Model 2

From Figure D6, it may be seen that the propagation of the waves through the liner are still very much planar for the frequencies of interest (under 1218Hz.). There is a slight discrepancy around the transition between the swirler and the diffuser and it is seen in Appendix F that this sudden change in area does cause some difficulties for the theoretical model.

The results for the harmonic analysis of Model 2 at 600Hz, with an excitation of 1m.s^{-1} placed at the location of the flame front (the interface between the ducts named “Flame Zone” and “Liner), are presented in the same order as those of Model 1 in Figure D7.

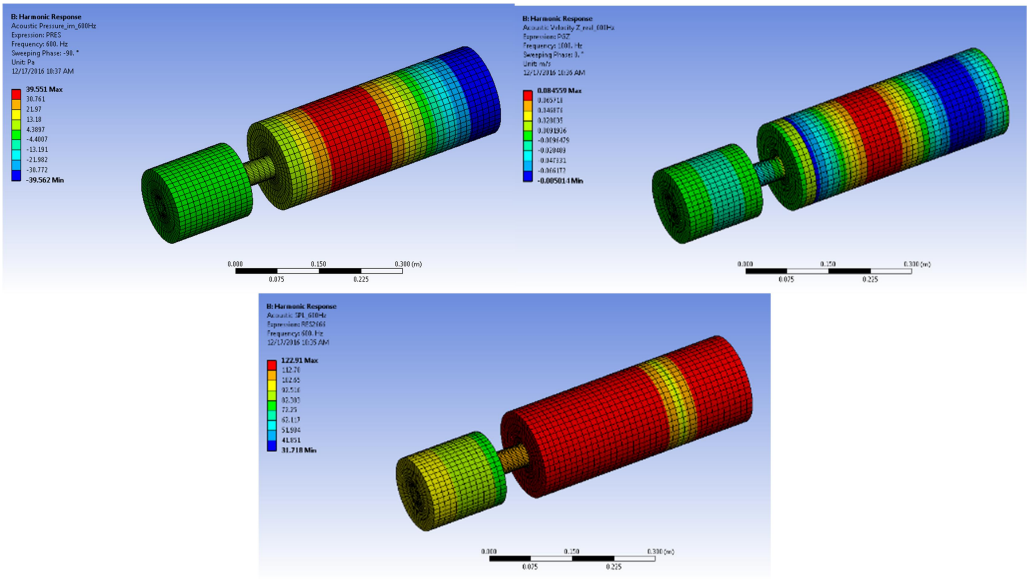


Figure D7: Results for harmonic analysis of Model 2

D4. Model 5

Model 2 is then repeated, with the inclusion of an additional section downstream of the liner, to approximate the shape of the outlet of the combustor to the tubine. The results of the subsequent harmonic analysis are shown in Figure D8 (for the case of a closed duct) and Figure D9 (for the case of an open ended duct).

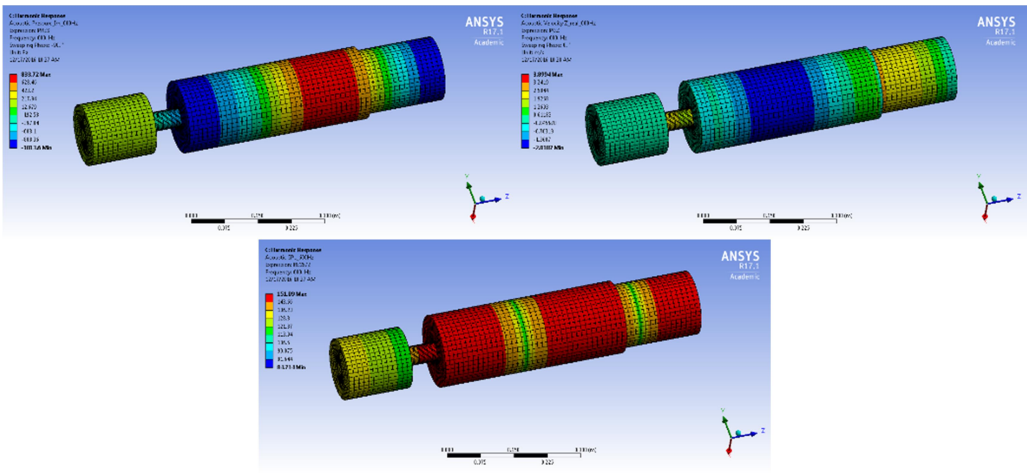


Figure D8: Results for harmonic analysis of Model 5, closed end

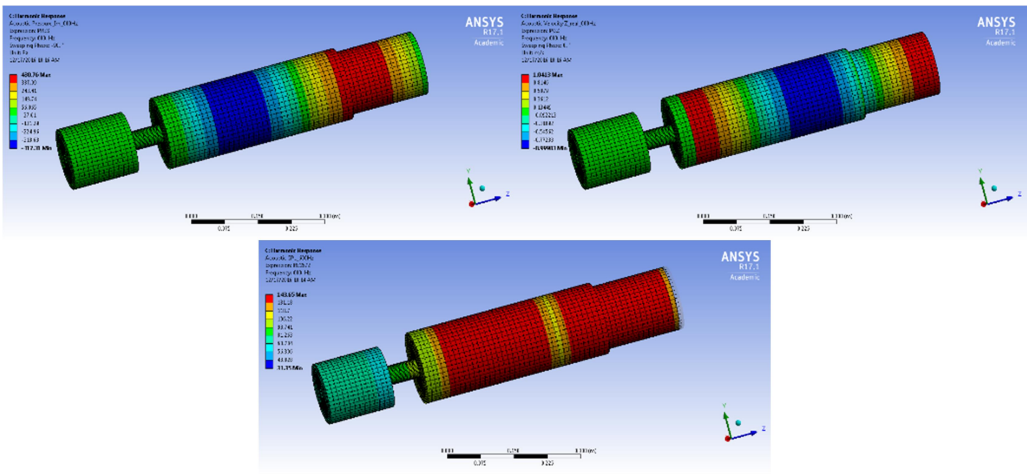


Figure D9: Results for harmonic analysis of Model 5, open end

The results of the harmonic analysis of the closed duct were compared with a theoretical model developed in MATLAB (described in Appendix F).

D5. Model 6

The geometry and mesh from Model 1 was used to create model 6, where the temperature was made to vary, first linearly in the manner described in (Howard & Cazzolato, 2014), and then to fluctuate in accordance with the temperatures obtained from Model 4 (See Appendix C – ANSYS CFX models). The temperature was developed in the model by running a thermal analysis in ANSYS mechanical, with the resulting temperatures mapped to the elements of the acoustic model, allowing the density and speed of sound of the calculations to vary accordingly. The thermal model of the linear case was produced by applying a temperature to the planes at either end of the cylinder, with the linear change in temperature shown in Figure D10.

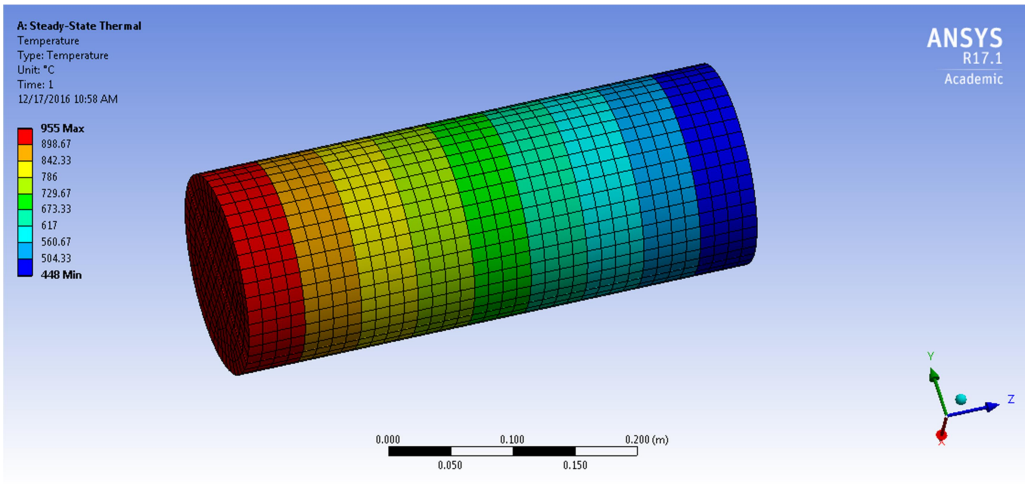


Figure D10: Linearly varying temperature across duct

With the material properties of the model suitably altered, a harmonic analysis is again conducted with an excitation of $1\mathrm{m.s}^{-1}$ for the frequency of $600\mathrm{Hz}$. The results of this analysis are presented in Figure D11 and were checked against those of the equivalent theoretical model developed in MATLAB and described in Appendix F.

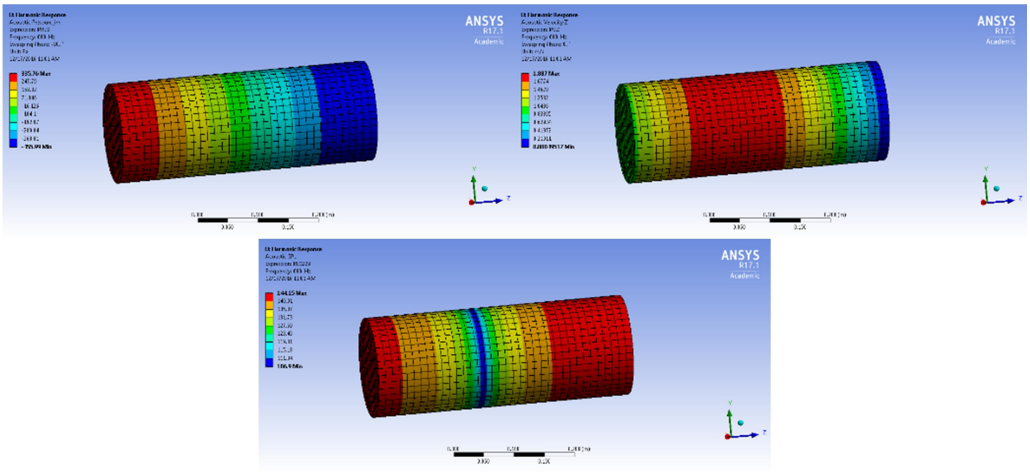


Figure D11: Results for harmonic analysis of Model 6 with linearly varying temperature

In order to produce the varying temperature field to more closely approximate what is likely to be experienced in the combustor, the mesh of the previous model is modified to insert the planes of different temperatures in Figure D12.

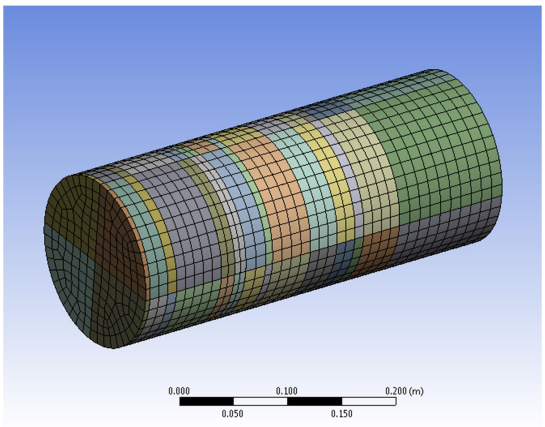


Figure D12: Mesh with multiple planes

The steady state thermal analysis was performed as before, but with multiple temperature values entered along the axis of the duct, giving a temperature profile that varies in a similar fashion to that of the CFD models of the combustor, described in Appendix B. This temperature profile is shown in Figure D13 and the results mapped to the acoustic model. The temperatures displayed are in degrees centigrade, while all calculations are performed in degrees Kalvin.

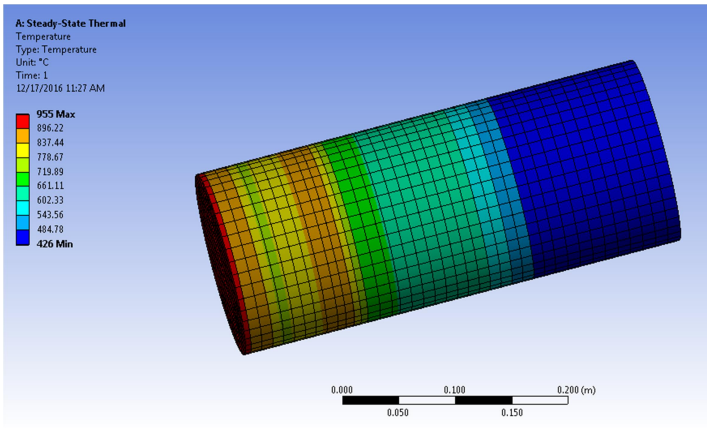


Figure D13: Varying temperature field of Model 6

As before, the modified material properties of the model were used to perform a harmonic analysis of Model 6 at 600Hz, with an excitation of 1m.s^{-1}. The results of this analysis are presented in Figure D14 and were later compared with the results of the theoretical model described in Appendix F.

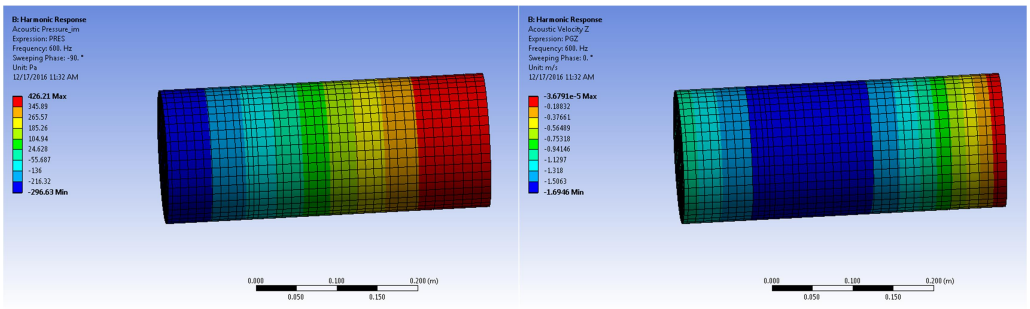


Figure D14: Results for harmonic analysis of Model 6 with variable temperature field

D6. Model 7

Model 7 was produced by combining the geometry of Model 5 with the procedure of Model 6. The diameter of the outlet was increased to that of the liner, to reduce the effect of any discontinuities on the model, with the geometry and mesh used visible in Figure D15.

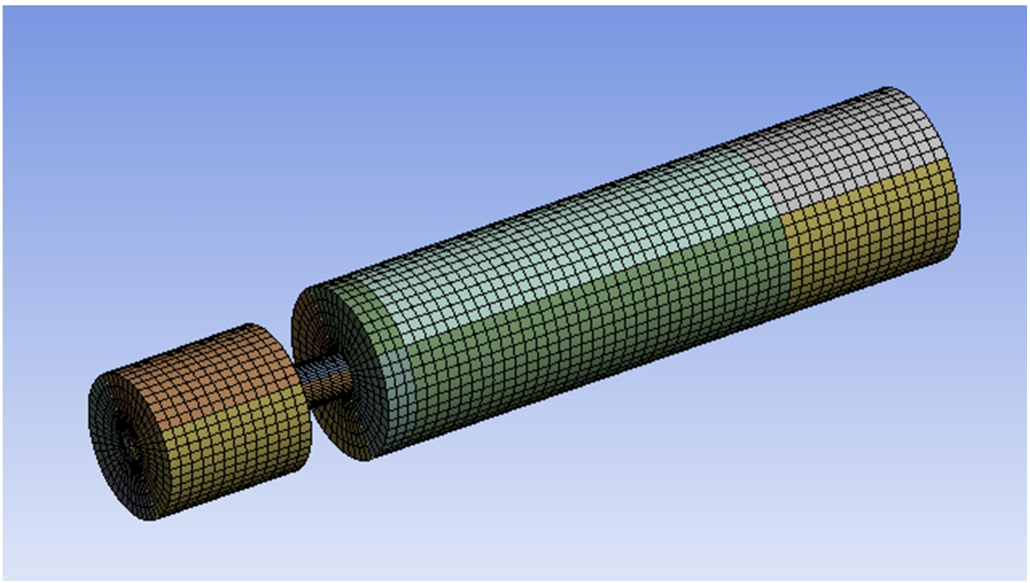


Figure D15: Geometry and Mesh of Model 7

As in Model 6, the temperature in the liner was made to vary linearly, with the results of the thermal analysis shown in Figure D16.

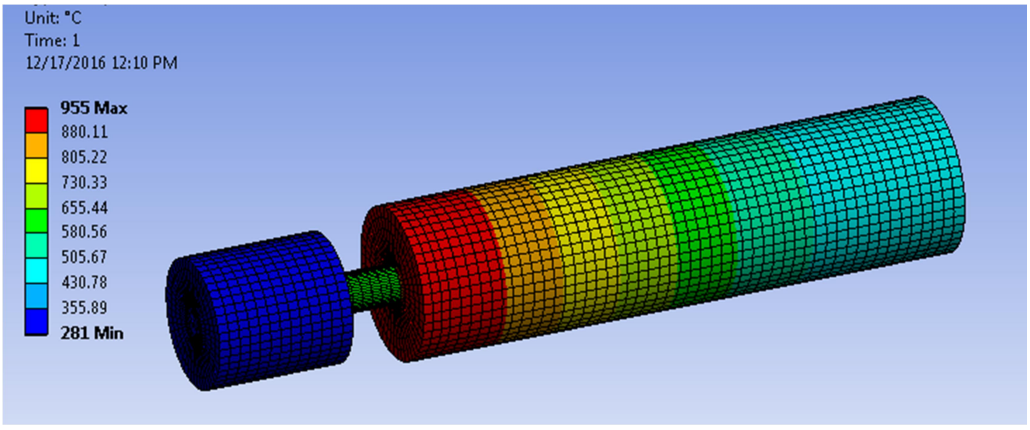


Figure D16: Linear temperature field of Model 7

The new material properties were used in the model to complete a harmonic analysis, the results of which are shown in Figure D17 and Figure D18 for closed and open duct conditions respectively.

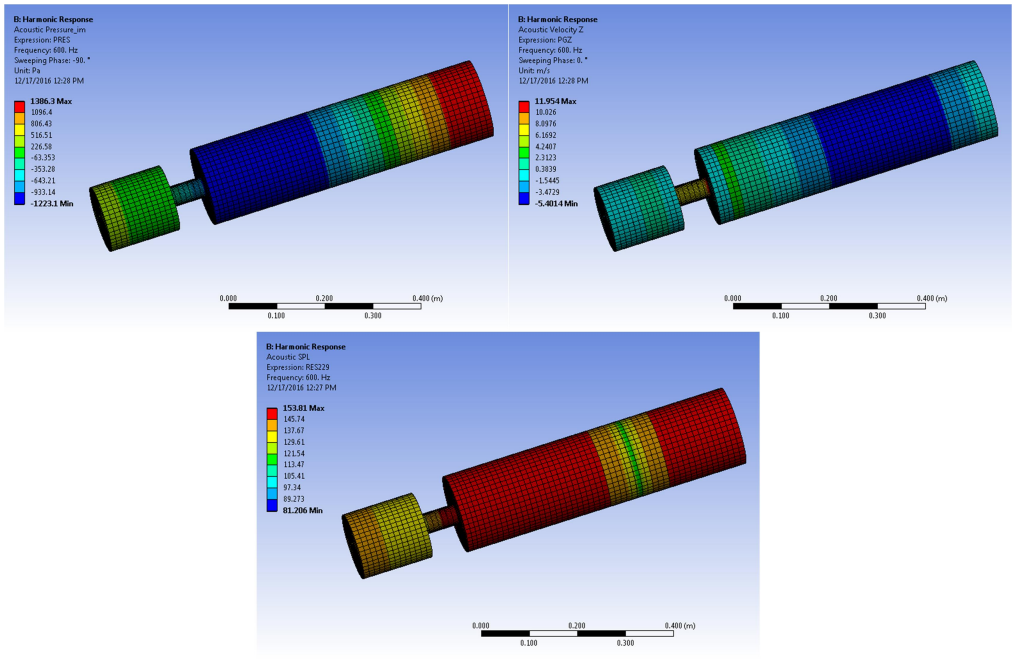


Figure D17: Results for harmonic analysis of Model 7 with linearly varying temperature, closed duct

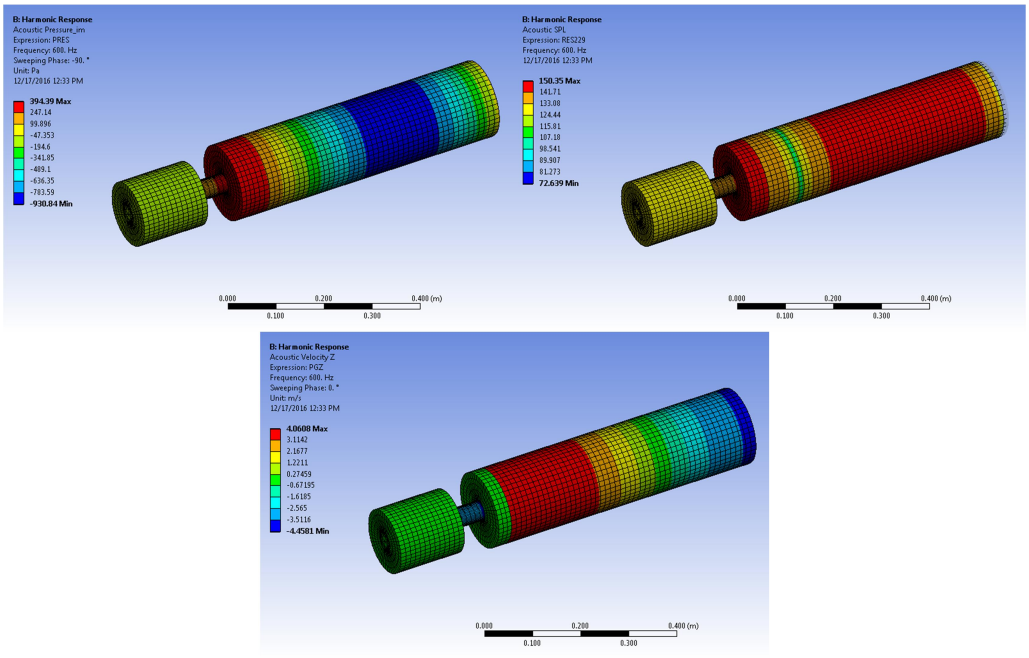


Figure D18: Results for harmonic analysis of Model 7 with linearly varying temperature, open duct

The values of the varying temperature field were applied to the planes shown in Figure D19, with the temperature field itself shown in Figure D20.

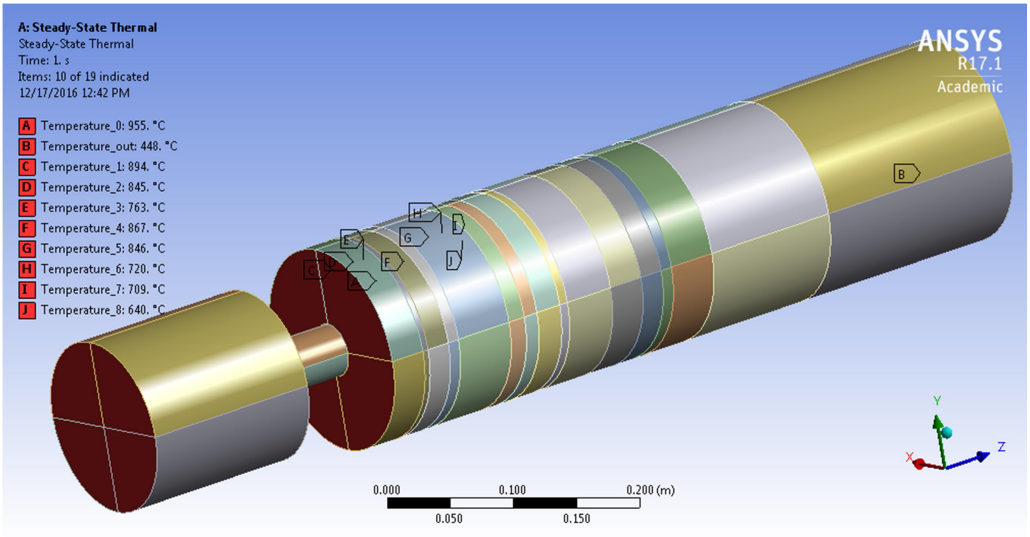


Figure D19: Temperature inputs for variable temperature field of Model 7

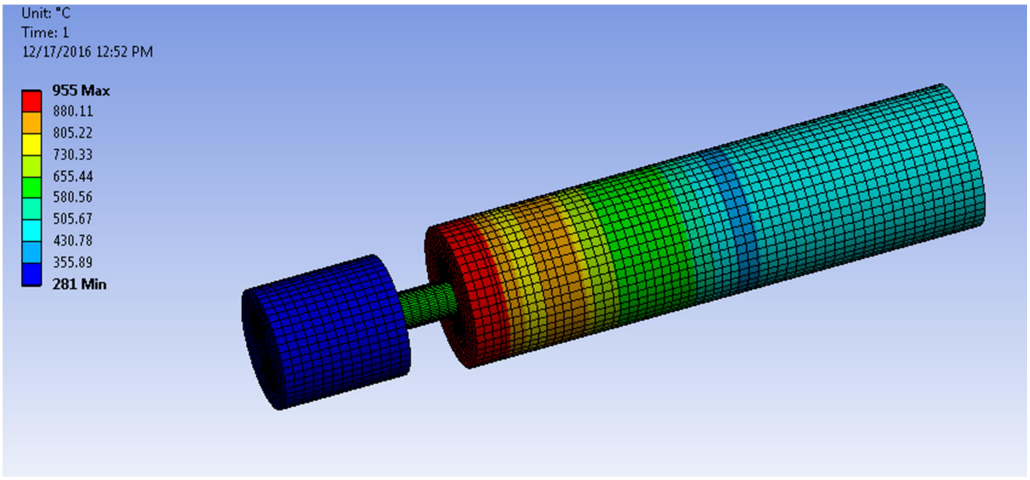


Figure D20: Variable temperature field of Model 7

The results of the final harmonic analyses, once again for a frequency of 600Hz, with an excitation of 1m.s^{-1}, for the geometry of Model 7 with a variable temperature field are shown in Figure D21 and Figure D22 for the closed and open

duct conditions respectively. These results show the slight deviation from the plane wave behaviour around the interfaces between the swirler and diffuser and flame zones.

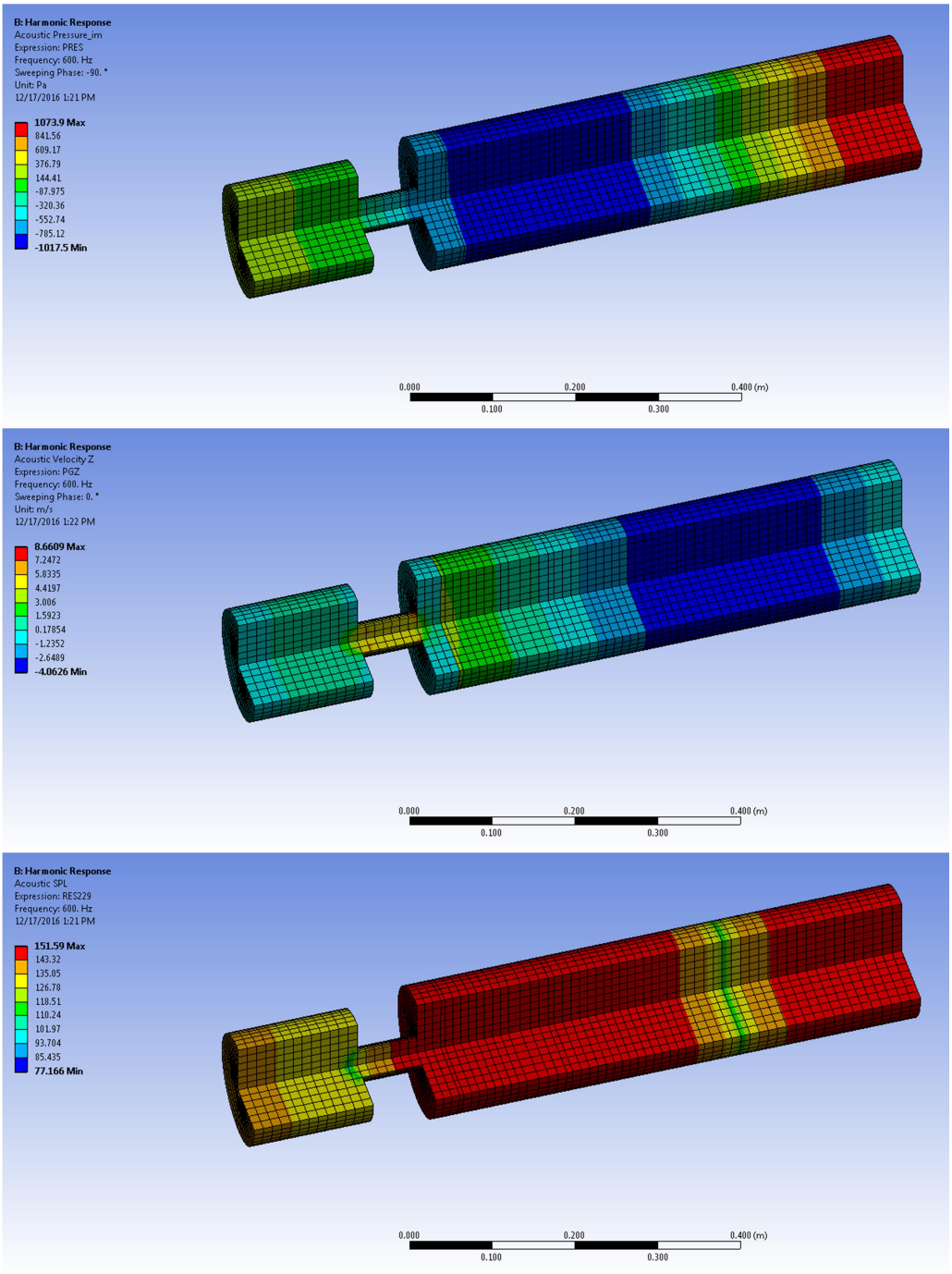


Figure D21: Results for harmonic analysis of Model 7 with variable temperature, closed duct

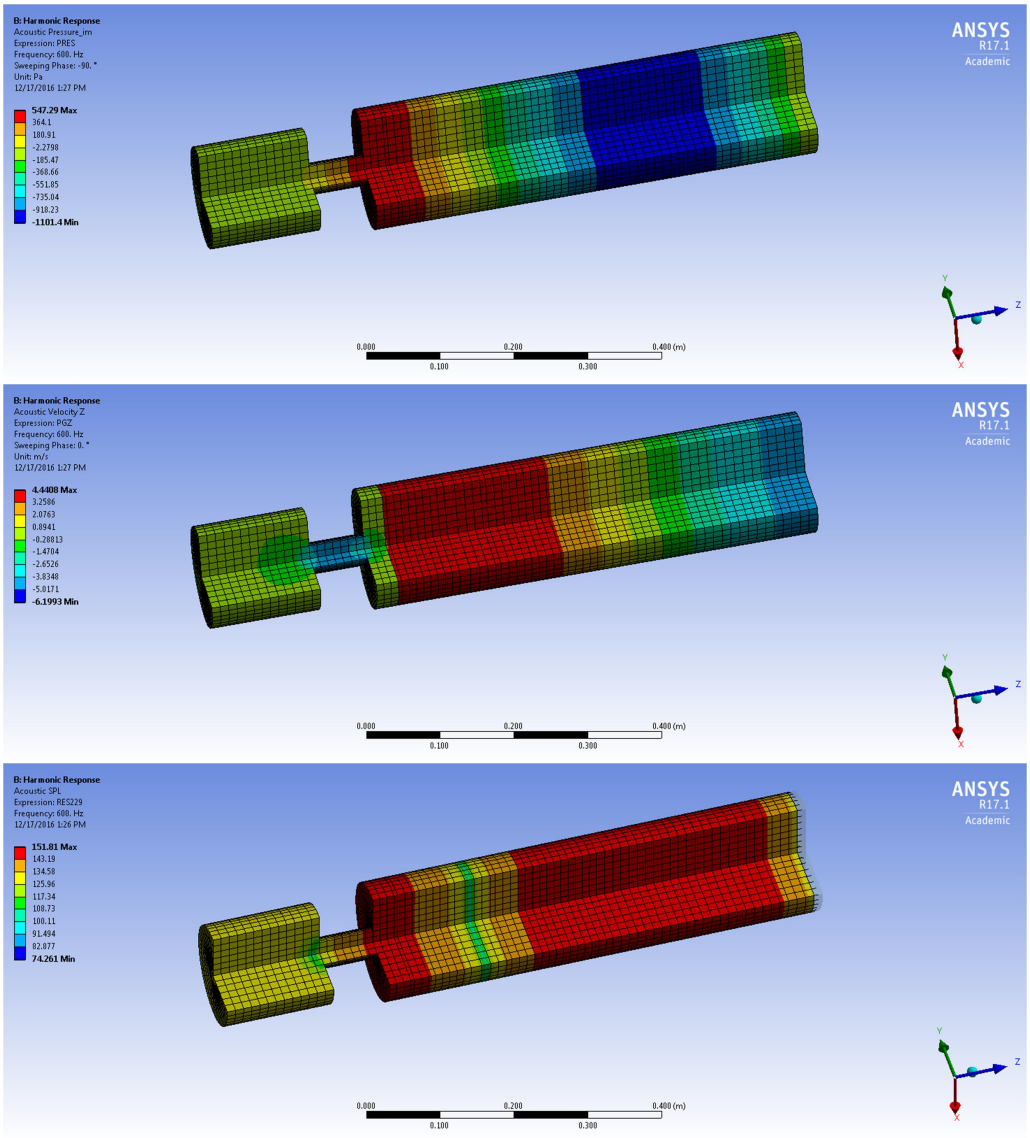


Figure D22: Results for harmonic analysis of Model 7 with variable temperature, open duct

D7. Exporting data from ANSYS to MATLAB

The values of the imaginary and real components of the Acoustic pressure and velocity, along with the SPL, along the axis ANSYS acoustic models described here were exported to Excel spreadsheets, using the export results function of ANSYS Mechanical. While this did not cause any difficulty for the simple geometries of Models 1 and 6, the models with multiple sections did have some complications.

When the results of the FEA models are exported to the spreadsheet, they are listed in order of node number. It may be seen from Figure D23 that, for the case of the composite section models, these nodes are not numbered in sequence along the axis of the model, meaning that the results exported spreadsheet require some manipulation to get them into the desired order for them to be compared to those of the theoretical models.

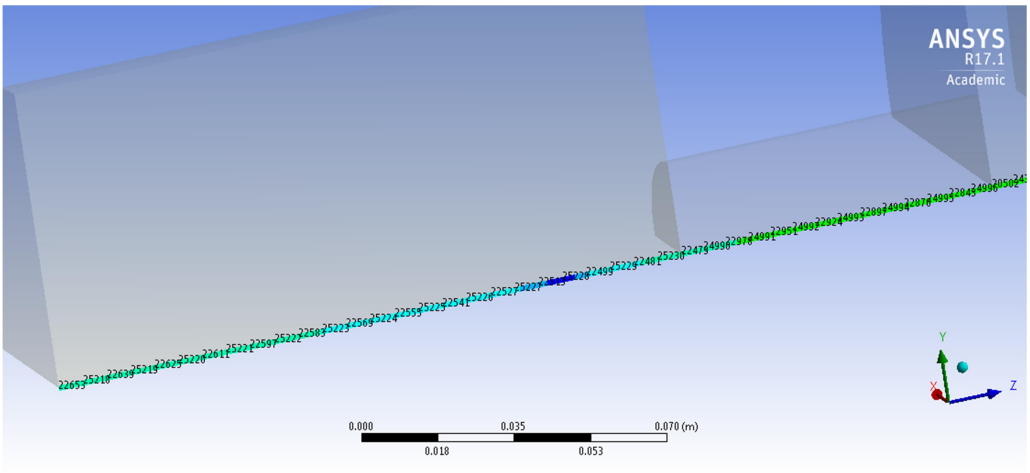


Figure D23: Nodes along axis of ANSYS Model

The position of each node along the axis of every model that encountered this difficulty was manually entered into a spreadsheet that contained the nodes in the order in which they were exported from ANSYS. This column was then copied to the spreadsheets that contained the calculated values in their exported order. The column with the node order was then sorted from smallest to largest (using the standard excel function for this task), placing the calculated values in the correct order.

Once the values of the acoustic pressures, velocities and SPLs were placed in the correct order, the results for each model were collected into one spreadsheet and saved in the working directory of the relevant MATLAB script. The Z-coordinate values were included in this spreadsheet by using the constant size of the elements as the step size along the axis.

Appendix

E - Transfer Matrices

Appendix E Contents

Appendix E Contents ..... Eii

List of Symbols ..... Eiii

E1. Introduction E1

E2. Derivation of 4-Pole matrix for cylindrical duct with constant temperature E1

E3. Model Orientation E4

E4. Alternative form of 4-pole matrix E6

E5. Four pole matrix for acoustic pressure and velocity in cylindrical duct of varying temperature...E8

List of Symbols

x	Coordinate on x-axis	m
S	Cross sectional area of duct	m^2
L	Length of duct	m
P'_x	Acoustic pressure at point x	Pa
P_I	Incident pressure wave	Pa
P_R	Reflected pressure wave	Pa
u'_x	Acoustic velocity at point x	$m.s^{-1}$
m'_x	Acoustic mass flow rate at point x	$kg.m.s^{-1}$
k	Wave number	$-$
ω	Angular velocity	$rad.s^{-1}$
T	Temperature	K
ρ_0	Density of air (constant)	$kg.m^{-3}$
ρ_x	Density of air at point x	$kg.m^{-3}$
c_0	Speed of sound (constant)	$m.s^{-1}$
c_x	Speed of sound at point x	$m.s^{-1}$
$\boldsymbol{A}, \boldsymbol{B}, \boldsymbol{C}, \boldsymbol{T}$	4-Pole Transfer matrices	$-$
R_i	Row of transfer matrix	$-$
ν	Defined constant	$(J.kg^{-1}K^{-1})^{\frac{1}{2}}$
γ	Ratio of specific heats	$-$
R	Universal gas constant	$J.mol^{-1}.K^{-1}$
R_S	Specific gas constant	$J.kg^{-1}K^{-1}$
M	Molar mass of air	$kg.mol^{-1}$
χ_i	Defined constant	$K.rad.s^{-1}.J^{-\frac{1}{2}}.kg^{-\frac{1}{2}}$

E1. Introduction

This Appendix serves to give a detailed development of the transfer matrices used in this project to give the relation between the acoustic particle velocities and pressures at any point along the axis of the duct, referred to in Appendix D.

E2. Derivation of 4-Pole matrix for cylindrical duct with constant temperature

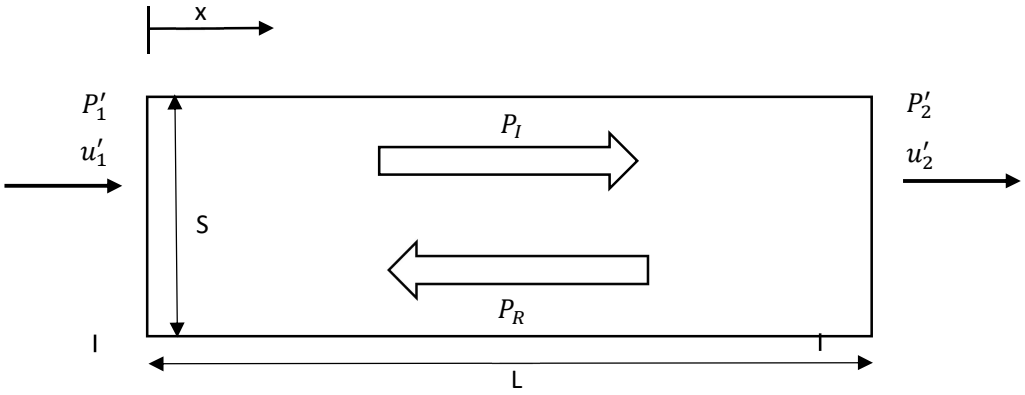


Figure E1: One dimensional wave propagation in a duct

Using:

$$\boldsymbol{u'(x) = -\frac{1}{\rho_0 c_0}\left(P_I e^{jk(x)} - P_R e^{-jk(x)}\right)} \quad \text{E-1}$$

$$\boldsymbol{P'(x) = P_I e^{jk(x)} + P_R e^{-jk(x)}} \quad \text{E-2}$$

The boundary conditions at $x = 0$ and $x = L$ are:

$$\boldsymbol{P_1' = P'(0) = P_I e^{jk(0)} + P_R e^{-jk(0)}} \quad \text{E-3}$$

$$\boldsymbol{u_1' = u'(0) = -\frac{1}{\rho_0 c_0}\left(P_I e^{jk(0)} - P_R e^{-jk(0)}\right)} \quad \text{E-4}$$

Which may be written as:

$$\begin{pmatrix} \boldsymbol{P_1'} \\ \boldsymbol{u_1'} \end{pmatrix} = \begin{pmatrix} \mathbf{1} & \mathbf{1} \\ -\frac{\mathbf{1}}{\boldsymbol{\rho_0 c_0}} & \frac{\mathbf{1}}{\boldsymbol{\rho_0 c_0}} \end{pmatrix} \begin{pmatrix} \boldsymbol{P_I} \\ \boldsymbol{P_R} \end{pmatrix} \quad \text{E-5}$$

And

$$\boldsymbol{P_2' = P'(L) = P_I e^{jk(L)} + P_R e^{-jk(L)}} \quad \text{E-6}$$

$$\boldsymbol{u_2' = u'(L) = -\frac{1}{\rho_0 c_0}\left(P_I e^{jk(L)} - P_R e^{-jk(L)}\right)} \quad \text{E-7}$$

Which may be written as:

$$\begin{pmatrix} \boldsymbol{P_2'} \\ \boldsymbol{u_2'} \end{pmatrix} = \begin{pmatrix} \boldsymbol{e^{jkL}} & \boldsymbol{e^{-jkL}} \\ -\frac{\boldsymbol{e^{jkL}}}{\boldsymbol{\rho_0 c_0}} & \frac{\boldsymbol{e^{-jkL}}}{\boldsymbol{\rho_0 c_0}} \end{pmatrix} \begin{pmatrix} \boldsymbol{P_I} \\ \boldsymbol{P_R} \end{pmatrix} \quad \text{E-8}$$

Let the matrix:

$$\boldsymbol{A} = \begin{pmatrix} \mathbf{1} & \mathbf{1} \\ -\frac{\mathbf{1}}{\boldsymbol{\rho_0 c_0}} & \frac{\mathbf{1}}{\boldsymbol{\rho_0 c_0}} \end{pmatrix} \quad \text{E-9}$$

Then

$$\begin{pmatrix} \boldsymbol{P_1'} \\ \boldsymbol{u_1'} \end{pmatrix} = \boldsymbol{A} \begin{pmatrix} \boldsymbol{P_I} \\ \boldsymbol{P_R} \end{pmatrix} \quad \text{E-10}$$

Multiplying both sides of the equation by $\boldsymbol{A^{-1}}$:

$$\boldsymbol{A^{-1}} \begin{pmatrix} \boldsymbol{P_1'} \\ \boldsymbol{u_1'} \end{pmatrix} = \boldsymbol{A^{-1} A} \begin{pmatrix} \boldsymbol{P_I} \\ \boldsymbol{P_R} \end{pmatrix} \quad \text{E-11}$$

$$\boldsymbol{A^{-1}} \begin{pmatrix} \boldsymbol{P_1'} \\ \boldsymbol{u_1'} \end{pmatrix} = \begin{pmatrix} \boldsymbol{P_I} \\ \boldsymbol{P_R} \end{pmatrix} \quad \text{E-12}$$

Solving for $\boldsymbol{A^{-1}}$:

$$\boldsymbol{A} = \begin{pmatrix} \mathbf{1} & \mathbf{1} \\ -\frac{\mathbf{1}}{\boldsymbol{\rho_0 c_0}} & \frac{\mathbf{1}}{\boldsymbol{\rho_0 c_0}} \end{pmatrix} \tag{E-13}$$

$$\left(\begin{array}{cc|cc} \mathbf{1} & \mathbf{1} & \mathbf{1} & \mathbf{0} \\ -\frac{\mathbf{1}}{\boldsymbol{\rho_0 c_0}} & \frac{\mathbf{1}}{\boldsymbol{\rho_0 c_0}} & \mathbf{0} & \mathbf{1} \end{array}\right) \tag{E-14}$$

$$\boldsymbol{R_2} + \frac{\boldsymbol{R_1}}{\boldsymbol{\rho_0 c_0}} \Rightarrow \left(\begin{array}{cc|cc} \mathbf{1} & \frac{\mathbf{1}}{\mathbf{2}} & \mathbf{1} & \mathbf{0} \\ \mathbf{0} & \frac{\mathbf{1}}{\boldsymbol{\rho_0 c_0}} & \frac{\mathbf{1}}{\boldsymbol{\rho_0 c_0}} & \mathbf{1} \end{array}\right) \tag{E-15}$$

$$\boldsymbol{R_2} \times \frac{\boldsymbol{\rho_0 c_0}}{\mathbf{2}} \Rightarrow \left(\begin{array}{cc|cc} \mathbf{1} & \mathbf{1} & \mathbf{1} & \mathbf{0} \\ \mathbf{0} & \mathbf{1} & \frac{\mathbf{1}}{\mathbf{2}} & \frac{\boldsymbol{\rho_0 c_0}}{\mathbf{2}} \end{array}\right) \tag{E-16}$$

$$\boldsymbol{R_1} - \boldsymbol{R_2} \Rightarrow \left(\begin{array}{cc|cc} \mathbf{1} & \mathbf{0} & \frac{\mathbf{1}}{\mathbf{2}} & -\frac{\boldsymbol{\rho_0 c_0}}{\mathbf{2}} \\ \mathbf{0} & \mathbf{1} & \frac{\mathbf{1}}{\mathbf{2}} & \frac{\boldsymbol{\rho_0 c_0}}{\mathbf{2}} \end{array}\right) \tag{E-17}$$

$$\boldsymbol{A^{-1}} = \begin{pmatrix} \frac{\mathbf{1}}{\mathbf{2}} & -\frac{\boldsymbol{\rho_0 c_0}}{\mathbf{2}} \\ \frac{\mathbf{1}}{\mathbf{2}} & \frac{\boldsymbol{\rho_0 c_0}}{\mathbf{2}} \end{pmatrix} \tag{E-18}$$

Combining Equations E-12 and E-8 gives:

$$\begin{pmatrix} \boldsymbol{P_2'} \\ \boldsymbol{u_2'} \end{pmatrix} = \begin{pmatrix} \boldsymbol{e^{jkL}} & \boldsymbol{e^{-jkL}} \\ -\frac{\boldsymbol{e^{jkL}}}{\boldsymbol{\rho_0 c_0}} & \frac{\boldsymbol{e^{-jkL}}}{\boldsymbol{\rho_0 c_0}} \end{pmatrix} \boldsymbol{A^{-1}} \begin{pmatrix} \boldsymbol{P_1'} \\ \boldsymbol{u_1'} \end{pmatrix} \tag{E-19}$$

$$\begin{pmatrix} \boldsymbol{P_2'} \\ \boldsymbol{u_2'} \end{pmatrix} = \begin{pmatrix} \boldsymbol{e^{jkL}} & \boldsymbol{e^{-jkL}} \\ -\frac{\boldsymbol{e^{jkL}}}{\boldsymbol{\rho_0 c_0}} & \frac{\boldsymbol{e^{-jkL}}}{\boldsymbol{\rho_0 c_0}} \end{pmatrix} \begin{pmatrix} \frac{\mathbf{1}}{\mathbf{2}} & -\frac{\boldsymbol{\rho_0 c_0}}{\mathbf{2}} \\ \frac{\mathbf{1}}{\mathbf{2}} & \frac{\boldsymbol{\rho_0 c_0}}{\mathbf{2}} \end{pmatrix} \begin{pmatrix} \boldsymbol{P_1'} \\ \boldsymbol{u_1'} \end{pmatrix} \tag{E-20}$$

$$\begin{pmatrix} \boldsymbol{P_2'} \\ \boldsymbol{u_2'} \end{pmatrix} = \begin{pmatrix} \left(\frac{\boldsymbol{e^{jkL}}}{\mathbf{2}} + \frac{\mathbf{1}}{\mathbf{2}\boldsymbol{e^{jkL}}}\right) & \left[\frac{\boldsymbol{\rho_0 c_0}}{\mathbf{2}}\left(\boldsymbol{e^{-jkL}} - \boldsymbol{e^{jkL}}\right)\right] \\ \frac{\boldsymbol{\rho_0 c_0}}{\mathbf{2}}\left(\boldsymbol{e^{-jkL}} - \boldsymbol{e^{jkL}}\right) & \left(\frac{\boldsymbol{e^{jkL}}}{\mathbf{2}} + \frac{\mathbf{1}}{\mathbf{2}\boldsymbol{e^{jkL}}}\right) \end{pmatrix} \begin{pmatrix} \boldsymbol{P_1'} \\ \boldsymbol{u_1'} \end{pmatrix} \tag{E-21}$$

Using the identities:

$$\sin x = \frac{e^{jx} - e^{-jx}}{2} \qquad \text{E-22}$$

$$\cos x = \frac{e^{jx} + e^{-jx}}{2j} \qquad \text{E-23}$$

$$\begin{pmatrix} P_2' \\ u_2' \end{pmatrix} = \begin{pmatrix} \cos kL & -j\rho_0 c_0 \sin kL \\ -\frac{j}{\rho_0 c_0} \sin kL & \cos kL \end{pmatrix} \begin{pmatrix} P_1' \\ u_1' \end{pmatrix} \qquad \text{E-24}$$

In order to make use of this matrix over multiple ducts of varying cross section, where the acoustic velocity will not be constant, it is necessary to compute the acoustic mass flow rate (m') instead. When u_2' and u_1' are multiplied by the density of the air and the area of the duct section ($\rho_0 S$), equation E-24 is modified to:

$$\begin{pmatrix} P_2' \\ m_2' \end{pmatrix} = \begin{pmatrix} \cos kL & -\frac{jc_0}{S} \sin kL \\ -\frac{jS}{c_0} \sin kL & \cos kL \end{pmatrix} \begin{pmatrix} P_1' \\ m_1' \end{pmatrix} \qquad \text{E- 25}$$

E3. Model Orientation

From E-24, let

$$\mathbf{B} = \begin{pmatrix} \cos kL & -j\rho_0 c_0 \sin kL \\ -\frac{j}{\rho_0 c_0} \sin kL & \cos kL \end{pmatrix} \qquad \text{E- 1}$$

The convention in acoustic calculations is to orient the model from right to left (as used in (Howard & Cazzolato, 2014) and (Singh, et al., 2008)), while that of fluid mechanics (on which the temperature field of the models is based) is from left to right. In both cases, the convention is to have the point on the left of the duct marked as point 1 and that on the right as point 2.

If the names of the points are kept constant, and the orientation of the waves are swapped (as would happen when alternating between the conventions described above, Equation E-26 becomes:

$$\begin{pmatrix} P_1' \\ u_1' \end{pmatrix} = \mathbf{B}\begin{pmatrix} P_2' \\ u_2' \end{pmatrix} \quad \text{E-27}$$

And, therefore:

$$\begin{pmatrix} P_2' \\ u_2' \end{pmatrix} = \mathbf{B}^{-1}\begin{pmatrix} P_1' \\ u_1' \end{pmatrix} \quad \text{E-28}$$

Solving for $\mathbf{B}^{-1}$:

$$\left(\begin{array}{cc|cc} \cos kL & -j\rho_0 c_0 \sin kL & 1 & 0 \\ -\frac{j}{\rho_0 c_0}\sin kL & \cos kL & 0 & 1 \end{array}\right) \quad \text{E-29}$$

$$\frac{R_1}{\cos kL} \Longrightarrow \left(\begin{array}{cc|cc} 1 & -j\rho_0 c_0 \frac{\sin kL}{\cos kL} & \frac{1}{\cos kL} & 0 \\ -\frac{j}{\rho_0 c_0}\sin kL & \cos kL & 0 & 1 \end{array}\right) \quad \text{E-30}$$

$$R_2 + \left(\frac{j}{\rho_0 c_0}\sin kL\right) R_1 \Longrightarrow \left(\begin{array}{cc|cc} 1 & -j\rho_0 c_0 \frac{\sin kL}{\cos kL} & \frac{1}{\cos kL} & 0 \\ 0 & \frac{1}{\cos kL} & \frac{j}{\rho_0 c_0}\frac{\sin kL}{\cos kL} & 1 \end{array}\right) \quad \text{E-31}$$

$$(\cos kL)R_2 \Longrightarrow \left(\begin{array}{cc|cc} 1 & -j\rho_0 c_0 \frac{\sin kL}{\cos kL} & \frac{1}{\cos kL} & 0 \\ 0 & 1 & \frac{j}{\rho_0 c_0}\sin kL & \cos kL \end{array}\right) \quad \text{E-32}$$

$$R_1 + \left(j\rho_0 c_0 \frac{\sin kL}{\cos kL}\right) R_2 \Longrightarrow \left(\begin{array}{cc|cc} 1 & 0 & \cos kL & j\rho_0 c_0 \sin kL \\ 0 & 1 & \frac{j}{\rho_0 c_0}\sin kL & \cos kL \end{array}\right) \quad \text{E-33}$$

Therefore:

$$\mathbf{B^{-1}} = \begin{pmatrix} \cos kL & j\rho_0 c_0 \sin kL \\ \frac{j}{\rho_0 c_0}\sin kL & \cos kL \end{pmatrix} \quad \text{E-34}$$

Note that $\mathbf{B}_{12}^{-1} = -\mathbf{B}_{12}$ and $\mathbf{B}_{21}^{-1} = -\mathbf{B}_{21}$, with the other two values identical. When using the method employed in the one dimensional MATLAB model of the project, any confusion over the orientation of the model will result in the values of the individual pressure values at each point on the axis being multiplied by -1.

This makes it very important to ensure that the points at either end of the duct, and the direction of the incident and reflected waves (P_I and P_R) are clearly defined and kept consistent throughout any efforts at computation.

For this project, the duct has been oriented from left to right, with the usual numbering system of the points applying (see Figure E1), in the same manner as (Huls, 2006). In the derivations above, the duct is oriented along the x axis, while the models produced in this project have been oriented along the y axis.

E4. Alternative form of 4-pole matrix

In order to make use of Equation E-25, both the acoustic pressure and velocity must be known at one of the points. For the case of a closed duct with an acoustic velocity source at one end (as used in some of the 1-D models in this project), it is the velocities at either end that are known and the pressures that must be found.

The values for the acoustic pressure at either end of the duct may be found by re-arranging the terms of matrix $\mathbf{T}$ in Equation , as used in the MATLAB scripts produced by Howard & Cazzolato (2014), giving the set of equations:

$$\boldsymbol{P_2'} = \boldsymbol{T_{11}P_1'} + \boldsymbol{T_{12}m_1'} \quad \text{E-35}$$

$$\boldsymbol{P_1'} = \frac{\boldsymbol{m_2'} - \boldsymbol{T_{22}m_1'}}{\boldsymbol{T_{21}}} \quad \text{E-36}$$

In cases where it the matrix T has not been solved, it is sometimes more convenient to use the matrix derived below, as used in (Huls, 2006).

The setup for the initial equations is the same as that for Equations E-5 and E-8, with the boundary conditions taken from Figure E1.

$$\begin{pmatrix} P_1' \\ P_2' \end{pmatrix} = \begin{pmatrix} e^{jk(0)} & -e^{-jk(0)} \\ e^{jkL} & -e^{-jkL} \end{pmatrix} \begin{pmatrix} P_I \\ P_R \end{pmatrix} \quad \text{E-37}$$

$$\begin{pmatrix} u_1' \\ u_2' \end{pmatrix} = \frac{1}{-\rho_0 c_0} \begin{pmatrix} e^{jk(0)} & -e^{-jk(0)} \\ e^{jkL} & -e^{-jkL} \end{pmatrix} \begin{pmatrix} P_I \\ P_R \end{pmatrix} \quad \text{E-38}$$

As before, the inverse of the matrix in E-37 must be found and used in E-38 to give a relation between the acoustic velocities and pressures at either end of the duct. If the matrix in E-37 is called $\mathbf{C}$, then $\mathbf{C}^{-1}$ is found by the following reduction:

$$\left(\begin{array}{cc|cc} 1 & 1 & 1 & 0 \\ e^{jkL} & e^{-jkL} & 0 & 1 \end{array}\right) \quad \text{E-39}$$

$$R_2 - e^{jkL} R_1 \Rightarrow \left(\begin{array}{cc|cc} 1 & 1 & 1 & 0 \\ 0 & e^{-jkL} - e^{jkL} & -e^{jkL} & 1 \end{array}\right) \quad \text{E-40}$$

$$\frac{R_2}{e^{-jkL} - e^{jkL}} \Rightarrow \left(\begin{array}{cc|cc} 1 & 1 & 1 & 0 \\ 0 & 1 & \frac{-e^{jkL}}{e^{-jkL} - e^{jkL}} & \frac{1}{e^{-jkL} - e^{jkL}} \end{array}\right) \quad \text{E-41}$$

$$R_1 - R_2 \Rightarrow \left(\begin{array}{cc|cc} 1 & 0 & 1 + \frac{e^{jkL}}{e^{-jkL} - e^{jkL}} & \frac{1}{e^{-jkL} - e^{jkL}} \\ 0 & 1 & \frac{-e^{jkL}}{e^{-jkL} - e^{jkL}} & \frac{1}{e^{-jkL} - e^{jkL}} \end{array}\right) \quad \text{E-42}$$

$$\mathrm{C}^{-1} = \begin{pmatrix} 1 + \frac{e^{jkL}}{e^{-jkL} - e^{jkL}} & \frac{1}{e^{-jkL} - e^{jkL}} \\ \frac{-e^{jkL}}{e^{-jkL} - e^{jkL}} & \frac{1}{e^{-jkL} - e^{jkL}} \end{pmatrix} \quad \text{E-43}$$

Using $\mathbf{C}^{-1}$, E-38 becomes:

$$\begin{pmatrix} u_1' \\ u_2' \end{pmatrix} = \frac{1}{-\rho_0 c_0} \begin{pmatrix} 1 & -1 \\ e^{jkL} & -e^{-jkL} \end{pmatrix} \begin{pmatrix} 1 + \frac{e^{jkL}}{e^{-jkL} - e^{jkL}} & \frac{1}{e^{-jkL} - e^{jkL}} \\ \frac{-e^{jkL}}{e^{-jkL} - e^{jkL}} & \frac{1}{e^{-jkL} - e^{jkL}} \end{pmatrix} \begin{pmatrix} P_1' \\ P_2' \end{pmatrix} \quad \text{E-44}$$

Which may be simplified to:

$$\begin{pmatrix} u_1' \\ u_2' \end{pmatrix} = \frac{1}{-\rho_0 c_0 \left(e^{-jkL} - e^{jkL}\right)} \begin{pmatrix} \left(e^{-jkL} + e^{jkL}\right) & -2 \\ 2 & e^{-jkL} \end{pmatrix} \begin{pmatrix} P_1' \\ P_2' \end{pmatrix} \quad \text{E-45}$$

To get to the form utilised in (Huls, 2006), a factor of 2 is taken out of the transformation matrix and use is made of the identities:

$$\sinh x = \frac{e^x - e^{-x}}{2} \quad \text{E-46}$$

$$\cosh x = \frac{e^x + e^{-x}}{2} \quad \text{E-47}$$

$$\sinh jx = j \sin x \quad \text{E-48}$$

Giving:

$$\begin{pmatrix} u_1' \\ u_2' \end{pmatrix} = \frac{1}{-j\rho_0 c_0 \sin kL} \begin{pmatrix} \cosh jkL & -1 \\ 1 & -\cosh jkL \end{pmatrix} \begin{pmatrix} P_1' \\ P_2' \end{pmatrix} \quad \text{E-49}$$

As with Equations E-24 and E-25, Equation E-49 needs to be modified from giving the relationship between the acoustic velocities and pressures to that of the acoustic mass flow rates and pressures. This final equation is given below.

$$\begin{pmatrix} m_1' \\ m_2' \end{pmatrix} = \frac{S}{-jc_0 \sin kL} \begin{pmatrix} \cosh jkL & -1 \\ 1 & -\cosh jkL \end{pmatrix} \begin{pmatrix} P_1' \\ P_2' \end{pmatrix} \quad \text{E-50}$$

E5. Four pole matrix for acoustic pressure and velocity in cylindrical duct of varying temperature

The equations dealt with so far all rely on the temperature (and, therefore, the density and speed of sound) of the air within the duct remaining constant. In the combustion chamber of a gas turbine, this is certainly not going to be the case. A transfer matrix that takes the effect of a variation in temperature into account such that:

$$\begin{pmatrix} P_2' \\ u_2' \end{pmatrix} = B \begin{pmatrix} P_1' \\ u_1' \end{pmatrix} \quad \text{E-51}$$

$$B = \begin{pmatrix} B_{11} & B_{12} \\ B_{21} & B_{22} \end{pmatrix} \quad \text{E-52}$$

$$B_{11} = \left[\frac{\pi}{2}\frac{\omega\sqrt{T_2}}{\nu}\right]\left[J_1\left(\frac{\omega\sqrt{T_2}}{\nu}\right)Y_0\left(\frac{\omega\sqrt{T_1}}{\nu}\right) - J_0\left(\frac{\omega\sqrt{T_1}}{\nu}\right)Y_1\left(\frac{\omega\sqrt{T_2}}{\nu}\right)\right] \quad \text{E-53}$$

$$B_{12} = \left[j\left(\frac{\pi}{2}\frac{\omega\sqrt{T_2}}{\nu}\right)\left(\frac{m}{|m|}\right)\left(\rho_2\sqrt{\gamma R_S T_2}\right)\right]\left[J_0\left(\frac{\omega\sqrt{T_1}}{\nu}\right)Y_0\left(\frac{\omega\sqrt{T_2}}{\nu}\right) - J_0\left(\frac{\omega\sqrt{T_2}}{\nu}\right)Y_1\left(\frac{\omega\sqrt{T_1}}{\nu}\right)\right] \quad \text{E-54}$$

$$B_{21} = \left[j\left(\frac{\pi}{2}\frac{\omega\sqrt{T_2}}{\nu}\right)\left(\frac{m}{|m|}\right)\left(\frac{1}{\rho_1\sqrt{\gamma R_S T_1}}\right)\right]\left[J_1\left(\frac{\omega\sqrt{T_1}}{\nu}\right)Y_1\left(\frac{\omega\sqrt{T_2}}{\nu}\right) - J_1\left(\frac{\omega\sqrt{T_2}}{\nu}\right)Y_1\left(\frac{\omega\sqrt{T_1}}{\nu}\right)\right] \quad \text{E-55}$$

$$B_{22} = \left[j\left(\frac{\pi}{2}\frac{\omega\sqrt{T_2}}{\nu}\right)\left(\frac{\rho_2\sqrt{\gamma R_S T_2}}{\rho_1\sqrt{\gamma R_S T_1}}\right)\right]\left[J_1\left(\frac{\omega\sqrt{T_1}}{\nu}\right)Y_0\left(\frac{\omega\sqrt{T_2}}{\nu}\right) - J_0\left(\frac{\omega\sqrt{T_2}}{\nu}\right)Y_1\left(\frac{\omega\sqrt{T_1}}{\nu}\right)\right] \quad \text{E-56}$$

Where:

$$\nu = \frac{|m|}{2}\sqrt{\gamma R_S} \quad \text{E-57}$$

$$R_S = \frac{R}{M} \quad \text{E-58}$$

To make the equations easier and neater to code in MATLAB, the following constants are defined:

$$\chi_1 = \frac{\omega\sqrt{T_1}}{\nu},\ \chi_2 = \frac{\omega\sqrt{T_2}}{\nu} \quad \text{E-59}$$

And it is noted that:

$$c_1 = \sqrt{\gamma R_S T_1},\ c_2 = \sqrt{\gamma R_S T_2} \quad \text{E-60}$$

With c_1 and c_2 representing the speed of sound at the inlet and outlet of the duct respectively. Equations E-53 to E-56 become:

$$\boldsymbol{B_{11}} = \left[\frac{\pi}{2}\chi_2\right][\boldsymbol{J_1}(\chi_2)\boldsymbol{Y_0}(\chi_1) - \boldsymbol{J_0}(\chi_1)\boldsymbol{Y_1}(\chi_2)] \quad \text{E-61}$$

$$\boldsymbol{B_{12}} = \left[\boldsymbol{j}\left(\frac{\pi}{2}\chi_2\right)\left(\frac{\boldsymbol{m}}{|\boldsymbol{m}|}\right)(\boldsymbol{\rho_2 c_2})\right][\boldsymbol{J_0}(\chi_1)\boldsymbol{Y_0}(\chi_2) - \boldsymbol{J_0}(\chi_2)\boldsymbol{Y_1}(\chi_1)] \quad \text{E-62}$$

$$\boldsymbol{B_{21}} = \left[\boldsymbol{j}\left(\frac{\pi}{2}\chi_2\right)\left(\frac{\boldsymbol{m}}{|\boldsymbol{m}|}\right)\left(\frac{\boldsymbol{1}}{\boldsymbol{\rho_1 c_1}}\right)\right][\boldsymbol{J_1}(\chi_1)\boldsymbol{Y_1}(\chi_2) - \boldsymbol{J_1}(\chi_2)\boldsymbol{Y_1}(\chi_1)] \quad \text{E-63}$$

$$\boldsymbol{B_{22}} = \left[\boldsymbol{j}\left(\frac{\pi}{2}\chi_2\right)\left(\frac{\boldsymbol{\rho_2 c_2}}{\boldsymbol{\rho_1 c_1}}\right)\right][\boldsymbol{J_1}(\chi_1)\boldsymbol{Y_0}(\chi_2) - \boldsymbol{J_0}(\chi_2)\boldsymbol{Y_1}(\chi_1)] \quad \text{E-64}$$

Appendix

F - Theoretical Models in MATLAB

Appendix F Contents

Appendix F Contents ..... Fii
Appendix F Figures ..... Fiii
F1. Introduction F1
F2. Method F1
F3. Model 1 ..... F3
F4. Models 2 and 5 ..... F4
F5. Model 6 ..... F7
F6. Model 7 ..... F10

Appendix F Figures

Figure F1: SPL for Model 1, theory vs ANSYS 3
Figure F2: Sections and endpoints of Model 5 4
Figure F3: SPL for Model 2, ANSYS vs Theory 6
Figure F4: SPL for Model 5, ANSYS vs Theory 6
Figure F5: SPL for Model 6a, ANSYS vs Theory 7
Figure F6: Linear and variable temperature profiles, as used in Models 6 & 7 8
Figure F7: SPL for Model 6b, ANSYS vs Theory 9

F1. Introduction

This Appendix serves to describe the methods and results of the theoretical, one dimensional MATLAB scripts developed in this project. These scripts are used to validate the acoustic FEA models produced in ANSYS Mechanical (through the Acoustic ACT extension) described in Appendix D. The acoustic pressures, velocities and SPLs are calculated in each case, with only the graphs of the SPLs presented here.

F2. Method

The scripts are based on those developed in (Howard & Cazzolato, 2014), with a 4 pole transfer matrix used to calculate the acoustic pressure and velocity along the axis of a duct by dividing it into multiple "slices" and treating these as the ends of successive ducts. Ducts of different diameters are then added to the script to imitate the models of Appendix C. For the interfaces between these ducts, constant acoustic mass flow and pressure is assumed. All transfer matrices used are in the forms that calculate the relationship between pressure and mass flow, with the mass flow converted to velocity once all calculations have been completed.

When using the transfer matrices to calculate the acoustic properties along the axis of the model, it is important to note that the direction of travel along the axis and the nomenclature of the boundary conditions is extremely important. If there is any confusion of these, the results of the calculated pressure values will be inverted about the axis (i.e. multiplied by -1). For details on the matrices that bring about this effect, see Appendix E.

The SPL is calculated using the equation from (Howard & Cazzolato, 2014), note the $\sqrt{2}$ in the denominator, which results in the peak SPL being calculated instead of the RMS value. This is necessary in order to agree with the results produced in the ANSYS program (Howard & Cazzolato, 2014):

$$\mathbf{SPL} = \mathbf{20}\log_{10}\frac{\mathbf{P}_x'}{(\sqrt{2})(\mathbf{20}\times\mathbf{10}^{-6})} \qquad \text{F-1}$$

The results of the relevant ANSYS models of Appendix C are imported from the spreadsheets in which they are stored and plotted against the values calculated in the MATLAB script.

F3. Model 1

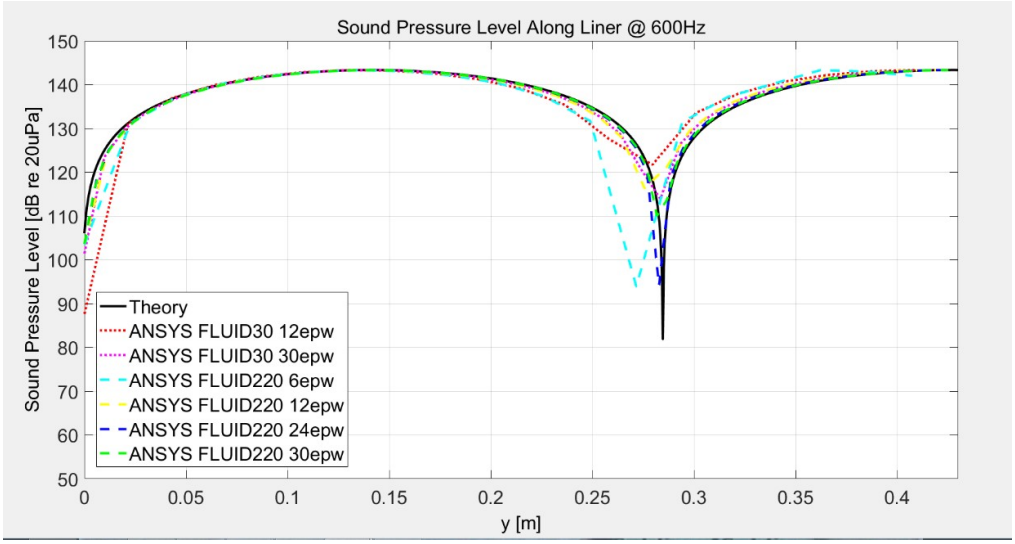


Figure F1: SPL for Model 1, theory vs ANSYS

The first 1 dimensional model is based on the script described in (Howard & Cazzolato, 2014) and modified for the dimensions and conditions of Model 1 (see Appendix D). The results of the SPL calculation are shown in Figure F1 and were used in selecting the element size for the acoustic FEA models produced in ANSYS Mechanical. The close agreement between the model using the FLUID 220 elements, at a size of 24epl, and the theory, was used as the basis for choosing this mesh configuration.

F4. Models 2 and 5

The geometries of models 2 and 5 are very similar, both consisting of several ducts of different dimensions. The difference being that Model 5 includes an additional duct downstream of the liner. The form of both of these geometries is similar to that of the theoretical model described in (A. P. Dowling, 2003) and has potential for further development of a source term that is more in line with that produced by the flame of a gas turbine combustor. This source term is not included in this project.

The values at each intersection between these composite ducts are calculated and used to verify the values that are later calculated along the axis of the entire model. The values at point -2 are used to determine the pressure at point 1, which is taken as the source of the sound propagating through the duct. Point 1 is located in line with the first primary air injection holes of the combustor described in Appendices A and B, which corresponds to the region where the majority of combustion occurs, as seen in Appendix C. The origin of the coordinate system is at point 1, as with the ANSYS acoustic models.

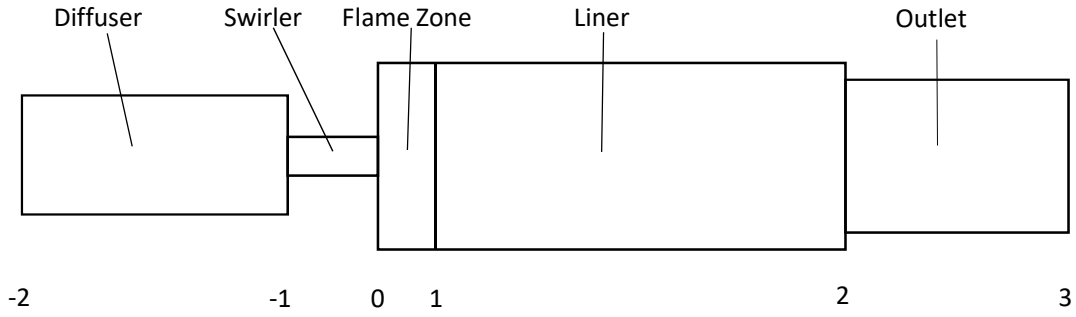


Figure F2: Sections and endpoints of Model 5

$$\begin{pmatrix} \mathrm{P}_2' \\ m_2' \end{pmatrix} = [\boldsymbol{T_L}] \begin{pmatrix} \mathrm{P}_1' \\ m_1' \end{pmatrix} \quad \text{F-2}$$

$$\begin{pmatrix} \mathrm{P}_1' \\ m_1' \end{pmatrix} = [\boldsymbol{T_{FZ}}] \begin{pmatrix} \mathrm{P}_0' \\ m_0' \end{pmatrix} \quad \text{F-3}$$

$$\begin{pmatrix} \mathrm{P}_0' \\ m_0' \end{pmatrix} = [\boldsymbol{T_S}] \begin{pmatrix} \mathrm{P}_{-1}' \\ m_{-1}' \end{pmatrix} \quad \text{F-4}$$

$$\begin{pmatrix} \mathbf{P}'_{-1} \\ \boldsymbol{m}'_{-1} \end{pmatrix} = [\boldsymbol{T_D}] \begin{pmatrix} \mathbf{P}'_{-2} \\ \boldsymbol{m}'_{-2} \end{pmatrix} \quad \text{F-5}$$

Combining Equations F-3, F-4 and F-5 gives:

$$\begin{pmatrix} \mathbf{P}'_{1} \\ \boldsymbol{m}'_{1} \end{pmatrix} = [\boldsymbol{T_{FZ}}][\boldsymbol{T_S}][\boldsymbol{T_D}] \begin{pmatrix} \mathbf{P}'_{-2} \\ \boldsymbol{m}'_{-2} \end{pmatrix} \quad \text{F-6}$$

With m'_1 used as the excitation and m'_{-2} assumed to be 0 due to the choked inlet conditions of the diffuser, P'_1 may be found as used as a starting point for the calculations done along the duct in either direction. For all scripts, the excitation is set in terms of the acoustic velocity, to match the format used in the ANSYS models, and converted to acoustic mass flow rate in the script.

As may be seen in Figure F3, there is still very good agreement between the theoretical values along the liner and those produced by the model in ANSYS. Around the swirler, however, there is a slight disagreement. From the cutaway figures of the results of this region in the ANSYS models, it appears that the sudden change in area causes a short region of non-planar behaviour of the wave. While the FEA model in ANSYS is able to model this non-planar behaviour, the one dimensional theoretical model is not able to do so and. The norm in producing one dimensional models of a combustor is to determine the transfer matrix of the burner (the swirler, injector and flame) experimentally, which was not an option here.

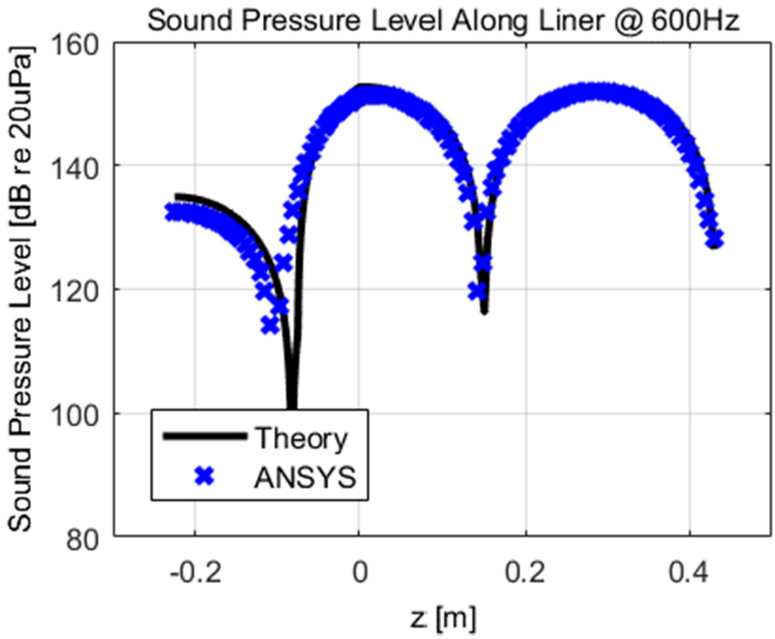


Figure F3: SPL for Model 2, ANSYS vs Theory

In Model 5, the results of which are shown in Figure F4 there is once again good agreement along the length of the liner, with the theoretical model showing signs of the discontinuities caused by the sudden changes of volume around the swirler.

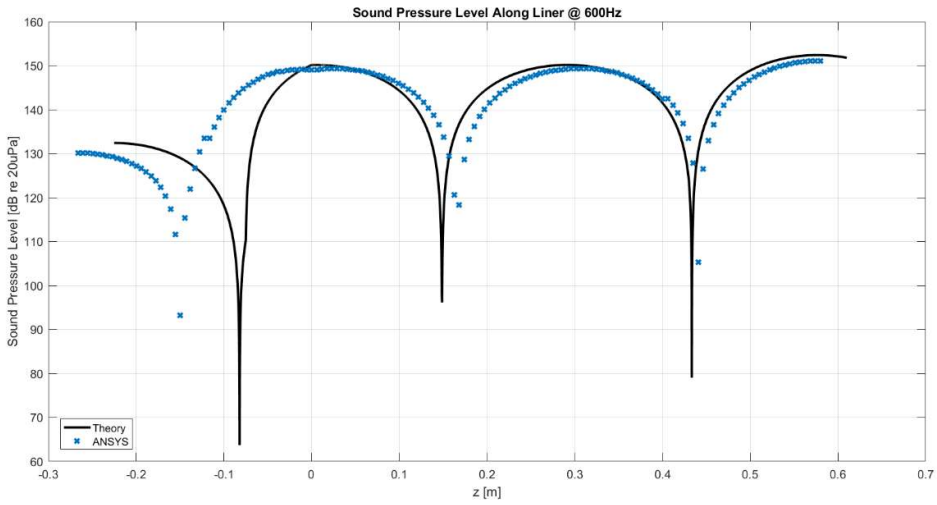


Figure F4: SPL for Model 5, ANSYS vs Theory

F5. Model 6

In Model 6, as with Model 1, the MATLAB script is based on that described in (Howard & Cazzolato, 2014) that makes use of the special transfer matrix derived in (Howard, 2013) for a duct with a linear temperature variation. The terms of this matrix are detailed in Appendix E.

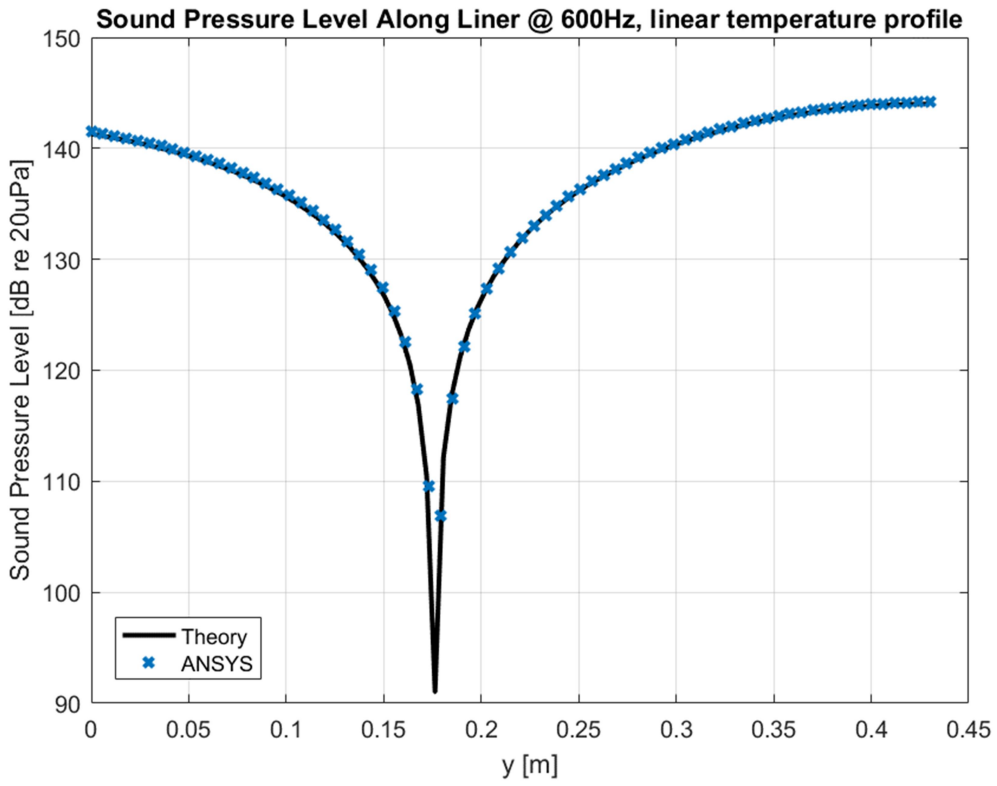


Figure F5: SPL for Model 6a, ANSYS vs Theory

The theoretical and ANSYS values for the SPL of Model 6 are shown in Figure F5 to be in very good agreement with each other, verifying the procedure used in altering the material properties of the model in ANSYS.

With the calculations of the linear temperature gradient calculated, a more complex temperature field was then introduced to the model. The results of the thermal analysis described in Appendix C (shown in Figure F6) were used as the individual

values of temperature along the axis of the theoretical model in MATLAB and the results calculated using the same transfer matrix as the first version of Model 6.

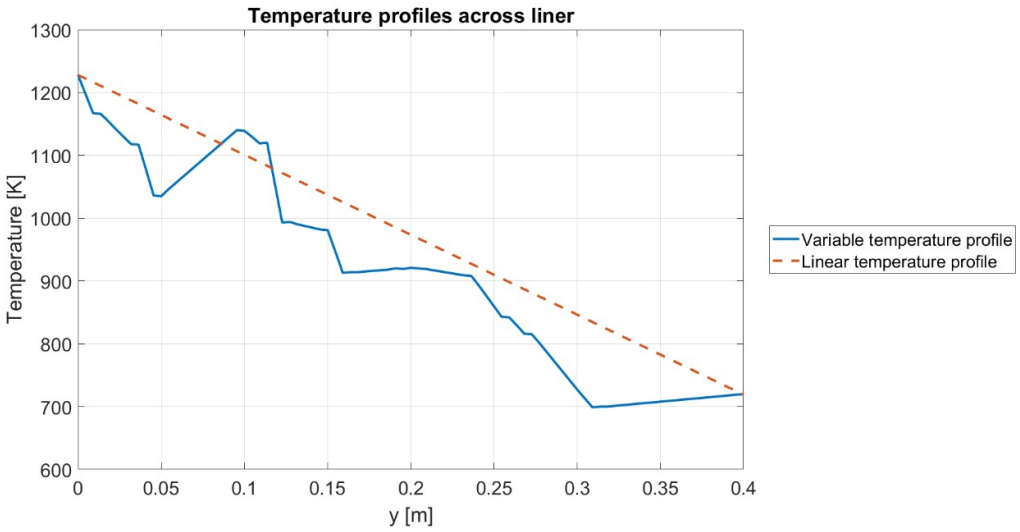


Figure F6: Linear and variable temperature profiles, as used in Models 6 & 7

While theoretical and ANSYS models agreed in the general form of the graph, it is clear from Figure F7 that the theoretical model does not handle the sudden changes in temperature gradient very well and a different analytical model would need to be developed for this method to be of any practical value other than a general verification of a more thorough method as is done here.

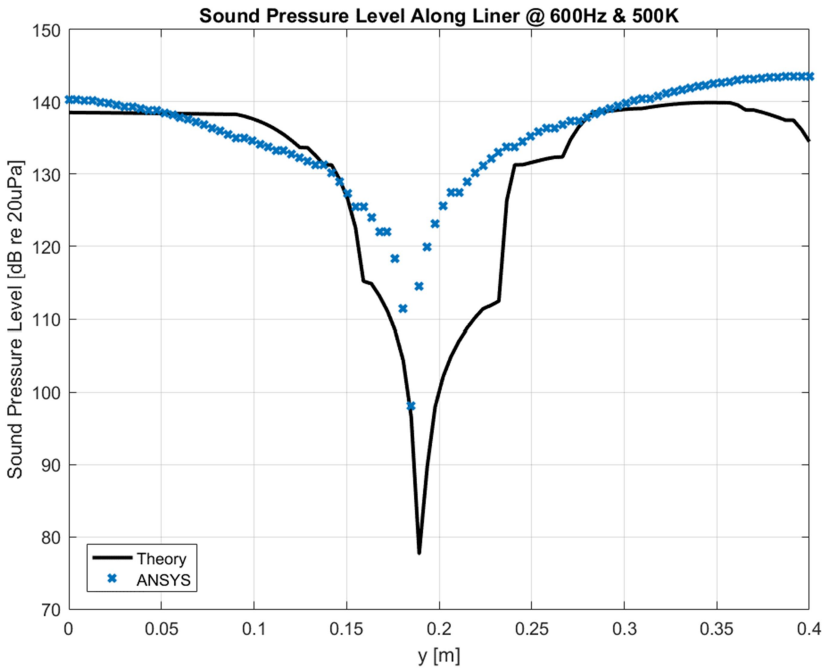


Figure F7: SPL for Model 6b, ANSYS vs Theory

F6. Model 7

The temperature is made to vary, as in Model 6, first linearly and then using the results of a thermal analysis. As may be expected, the theoretical model encounters the same difficulties as Models 5 and 6 with the discontinuities of area and temperature gradient. The agreement between the results, however, is good enough to serve as a verification of the FEA models, which are better equipped to handle these changes in input variables. The results of both analyses are presented in Figure F24 and Figure F25

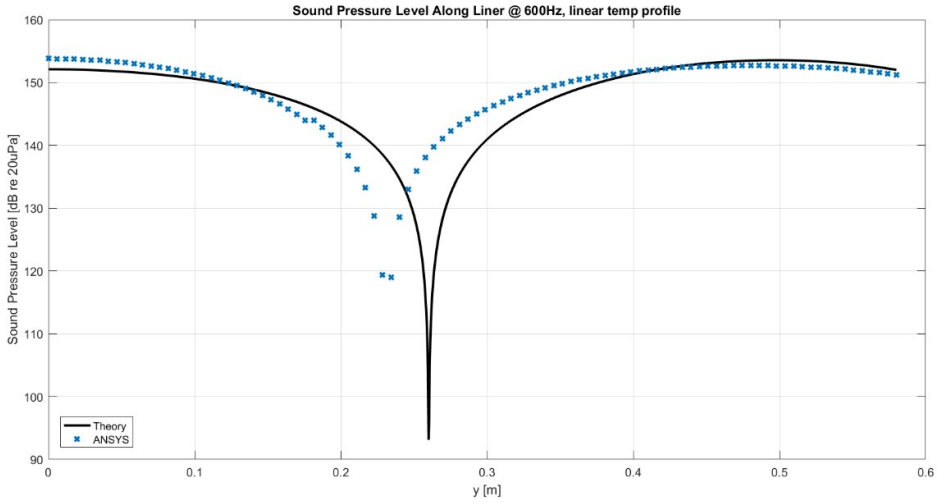


Figure F24: SPL for Model 7a, ANSYS vs Theory

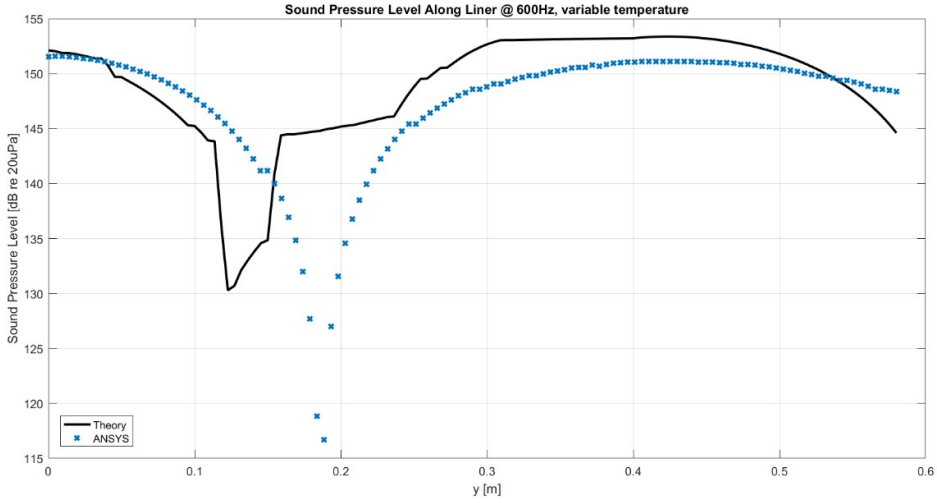


Figure F25: SPL for Model 7b, ANSYS vs Theory